Dissertation

submitted to the

Combined Faculties for the Natural Sciences and for Mathematics

of the Ruperto-Carola University of Heidleberg, Germany

for the degree of

Doctor of Natural Sciences

presented by

Alexandre, François, André Micoulet

born in Saint Vallier-sur-Rhône, Drôme, France

Oral examination the 15th December 2004

Uniaxial Mechanical Assays

on

Adherent Living Single Cells:

Animal Embryonic Fibroblasts

and

Human Pancreas Cancer Cells

Referees: **Prof. Dr. Joachim P. Spatz**

Prof. Dr. Heinz Horner

Trotz der enormen Komplexität lebender Materie, wie beispielsweise Gewebe und Zellen – die kleinste lebende Einheit – folgt diese physikalischen Prinzipien. In lebendem Gewebe sind andauernde oder zeitweise regulierte Prozesse, wie beispielsweise biochemische und mechanische Wechselwirkungen zwischen einzelnen Zellen und ihrer Umgebung grundlegend für den Aufbau von Gewebestrukturen und deren Funktion. Diese Wechselwirkungen regulieren beispielsweise die Differentiation und die Genexpression von Zellen grundlegend. Hierzu steht das Verhalten von Krebszellen im Gegensatz. Krebszellen vermehren sich und bewegen sich durch Gewebe unkontrolliert. Das mechanische Verhalten und das Adhäsionsverhalten sind von normalen Zellen sehr verschieden.

Die vorliegende Arbeit beschreibt Experimente welche die Bedingungen einer Zelle im Gewebe nachahmen, indem ein uniaxialer, mechanischer Stress unter physiologischen Bedingungen an eine einzelne Zelle angelegt wurde. Gleichzeitig wurde die angelegte Kraft, die Zelldeformation und die zelluläre Form mit höchster Genauigkeit gemessen. Die uniaxiale Deformation wurde mittels zweier Mikroglasplatten einer einzelnen Zelle aufgezwungen. Diese Experimente konnten entweder mit konstanter Kraft oder konstanter Deformation kontrolliert werden und erlaubten die Quantifizierung der zellulären viskoelastischen Eigenschaften und deren Beschreibung mittels linearer Kraftgesetze oder dem Kelvin-Modell. Biolipde, wie beispielsweise Sphingosylphosphorylcholin und Lysophosphatidsäure, verändern die Architektur des Zytoskeletts. Dies zeigte fatale Konsequenzen bezüglich der mechanischen Eigenschaften von embryonalen Fibroblasten von Ratten und menschlichen Pankreas-Krebs-Zellen. Zelluläre Versteifung und Erweichung, die Leistung und der Energieverbrauch einer einzelnen Zelle konnte quantitativ bestimmt werden. Beispielsweise betrug die Kontraktionsleitung einer einzelnen Zelle ca. 10^{-18} Watt, was einem Verbrauch von ca. 2500 Molekülen ATP/s bei 10 k_BT/ATP pro Molekül entspricht.

Despite their biological complexity, animals, living tissues and cells, the smallest unit of live, are subjected to physical principles. In living tissues, permanent or transient regulation processes, such as biochemical and mechanical interactions between a single cell and its environment are essential to develop tissue structure and function. These interactions play a major role in biological processes such as differentiation and gene expression of cells. In contrast, metastatic cancer cells escape such regulations. These cells proliferate and migrate through tissues unregulated, ignoring input from environment. Their mechanical and adhesion properties are drastically different than those of non-tumour cells.

The presented studies describe experiments which mimic conditions in vivo by applying uniaxial stress to a single living cell under physiological conditions. Simultaneously, applied force, cell deformation and cellular shape are determined with highest accuracy. Uniaxial deformation is applied to a single cell which adheres between two parallel glass plates. Such mechanical assays accomplished at constant displacement or constant force allow for quantifying cellular viscoelastic properties and for describing the data by using linear force relations or the Kelvin model. Biolipids such as sphingosylphosphorylcholine and lysophosphatidic acid modulated the cytoskeleton architecture which showed to cause fatal consequences for mechanical properties of rat embryonic fibroblasts and human pancreatic cancer cells. Cellular stiffening or softening, power generation and energy consumption upon cellular contraction of a single cell are quantitatively measured. For example, the contraction power of a single cell was measured to be ca. 10^{-18} Watt which corresponds to approximately 2500 molecules of ATP/s at 10 k_BT/ATP per molecule.

Bien que grandement complexes, les animaux, les tissus vivants et les cellules, la plus petite unité de vie, sont assujettis aux lois de la physique. Dans les tissus vivants, des processus de régulation permanents ou transitoires, tels que des interactions biochimiques et mécaniques entre une cellule isolée et son environnement, sont essentiel au développement et au maintient de la structure et des fonctions du tissu. Ces interactions interviennent dans des processus biologiques tel que la différentiation cellulaire et l'expression génétique. Les cellules cancéreuses et les métastases échappent au contraire à toutes régulations. Elles prolifèrent et migrent à travers les tissus, ignorant les signaux de régulation environnant. Leurs propriétés mécaniques et d'adhésion sont très différentes de celles des cellules saines.

L'étude suivante présente différentes expériences qui cherchent à mimer les conditions in vivo en appliquant un stress uniaxial à une cellule isolée sous conditions physiologiques. Simultanément, la force appliquée à la cellule, sa déformation et sa forme sont mesurée. La déformation uniaxiale est appliquée à une cellule isolée adhérant sur deux plaques de verre. De tel essais mécaniques réalisés à constante déformation ou à constante force permettent la quantification des propriétés mécaniques cellulaire et une description physique des données par le modèle de Kelvin. Des lipides bioactifs tel que la sphingosylphosphorylcholine et l'acide lysophosphatidique, modifient l'architecture du cytosquelette. Ces modifications influencent fortement les propriétés mécaniques des fibroblastes ou les cellules cancéreuses du pancréas. Durcissement ou ramollissement, génération de force, consommation d'énergie leur de la contraction cellulaire ont été mesurés quantitativement. Par exemple, l'énergie de contraction d'une cellule a été mesurée à approximativement 10^{-18} W ce qui correspond à approximativement 2500 molécules d'ATP/s considérant 10 k_BT/ATP par molécule.

à mon père,

Table of Contents

1 Introduction

A living cell is essentially a compartment, the basic structural and functional unit of all organisms. Cells may also exist as independent units of life e.g., yeast, bacteria, amoeba, etc. Cells may cluster to form colonies or assemblies of cells. For example, the amoeba, scientifically known as *dictyostelium discoideum*, is a model system in biology to study cell assembly and morphogenesis. Embryo, tissues and organs, *i.e.* assemblies of eukaryotic cells, are even more complex because they are composed of cells, which assume different structure and functions. Each cell in such an assembly receives signals from multiple pathways. These signals, persistent or transitory, define and regulate the biophysical state of a cell, as well as cell differentiation and growth at a defined location of the assembly. In response, the cell adjusts or strongly modifies its structure and consequently its functions. These signals are regulate by the genetic program, as well as by the cell neighbourhood and the necessity to physiological adaptation of the whole body to its environment. Signals may be in the form of mechanical interactions with neighbouring cells, extracellular ligands which modulate cell adhesion and shape, as well as biochemical molecules or proteins (such as bioactive lipids, growth factors, hormones…) present in the cell's environment. However, in many cases, the most prominent signal arises from mechanical interactions (Janmey, P. 1998) e.g., sense of hearing and touch are initiated by such interactions. The functional 'tool' which cells employ in order to sense and generate mechanical forces, is the cytoskeleton, which is basically composed of protein polymers. The cytoskeleton spreads through the cell body between the nucleus and the cell membrane, and is responsible for mechanical sensing and force generation (Ballestrem C. 2004; Choquet, D. 1997; Thoumine, O. and A. Ott 1997).
It may happen that a signal path is damaged, due to an inappropriate protein mutation in receptor-proteins or in signal-carriers. This is typically the case in cancer, whereby, transformed cells escape to proliferation regulation. This control deficiency results in local disordered proliferation leading to the formation of a tumour, an abnormal tissue without any functions and which grows independently. It disorganises the normal tissue and disrupts its functions because the tumour consumes energy and requires space for its room for growth and enlargement. In healthy tissue as well as in abnormal tissue, the structure-property-function connection plays in most cases, a key role in understanding of the control mechanisms of cell assembly (Fuchs, E. 1998). Organisms, organs and cells are complex systems because they can be influenced by various physical and biological parameters, which are however sometimes unknown. A subtle parameter is the history of the considered system. Cell and tissue characteristics are strongly dependent on their history. Hence, before conducting measurements, cell culture as well as cell/tissue preparation must proceed with great care. Despite the structural complexity and difficulty to set parameters, cells and tissues are objects of interest for the physics of mechanical forces such as shear, tensile and compressive forces. The first step for the study of cells/tissues is via observation of the system in order to determine its morphological and internal structure. The physical properties of the system are then characterised and usually present strong correlations to its internal structure. Finally, taking the biological information into account, one determines the cell functions through the understanding of its properties. Such a study not only permits the understanding of the normal function of the system, but also enables the prediction of physical changes related to

physiological adaptation or resulting from external factors such as infection or disease. Eventually methods could be proposed to re-establish normal functions.
Blood circulation, force balance in the skeleton, force-generation in muscles and the viscoelastic properties of the lungs are amongst the first subjects of interest in biomechanics. However, the understanding of single cell mechanics is the most attractive research area in this field. The coupling between diseases and structure is fascinating and the focus of an intensive research, e.g. for skin disorders, malaria infection in red blood cells, cancer of the pancreas, etc (Fuchs, E. 1998; Kemkemer, R. 2002; Russel, D. 2004; Lim, C.T. 2004; Micoulet, A. 2003; Suresh, S. 2005). Several developments in physics provide tools and techniques for the manipulation of single living cells. They can be fruitfully used to measure mechanical properties of the cells e.g., optical and magnetic tweezers, micro- and nano-designed cell-adhesion surfaces, etc (Arnold, M. 2004, Balaban, N.Q. 2001, Lehnert, D. 2004, J. L. Tan, 2003; Zatloukal, K. 2004). These techniques enable the probing of cell's elasticity or viscoelasticity either locally (meaning at a sub-cellular scale) or globally i.e. the entire cell is probed. Depending on the technique, cells may or may not be allowed to adhere to a surface.

1.1 Cells in Tissues

In order to evaluate the complexity of tissue architecture and the role played by mechanics in the stability of this living structure, we focus on three examples of tissues: the pancreas, the connective tissues and in more details, a particular connective tissue, the periodontal ligament (PDL).

1.1.1 The Pancreas

In the human body, the pancreas is a secretory gland situated transversely across the posterior wall of the abdomen. A duct, called "pancreatic duct" extends through the pancreas. "It commences by the junction of the small ducts of the lobules situated in the tail of the pancreas, and, running from right to left through the body, it constantly receives the ducts of the various lobules composing the gland. Considerably augmented in size, it reaches the neck and turning obliquely downwards, backwards and to the right, it comes into relation with the common bile duct, lying to its left side; leaving the head of the gland it passes very obliquely through the mucous and muscular coats of the duodenum, and terminates by an orifice common to it. […] Each lobule consists of one of the ultimate ramifications of the main duct, terminating in a number of alveoli which are tubular." (Gray, H., 1995, pp. 929-932).

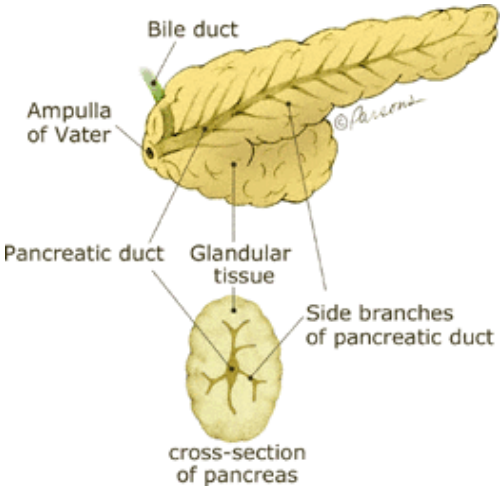

Figure 1: Schematic of the pancreas
up, 3D schematic of the pancreas. down, schematic of pancreas cross-section

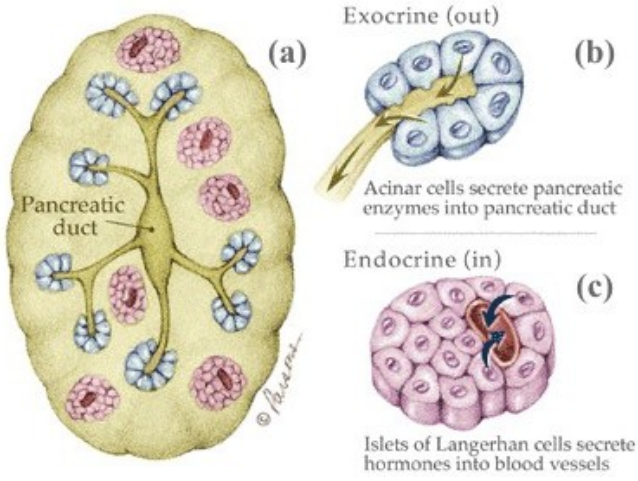

Figure 2: Schematic of the pancreas internal structure
(a) schematic of pancreas cross-section. (b) acinar cells organized in alveolus, (c) schematic of an islets of Langerhan. (John Hopkins University, Pathology dept., web site)

The alveoli compose the buck exocrine glandular tissue. The acinar cells (Figure 2, hell blue) form the wall of the alveoli. These cells produce the pancreatic fluid, which is then collected in the pancreatic duct and flows into the small intestine. The pancreatic fluid contains sodium bicarbonate ($NaHCO_3$), which neutralizes, in the small intestine, the acidity of the fluid arriving from the stomach. It contains also enzymes, such as amylase, lipase, trypsin, which take part to the hydrolysis of respectively starches (a kind of polysaccharide), fatty acids and proteins. There are two other kinds of cells in the pancreas: the duct cells, which compose the epithelium of the duct and, scattered through the acinar tissue, several hundred thousand clusters of cells, called islets of Langerhans. These islets represent 2.5-3.0 % of the pancreas weight (European Pancreas Centre, web site). These islets are an endocrine tissue. Cells aggregated in those islets produce hormones, the insulin and glucagons. These hormones, collected by webbed blood capillaries, are released in the splenic and superior mesenteric

veins (ending to the liver). The secretory functions of the pancreas are very important for the body, because the secretions are involved in the digestion and the control of glucose content in the blood. For cells, the glucose is the most important sugar. Cells produce their energy by degradation of the glucose (glycolysis).

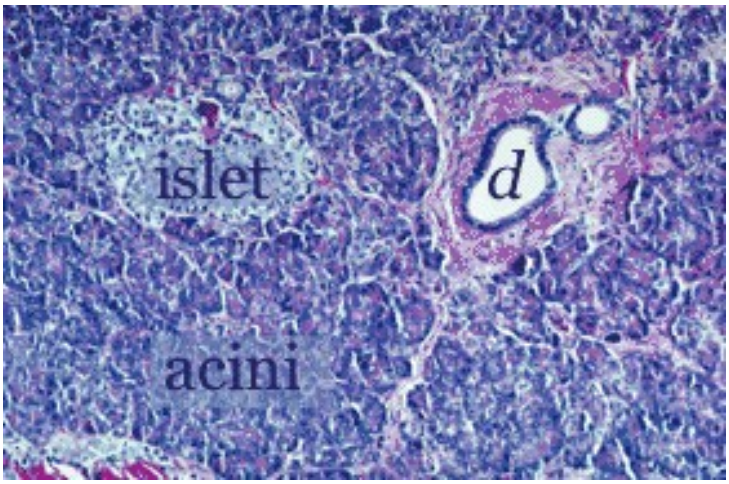

Figure 3: Pancreas histological section.
Three kinds of pancreatic cell assemblies are clearly visible: islets, acini and duct.
(John Hopkins University, Pathology dept., web site)

The pancreas is an assembly of the epithelial cells (islet cells, acinar cells, duct cells) but also endothelial cells (cells building the walls of blood vessel) and finally blood cells. The functions of these cells together determine the organ functions. As it was mentioned earlier, cell functions depend on cell structure and the structure itself depends on the interaction of the cell with its environment. Consequently, organ functions depend indirectly on single cell communication and structure. This point will be illustrated with more detailed examples in chapter 4. As each organ of the body, the pancreas is enveloped in a protective tissue, called areolar tissue or loose connective tissue.

1.1.2 Connective Tissues

Connective tissues (CTs) are one of the four tissue categories present in mammalians, besides epithelial, muscular and neuronal tissue. The pancreas is an example of epithelial tissue. CTs are composed of cells and of a matrix, called extra-cellular matrix (ECM). The ECM is itself composed of organised and non-organised substances, respectively: fibres and amorphous ground substances. Depending on the contents of cells and ECM in the CT, and also on the degree of ECM organization, properties and functions of CTs are modulated. This generates a specialisation of the CTs, a wide variety of mechanical properties and ability to undergo turnovers. In order to point out the CT diversity, several CTs could be mentioned: the blood, the bones, the sinews, the cornea, the dermis... The three main categories are: embryonic CT, CT proper and specialized CT.
The functions of CTs are: transport, immunological defense, mechanical support and protection, tissue repair, energy storage, heat generation and blood cell formation. The transport of nutriments and metabolites through the body is mainly achieved by the blood vessels, but not all the cells are located against capillaries. The water stored in the ground substance provides a final pathway by diffusion between cells and the blood circulation system. The adipose CT stores fat (energy), provides thermal insulation and eventually generates heat. CTs provide a safety barrier against infections: in the ECM, specialised cells such as mast cells, macrophages, white blood cells (lymphocytes, neutrophils…) react to infection and organise the destruction of invading micro-organisms in the inflamed tissue.

	embryonic CT	
	mesenchyme	mucous CT
resident cells	mesenchymal cells (undifferentiated)	stellate fibroblasts
immigrant cells	-	-
fibres	lacking	collagen fibres type I in small quantities
network	via cellular branching wide intercellular spaces	via cellular branching wide intercellular spaces
properties	plastic	
ground substances	large quantities, a lot of water	large quantities, a lot of water
function	embryonal and fetal development	
localisation	embryo	placenta fetalis, umbilical cord, dental pulpa

	CT proper			
	reticular CT	loose CT	dense CT	
			irregular	regular
resident cells	fibroblastic, reticular cells	fibroblasts, mast cells, macrophages	fibrocytes	fibrocytes
immigrant cells	lymphocytes	lymphocytes, neutrophils	lymphocytes	
fibres	fine collagen type III fibres	collagen type I fibres	abundant, type-I collagen fibres bundles	abundant, type-I collagen fibres bundles
network	composed of reticular cells and collagen fibres	random	random	parallel alignment
properties	flexible, non elastic	plastic	elastic	elastic
ground substances	abundant	abundant, high quantities of proteoglycans	minimum	minimum
function	to ensheath organs, protection, transport	to pat space between tissues, protection	to connect	to sustain tension
localisation	stroma	support for blood and lymph vessels and nerves to ensheath muscles beneath the skin	dermis sclera	tendon ligament

	specialised CT			
	cartilage	bone	blood	adipose
resident cells	chondrocytes	osteoblasts, osteoclasts	lymphocytes, neutrophils, hematocrits	adipocytes
immigrant cells				
fibres			lacking	fine collagen type III fibres
network				random
properties				
ground substances				a few
function	support	support		storage protection
localisation				

Table 1: List of the different kind of CTs.
This table contains the different kind of CTs, their components, properties, functions and location in the body.

After inflammation or if a wound occurs, the ECM has to be regenerated and reorganized in order to recover suitable functions. Fibroblasts and fibrocytes produce and secret new materials: jelly-like ground substance and building-units for ECM fibres, such as collagens,

elastin and adhesion protein, such as fibronectin (FN), vitronectin, laminin. Collagens assemble in 100-500 nm diameter fibres. These fibres aggregate in parallel to form collagen bundles, whose diameter is 1-10 µm. Collagen bundles are randomly distributed in the dermis, but well aligned in the direction of the applied force in tendons. The jelly-like ground substances contain high quantities of proteoglycans (hyaluronic acid), which provide a lubricant-like viscosity, a high elasticity, resistance against pressure and a good absorbency for water the CTs. Large quantities of ground substances are favourable to metabolism. The ECM fibres give mechanical properties to CTs. These properties allow CTs to fulfil the following mechanical functions: to pad spaces between tissues, to support and to anchor tissue, to connect and to bind tissues together or oppositely to separate them from each other. For example, bones hold obviously a supporting function; tendons, elastic CT, connect bones to muscles.
Depending on their function and also contingently on other new external parameters such as infection, wounds, mass to support, forces to balance, CTs develop and adapt. For example, a bone can grow or resorb with respect to the physical activity of the patient or resorb under micro-gravity conditions. In order to balance a new persistent force on the skeleton, the bone bends following the Wolff's law on the bone-apposition. Like bones, the other CTs are currently subjected to turnovers, but more or less consequent. As an example, the periodontal ligament is well known to achieve active turnovers, allowing tooth movement as big as several millimetres in several months.

1.1.3 The Periodontal Ligament

The periodontal ligament (PDL) is a dense CT. Because of the importance of this tissue in orthodontic treatment, its response to stress has been studied. Controlled forces applied to teeth induce stress in this tissue. Stress and strain are distributed between fibres of the ECM and cells.

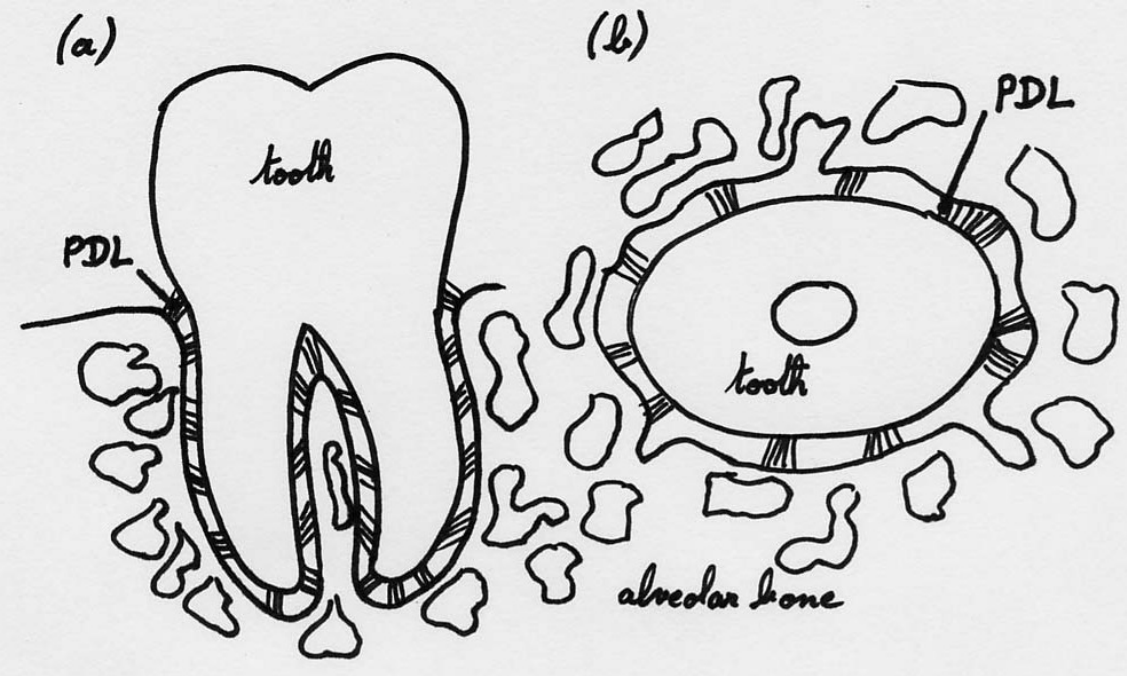

Figure 4: Schematic cross-sections of a tooth.
(a) vertical and (b) horizontal cross-section of a tooth. The alveolar bone is around the tooth. It is composed of bone and marrow. The periodontal ligament (PDL) fibres show a radial orientation to the centre of the root.

The PDL is localized around the roots of teeth between the alveolar bone and the teeth (Figure 4). Its function is to connect teeth to the alveolar bone of the jaw. The PDL is present as a layer covering the whole cavity receiving a tooth. The thickness of this layer is ~ 250 µm in rats or less in human. Fibroblasts, osteoblasts, osteoclasts and collagen fibres bundles constitute chiefly the PDL. Figure 4 shows the radial alignment of the PDL-filament bundles to the tooth axis. The PDL undergoes forces during the mastication. In order to perform the balance of force and the tooth stability, PDL-filament bundles located along the tooth sides make oblique angles with the tooth axis and connect the tooth to the alveolar bone (Figure 7). The variation of angles between bundles is designed in such a way that the tooth is brought back to the same position, when the tooth is slightly pushed or pulled.
Osteoblasts produce the collagenous matrix, which will be calcified to become bone (alveolar bone). Osteoclasts are giant cells, which destroy bone by local release of protons. Loose CT is also present between the collagen fibres to support blood capillaries and nerves.
The mechanical properties of the PDL have been measured on samples taken from the mandibles of adult pigs (Dorow, C. 2003). Mandibles were cut into segments, each containing one complete anterior tooth. A rotating saw was then used to cut the segments into slices perpendicular to the longitudinal axis of the tooth. The cuboid samples contained a bone part, a root part and the PDL part between them (Figure 7). Such samples were used for the mechanical assays. The stress-strain relationship is similar to dense CTs such as tendons. As the ligament is loaded at constant strain rate, the stress increases first exponentially (in Figure 5, from O to A). Second, the PDL is in a linear regime (from A to B). Finally, after a short non-linear regime, the PDL ruptures. The stress reaches the maximal value of 3.75 MPa. As a comparison, the ultimate stress from human tendon is in the range 50-100 MPa (Fung, Y.C. 1993, p. 260). The physiological regime, in which the tissue usually functions, is the first exponential regime.

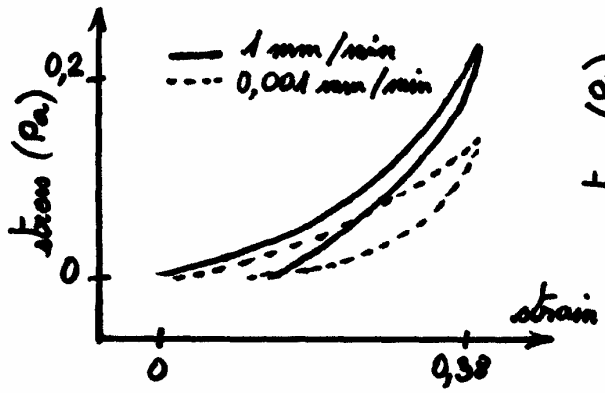

Figure 5: PDL stress-strain relationship in physiological range.
Adapted from Dorow and al. (Dorow, C. 2003).

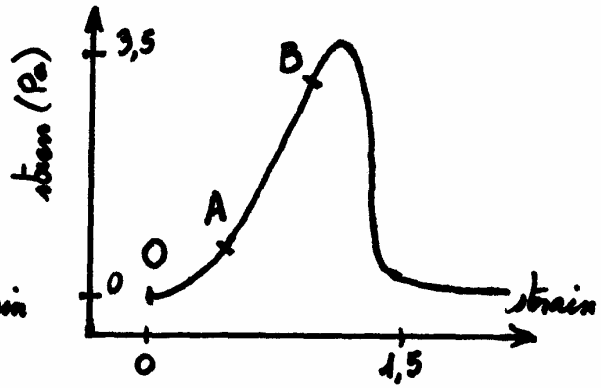

Figure 6: PDL stress-strain relationship until rupture.
Adapted from Dorow and al. (Dorow, C. 2003).

The PDL and particularly PDL fibroblasts are chronically exposed to high levels of physical force. In the PDL, turnovers are much higher than in most other CTs. The main reason is the high stress present in this tissue (Graber, T.M. 1994). The stress has two origins: functional stress (mastication, tong movement) and adaptational (movement of teeth during the growth of the jaw bone, or during orthodontic treatments). The application of a persistent or intermittent force to a tooth induces its movement. Occurring turnovers are not limited to the PDL. Progressively, the bone resorbs where a pressure is applied and new bone is formed where a tension is applied. In the case of orthodontic movement, in human, a tooth can typically move of 1 mm over 15 days! In rats, cells migrate in association with the bone

apposition incident to orthodontic tooth movement. New osteoblasts appear (because of activation of proliferation) in response to necessity of bone production. They derive solely from the proliferation of local precursor cells (Roberts, W.E. 1981). In contrast, osteoclast precursors are suspected to be recruited in the bone resorbtion region through chemotaxis. If an alveolar bone space is filled with fatty cells and undergoes pressure from a tooth in movement, the adipose CT becomes progressively loose CT, before entering in contact with the tooth. Consequently, the PDL at the resorbtion side is always in contact with either bone or bone marrow, loose CT.

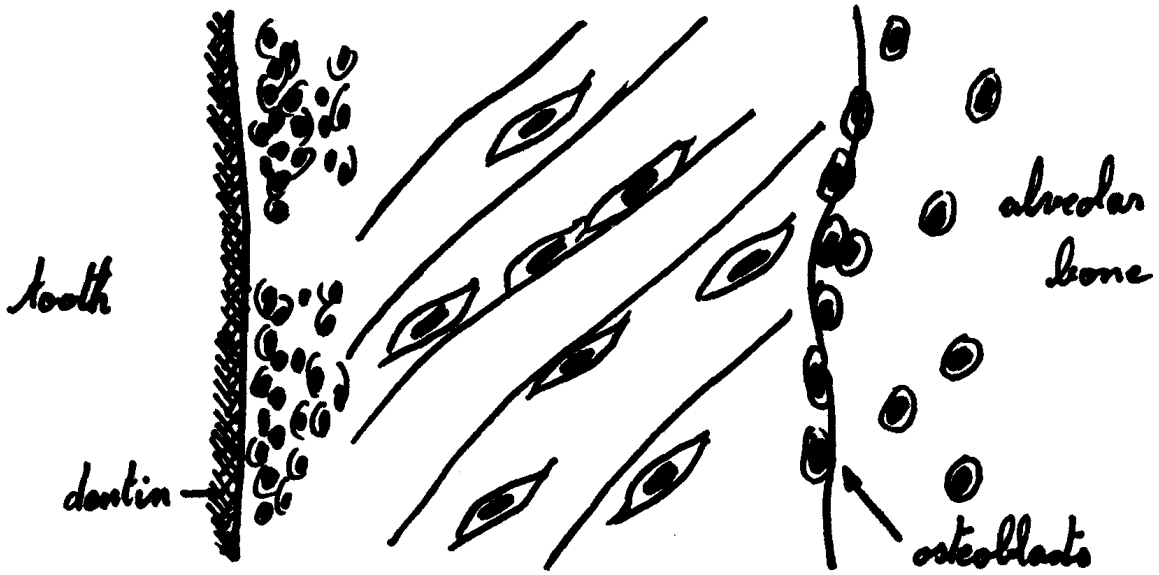

Figure 7: Schematic representation of the PDL
A cross-section parallel containing the tooth axis is represented. Cell nuclei appears as black points. Alveolar bone appears as a vertical band (right); Osteoblasts form a layer on the bone surface and some of them are embedded in the bone. The dentine of the tooth appears as a vertical band (left); the juxtaposed darker vertical band is calcified cementum; cementoblasts are accumulated on it. The space in between is the PDL; it is composed of fibroblasts spread along collagen bundles connecting tooth and bone.

How is the mechanical stimulus converted in such synchronized events? A first consideration is that a force cannot always induce turnover and adaptation of the PDL. The tooth movement can be blocked, even if the force is still applied. It happens, when the initial stress is too high: the PDL undergoes local necrosis and no turnover anymore can occur. To continue the orthodontic treatment, the PDL has first to recover. The mechanical signal has to be adapted to the turnover time-constant and force range of the PDL. If the limits of the mechanical signal conversion are known, the mechanism itself is so far not well understood. Nevertheless, two mechanisms are traditionally considered as to be involved: the pressure-tension theory and a second theory, which considers bioelectric phenomena. First, a force applied induces disorder in the PDL: at the compression site blood capillaries can be destroyed and cell depletion can be observed, leading to a mild inflammatory reaction. Local secretions of signalling molecules, such as prostaglandin, are present in stressed regions. The stress applied to cell membrane is known to control the opening of ion channels (Glogauer, M. 1997) and thus influence the intracellular second messenger cAMP, which can act as a chemo-attractant. Second, bioelectric phenomena might be involved (Roberts, W.E. 1981). Beside these two mechanisms involving the transduction to biochemical reactions of the mechanical signals, the direct mechanical response of a single cell in correlation with the sensed mechanical signal is part of the turnover. This response has two levels: first, the intracellular structure of the cell is adapted and second, the cell can generate an extra-cellular mechanical signal to

control the assembly reorganisation. *In vitro* studies on cultured periodontal fibroblasts show that the filamin A confers mechano-protection to stressed cells (Kainulein, T. 2002). The behaviour of periodontal fibroblast is clearly dependent on mechanical tension in the matrix. Actin polymerisation and stress fibre formation in response to mechanical stress occur in gingival fibroblasts, but not in PDL fibroblasts (Pender, N. 1991). The culture of PDL fibroblasts in an artificial collagen matrix shows, that mechanical tension seems to prevent degradation of the matrix. In contrast, relaxation of the tension enhances the resorptive activity. The sensitivity of PDL cells to mechanical tension may be essential for the remodelling of PDL and their adaptation to physiological and orthodontic forces (Von den Hoff, J.W. 2003).
The high activity of stressed PDL that has been briefly described here, shows the ability of cells to sense forces in tissues. The response depends strongly on tissue intrinsic parameters, such as the kind of cell present in the tissue and the ECM structure surrounding cells. In this example well controlled tissue turnovers, it occurs that turnovers are completely disorganised. The result is a tumour.

1.1.4 An Example of Assembly Disorder: Cancer of Pancreas

As it is displayed in pancreas or in PDL, external signals (mechanical or bio-chemical) are very important in eucaryotic cell assemblies. The function and the proliferation of cells in assemblies are controlled. Cells which can escape to the assembly regulation mechanisms develop cancerous tumours. Most of the primary tumour originates from a single abnormal cell. In a lifetime, in any human individual being, 10^{10} separate occasions of DNA mutation occur (Alberts, B. 2002, p. 1317), but a single mutation is not enough to lead to the development of cancer: the resulting tumour is benign. Cancerous growth often depends on defective control of cell death or cell differentiation due to mutations. A stem cell division produces normally a new stem cell and a daughter cell. Daughter-cells proliferate a finite number of times and differentiate. If the stem cell fails to produce a daughter cell, a tumour of stem cells occurs. If the daughter cells cannot differentiate, a tumour of daughter cells occurs.
Isolated in culture, cancer cells often behave as ‘immortalised’. For example, cells from human cancer cell line named Panc-1 originated from a human pancreatic duct carcinoma (Lieber, M., 1975). The development of cancer requires mutations in many genes and appears to be the result of a subtle equilibrium. If a cell, which is the origin of the benign tumour, presents a genetic instability, more tumour-cells accumulate mutations faster and some of them can develop dangerously outgrowing the neighbouring cells of the benign tumour and the normal tissue. A malignant tumour enlarges rapidly. These cells adapt to the physiological conditions in tumour, meaning lack of oxygen, of nutriments, rate of apoptosis increase. In contrast, if the genetic instability is too high, cells fail to adapt and just die. The tumour does not develop further.

Figure 8: Pancreatic-duct representation.
Morphology of the duct in different typical cancer evolutions. (European Pancreas Centre, Heidelberg, Germany, web site)

Figure 8 presents the different evolution of cancer occurring in the simple epithelium of the pancreatic duct. The disordered growth of cells disturbs the structure and then the functionality of the pancreatic duct. The capillaries structure is lost. As a consequence, the duct function of collecting secreted fluid is not achieved anymore. Proliferating on their own, cancerous cells may not keep contact with the normal duct leading to a cut or a shrinking of the duct. A possible development of the malignant tumour (called primary tumour) is the metastasis. It is the less understood aspect of cancer. Tumour cells become metastases, when they acquire the ability to move in tissues. Cells break away from the primary tumour; they invade normal tissues, blood and lymphatic vessels. Using fluid circulation or migrating through tissues, metastases settle in other part of the body and new tumours (called secondary tumours) develop. Cancers originate mainly in epithelial tissue, because these tissues are more exposed to mutations than others tissues. An epithelium is a layer of cells closely packed and adhering strongly together due to building of tight junctions. Often cancerous cells keep characteristics of normal tissue cells. For example, cells from an epidermal basal-cell carcinoma, derived from keratocyte stem cell in the skin, will generally continue to synthesize in culture a keratin network as normal cells. How these cells, having the ability to bind strongly to each other, can suddenly detached and migrate? It is known that it can happen through mutations, but the mechanisms in cellular assembly are not known in details. Definitively, two modifications have to be preformed. From one hand, the adhesion properties have to change in order to allow the release of cells from the tumour and after an efficient binging to the ECM (Hood, J.D. 2002). From the other hand, the mechanical properties of cells have to be modified to enable movement. Metastatic cells invade other tissues, migrate through CTs and spread in the body through the blood circulation. Consequently, metastases have to adapt to a different environment: initially to a tumour poor in nutriment and then to the dense ECM of the CTs or oppositely to the reduced adhesion in blood. Metastases experience various adhesions: cell-cell contacts in the tumour and at the contact with blood vessels, cell-ECM contacts in the CTs. They undergo various forces: compression in the tumour, stretching in CTs, and shearing force in blood. One could summarise these changes by the following picture: metastases are like an epithelial cell, which displays fibroblast-like and neutrophil-like mechanical properties. Consequently, metastases have to display various mechanical properties. The cytoskeleton is the part of a cell, which performs and structurally supports the cell's mechanical properties and functions. In metastases, structural modulations of the cytoskeleton give them unexpected mechanical properties.
The cytoskeleton is composed of protein-polymers. Their versatile assembly is regulated by the cell in adaptation with its environment.

1.2 The Cytoskeleton

The cytoskeleton components are protein-polymers and associated proteins: motor-proteins and proteins behaving as cross-linker. The cytoskeleton is connected with the plasma membrane, the nucleus and various organelles. The polymerisation and assembly of these filaments cost energy. The cytoskeletal has multiple functions, as it organises the transport in the cell, participates to cell division and generates forces for the maintenance of the cell shape and is responsible for the mechanical sensitivity of the cell to its environment.

1.2.1 Cytoskeletal Filaments

Three kinds of protein-polymers compose the cytoskeleton: the actin filaments, the microtubules (MTs) and the intermediate filaments (IFs). Their structures are different, conferring them different properties. Only actin filaments and MTs will be described in this section. IFs will be only cited. Their detailed description will be presented in chapter 4.

Protein-Polymer Structures

The protein actin (42 kDa) polymerises simultaneously in two strands forming a coil. Actin filaments are polar. Their diameter is ~ 8 nm and their period is 37 nm (Moore, P.B 1970). MTs are heteropolymers. Heterodimers (110 kDa) of α-tubulin and β-tubulin form and are polymerised in a tube-like structure composed of 13 juxtaposed linear protofilaments. This structure of ~ 25 nm diameter is polar (Chrétien, D. 1996). IFs are rope-like filaments of ~ 10 nm diameter (Strelkov, S.V. 2003). They lack polarity. Monomers (40-180 kDa) forming the IFs constitute a very large protein-family. Vimentin and keratin proteins are two examples. If a large majority of cell express actin filaments and MTs, the expression of IFs is, in contrast, strongly cell-type dependent.

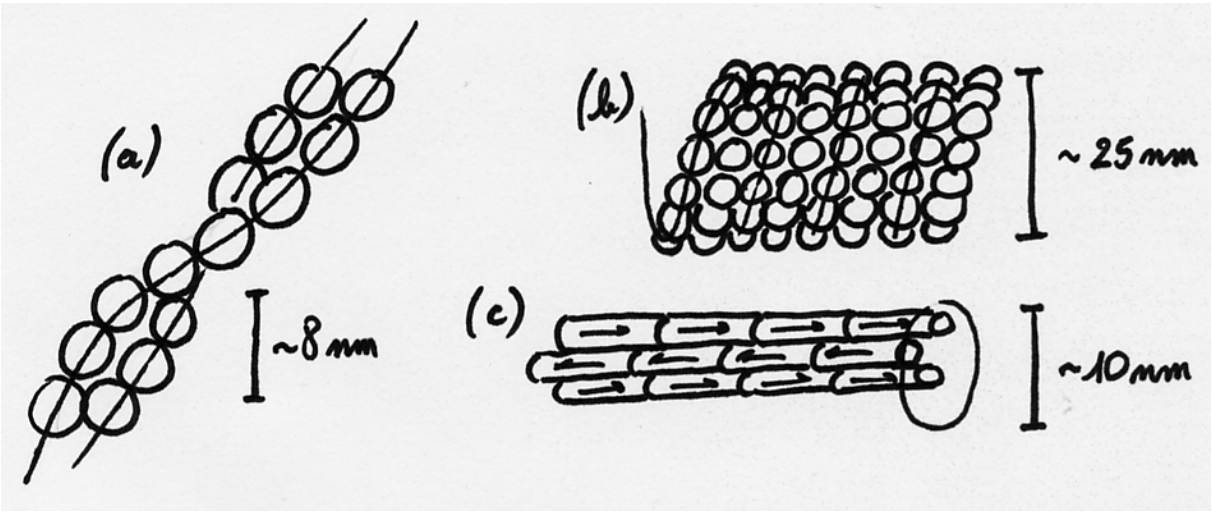

Figure 9: Schematics of protein-polymers of the cytoskeleton.
(a) actin filament, (b) microtubule and (c) intermediate filaments

Protein Polymerisation

The polymerisation of the protein-filaments (actin filaments, MTs and IFs) is a physical-chemical process that depends on several parameters *in vitro*. In a cell, this

polymerisation is not only a physical-chemical phenomenon because the regulatory mechanism of polymerisation occurs. This mechanism involves in fact filament-associated proteins, which modulate the polymerisation and assembly by binding to filaments or monomers (Pollard, T.D. 2001). The phosphorylation of monomers is also a way to control filament formation (Chang, L. 2004).

In vitro, the polymerisation of actin monomers can be induced in presence of ATP by increase in ionic strength (addition of KCl, $MgCl_2$, $CaCl_2$). The polymer concentration reaches steadily a plateau value at which the monomer concentration is about 0.2 µM (critical concentration). For instance, for a monomer concentration of 24 µM, it takes ~ 1 min to reach 95% of the steady-state polymer concentration (Xu, J. 1998). If the monomer concentration of the polymerised solution is increased, the filaments will grow further. Actin filaments can be as long as several µm and are polar. It implies that their both ends are not equivalent. These ends are named: barbed end and pointed end. Interestingly the critical concentration of pointed ends equals 2 µM and, as mentioned previously, 0.2 µM for the barbed ends. It means that as the monomer concentration decreases below 2 µM, the pointed ends begin to shrink and the barded ends grow. Because the growth is faster than the shrinking, the polymerised solution rises an equilibrium in the range of 0.2-0.3 µM. The ATP-actin complex polymerises more efficiently than the ADP-actin complex. The hydrolysis (ATP to ADP) occurs at a slower rate than the monomer binding rate. It results that the filaments ends are made only with ATP-actin complexes, which bind stronger than ADP-actin complexes. ATP catalyses and stabilises the polymerisation.
The actin polymerisation requires energy: only the complex ATP-actin monomers are able to polymerise. Beside the dependence on ATP and actin concentrations, *in vivo,* the polymerisation is also subject to control by actin-associate proteins, small proteins (14-15 kDa) such as profilin, cofilin and thymosin bind ATP-actin or ADP-actin and regulate the polymerisation.

MTs polymerise in a similar way to actin filaments. It has to be remarked that MTs are instable in presence of Ca^{2+} at a concentration above 10 µM. In contrast to actin filament, they present dynamic instabilities, i.e. they alternate phase of growth and phase of shrinkage.

IFs polymerisation, which is also a self-assembly process, will be explained in details in the introduction to chapter 4.

Protein-Polymer Mechanical Properties

Because of their linear molecular structure, single protein-filaments can be described as rods and ropes (Boal, D. 2002). The persistence length L_P characterises the spatial configuration of a filament at a defined temperature T, i.e. if the filament looks like a rod or a coil. The persistence length is the quotient of the bending modulus (in units [J.m]) to k_BT. It equals 10-20 µm for actin filaments and 1-6 mm for MTs.

1.2.2 Assembly of Protein-Filaments

Protein-Polymer Networks

In cells, the actin-filament assembly are various (Revenu, C. 2004). Without going in details, several examples will be cited. Microvilli in intestinal cells, stereocilia of inner-ear cells and filopodia in fibroblasts, are based on actin bundles. Filamin, fimbrin and α-actinin are involved in bundle formation. Lamellipodia are based on branched actin-filaments. The protein complex Arp2/3 binds to actin filaments and induces from the binding site the

nucleation of a new actin filament making an angle of 70 degrees with the old filament (Figure 10) (Svitkina, T.M. 1999). Profilin and cofilin bind actin monomers, capping-proteins stabilise actin-filaments and thus, they modulate the dependence of the actin polymerisation on actin-monomer and ATP concentration.
Myosins bind also actin-filaments and connect them. The actomyosin complex will be detailed in the section 1.2.3.

MTs are oriented from the nucleus to the cell membrane. They do not form meshwork in cell.

Mechanical Properties

Rheological studies have been conducted for example on purified actin-filaments, keratin- and vimentin-filaments assembly. Keratin and vimentin are presented in Chapter 4.
After polymerisation, gelation occurs. The elasticity of a pure actin-filament solution reaches a steady-state only after 8-10 hours. The loss modulus slightly dominates at the earliest times of the network formation, the elastic modulus dominates at long times. From liquid-like at the early stage, the actin network is solid-like at steady-state. The frequency-dependent viscous moduli, $G'(\omega)$ and $G''(\omega)$, demonstrate that 24 μM actin-filament solution are viscoelastic solids ($G' > G''$) at $\omega <$ 80-100 rad.s^{-1} and viscoelastic liquid ($G' < G''$) at $\omega >$ 80-100 rad.s^{-1} range in which the phase shift reaches ~ 67.5 degrees (Xu, J. 1998).

The addition of cross-linkers, for instance α-actinin, in the in the actin filament solution changes the mechanical properties of the gel (Xu, J. 2000). α-actinin localises in cell along the contractile stress fibres. Rheological shearing assays demonstrate that gel hardening occurs due to reduced motion of filaments at low strain (< 1%). Furthermore, α-actinin enhances the strain hardening, particularly at high rates of shear, but also allowed the gel to withstand larger deformation. The network ability to withstand deformations decreases with the solution temperature (coupling with the binding time of α-actinin to filaments) and the probed time scale.

1.2.3 Function of the Cytoskeleton

Force Generation by a Protein-Polymer

Protein-polymers generate a counter force if a force is applied on their tip along their axis or perpendicular to it. They bend immediately if the force is perpendicular. If the force is applied along the axis, they bend only when a critical force is attained. More interestingly protein-polymers are also able to generate a force by polymerisation. This force has the filament axis for direction. It can be generated without bending as long as the counter force is lower than the critical force of buckling. If the external force is greater than this critical value, the filament bends. For MTs, an elegant way to demonstrate this force generation is the following experiment conducted by Fygenson and al. (Fygenson, D.K. 1997). The polymerisation of MTs has been initiated in lipid vesicles. As the MTs grow, they deform the vesicle in which they are. The more deformed is the lipid membrane, the greater the membrane tension. As the resultant force of the membrane tension on MTs reaches the critical force, the MTs buckling is observed. It occurs at ~ 2 pN.

Force Generation by a Protein-Polymer Network

Cells generate forces for spreading and locomotion on a surface. The cell motility *in vitro* has been well studied. *In vivo*, besides the pathologic origin of the motility of metastatic cells, different kinds of cells present in the body are designed to be motile e.g., neutrophils,

keratocytes and fibroblasts. Cell motility is linked to the ability to adhere and to generate forces.
Neutrophils are white blood cells. They take part to the inflammatory response by their ability to phagocyte bacteria. Present in the blood as a spherical object of ~ 15 µm in diameter, neutrophils are stimulated by chemotactic factor produced in inflamed region. The stimulated neutrophils are able to enter the blood vessel wall, to invade tissues and achieve phagocytosis. All these processes require force-generation. The use of a detergent shows two states of actin in cells: soluble as monomer and insoluble as polymer (actin filaments). In stimulated neutrophils, the percentage of polymerized actin reaches 75% in comparison with 25% in non stimulated one. The content of myosin bound to actin increases slightly from 70% to 75% (White, J.R. 1983). This demonstrates the importance of actin filaments and myosin in locomotion. Myosins are a motor-protein which can move on actin filaments.

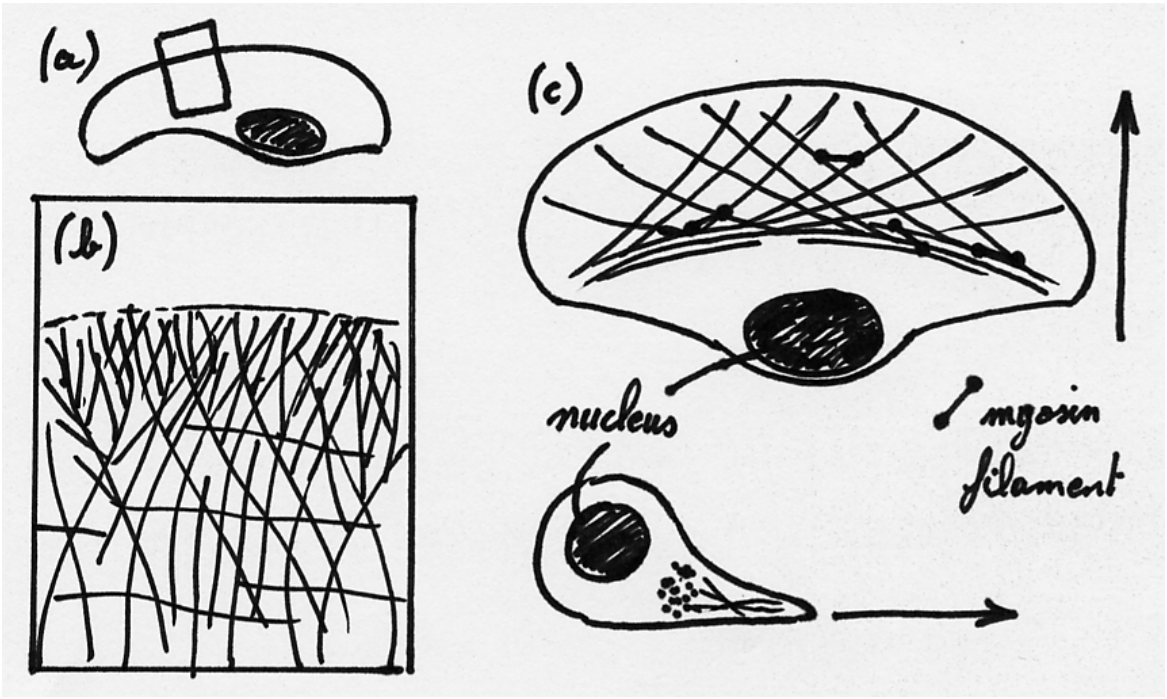

Figure 10: Organisation of actin filaments in keratocyte lamellipodium.
Representation inspired of electron-micrograph of detergent-extracted fish keratocyte. (a) Overview of a locomoting cell; (b) magnification of the leading edge (see frame in (a)). (c) Schematic of the dynamic network contraction model. Adapted from Svitkina et al. (Svitkina, T.M. 1997).

The crawling of a keratocyte *in vitro* is an interesting system to study the actin and actin-associated proteins assembly in cell (Svitkina, T.M. 1997). These cells form a very large lamellipodium extended in the direction of the movement (Figure 10, (a)). This lamellipodium is composed of meshwork of actin filaments cross-linked mainly by the protein-complex Arp2/3. In eukaryote cells, the polymerised actin is concentrated under the plasma membrane in a layer of 0.1-0.5 µm (actin filaments are typically ~ 0.5 µm long). This layer is named actin cortex. During keratocyte locomotion, the lamellipodium spreads on the surface in the direction of movement. The lamellipodium progresses under the pressure applied to the membrane border by the growing barbed ends of actin filaments. Densely branched the actin gel applies a constant force and homogeneously distributed, resulting in the directed progression of the lamellipodium. The motor-protein myosin II present in muscle cell is also present in the eukaryote cell cytoplasm. Myosin II is a dimer composed of two motor-heads and a tail. The movement of myosin along actin is the result of coupling of mechanical and chemical cycles. The low affinity of the ATP-myosin complex for actin filament induces the

separation of myosin from actin filament. The hydrolysis of the ATP by the myosin head results in a complex ADP-P-myosin, which binds actin filaments efficiently after a myosin-head conformation change. After binding to the actin filament, the phosphate ion is released inducing the opposite myosin conformation change, which produces a force acting through the working distance δ during the time τ_{on}. The myosin head is now again in the initial conformation. Depending on the myosin affinity for the ADP, it is released. The myosin stays bound to the actin filament, until a new ATP molecule binds to it. In the stochastic way, myosin can generate movement of actin filaments. Myosin II copies form bipolar filaments remembering the thick myosin II filaments of the muscle cells. *In vitro*, at low salt concentration, myosin tails interact to form octamers (Sinard, J.H. 1989). Myosin heads are concentrated at the ends of the bipolar filament in such a way that heads of one end are walking on actin filaments in opposite direction than the ones of the other end. Thus, when the heads are working, actin filaments are bring together in a bundle and translated along each others in a contraction movement. Myosin bipolar filaments have been observed in fish keratocyte (Svitkina, T.M. 1997) and in mouse 3T3 fibroblasts (Verkhovsky, A.B. 1993). The movement of keratocyte is explained by the dynamic network contraction model (Figure 10, (c)). The myosin bipolar filaments pull the actin filaments out of the actin filaments meshwork present in the lamellipodium and collect them in a contractile bundle orientated perpendicular to the movement direction close to the nucleus and the rear side of the keratocyte. In this region of the cell, actin filaments depolymerise.

In eucaryotic cells, both mechanisms are used to generate forces: the actin polymerisation and actomyosin as work producing units. Cells have the ability to activate or deactivate these mechanisms and control their location and their amplitude.

For physicists, it is very interesting to notice that these polymerising actin filament assemblies can be described by physical models, such as the thermal ratchet (Prost, J. 1994) or the motion of adhesive gel (Joanny, J.-F. 2004). The last model predicts that the motion results from a competition between a self-generated swelling gradient and the adhesion on the substrate. The resulting stress provokes the rupture of the adhesion points and allows for the motion. It may allow postulating that cells activate/deactivate robust physical phenomena in order to accomplish biological function, such as motility or maintaining cell shape. Taking in account the presence of dynamic cross-linker, the cytoskeleton (a network of cross-linked filaments) is expected to be able to resist rapid deformation but allow slow deformation in response to sustained force (Heidmann, S.R. 2004; Xu, J. 2000).

Adhesion

Only some main principles and processes of cell adhesion will be presented.

The cell builds protein-complexes in its plasma membrane in order to connect the cytoskeleton directly with the surface. Integrins, trans-membrane proteins, bind to ECM protein such as FN and in the cell to the protein-complexes. Various proteins are involved in these complexes. Depending on their maturation, which is coupled to the force applied to them, they are called focal adhesions (FAs)or focal complexes (FCs) (Zamir, E. 1999).

FCs are believed to be able the sense the stiffness of the ECM.

Sensing and Transmission of Mechanical Stress

The cell response to mechanical properties of the ECM has been examined by culturing cells on a collagen-coated polyacrylamide substrate. Thus, the flexibility of the substrate can be varied and simultaneously bio-chemical environment is maintained.

Compared with cells on rigid substrates, those on flexible substrates shows reduced spreading and increased rates of motility or lamellipodial activity. Microinjection of fluorescent vinculin indicated that FCs are irregularly shaped and highly dynamic on flexible substrates whereas those on rigid substrates display the expected morphology and are much more stable (Pelham, R.J. 1997). FCs are usually extended in the direction of stress. If the stress is increased, the FCs extend probably in order to maintain the balance of forces in the cell (Riveline, D. 2001).
Stretch-induced sub-cortical actin assembly is detectable within 30 seconds after stretch (Pender and McCulloch, 1991). A small increase in actin binding to beads in the FAs within 5 minutes after initiation of stretch is observed. It increases up to 30 minutes. The local increase of actin filaments provides structural stability to withstand increased physical stress. It also serves to shield cellular elements involved in mechano-transduction from the full effect of the physical stress.
The cytoskeleton couples the site at which the force applied to the cell membrane to the site of ultimate response, which can be an organelle or the nucleus. For example, a local force, coupled to the cytoskeleton by integrin binding and applied at many micrometers from the nucleus, induces its deformation and elongation in the direction of the pull (Maniotis A.J. 1997). Because the DNA structure and function can be affected by forces (Bensimon, D. 1996), it is likely possible that the cytoskeleton, chiefly the IFs cytoskeleton, mediates external mechanical signals. Such a signalling path could be involved in gene-expression control.
A model to explain measurement connects the force applied locally to the cell membrane and the intracellular calcium-ion content. It is hypothesised, that the local membrane deformation activates calcium-ion channels, which pump calcium ion from the cell medium into the cytosol. In response, actin filaments link at the force-application point and generate a counter force. The plasma membrane is less deformed and thus the channels are deactivated. In this case, the actin cytoskeleton behaves as a force sensor (Glogauer, M. 1997).
Recently, myo-tubes (assembly of muscle cells) have been subjected to cyclic uniaxial or multiaxial stretch. The multiaxial stretch was characterised by the specific phosphorylation (ribosomal S6 kinase, p70S6k), which was elicited by forces delivered through the elastic culture membrane. Specific types of mechanical stretch activate distinct signaling pathways. It may occur through direct mechano-sensory/transduction mechanisms and not through previously defined growth factor/receptor binding pathways (Hornberger, T.A. 2004).

The mechanical interaction of a cell with its environment and the adaptation of its internal structure in response appear to be relevant topics in order to understand better cells assemblies and their disfunctioning. How can be the cell mechanical properties measured?

1.3 Measurements of Cell Mechanical Behaviour

Single cell mechanics are important to understand the architecture and the function of a normal organ as well as to understand certain diseases. An approach developed in biology is to bring into being mammalians, such as mice, with specific deletions of genes. The result is that the protein assembly is perturbed because the expression of a target-protein is lacking. For example, the integrin β_1 can be deleted. Chondrocytes of integrin β_1-null mice have an abnormal shape and fail to arrange into the expected columns in the growth plate (Aszodi, A. 2003). Keratin-null mice (K8 (-/-), K18(-/-)) die at a rate of 50% at the embryonic state. The pancreas of surviving adults is (surprisingly) histologically normal, but the viability of cells is affected (Toivola, D.M. 2000). The human truncated keratin K14 gene has been expressed in transgenic mice. The skin of these mice exhibits blistering upon mild mechanical trauma indicating a modification of tissue function (Fuchs, E. 1998). The advantage of these experiments is that they are achieved in living animals. Another approach is to work with cell lines or primary culture (cell freshly extracted from a living tissue). Mechanical assays can be achieved on sparse assembly of cells or even on single cell. The disadvantage is that it is technically difficult to maintain experimental conditions, which are close to living conditions. The advantage is that the cell's structure dynamics can be observed and the measurements can be correlated with cell behaviour. The initial conditions and parameters, such as the presence and concentration of bio-chemicals involved in signalling can be set. This last point is very important because a cell is an adapting object, the signalling should not be neglected in order to facilitate and clarify interpretations of measurements. Measurements highlighting this point will be present later (see chapter 3). Mechanicals assays on single cell can be divided in two kinds: the local measurements probing the cell at the sub-cellular level and the global measurement probing the whole cell. These both categories contain two sub-categories defined on the fact that the cell adheres or not to a substrate. Some of these measurement techniques will be now briefly described. We will see through some examples that techniques used reveal different mechanical properties of cells.

1.3.1 Local Mechanical Assays with Adherent Cells

Optical Microscopy and Fluorescence Microscopy

In tissue as well as in culture flasks, cells adhere on an ECM. As this matrix is destroyed by the action of digestive enzymes, such as trypsin, cells loss adherence and round up. The observation in phase contrast microscopy or in differential interference microscopy (DIC) of cells in presence of trypsin can give pieces of information about the cellular scaffold. If the trypsin is removed, cells spread again. To do it, they need to generate forces. Observation of cell spreading is also a possibility to study cell mechanics (Döbereiner, H.-G. 2004). The fluorescence microscopy provides more details in this case. The transfection of cells with the GFP-human b-actin DNA construct allows direct observation of the actin organisation in living cells. Transfected cells synthesise GFP-labelled actin monomers (GFP-actin). GFP-actin integrated in the actin cytoskeleton with the wild-type actin can be visualised in fluorescence microscopy, because the protein GFP (green fluorescent protein) emits green light at ~ 503 nm, when it is excited at ~ 488 nm. The internal scaffold and its dynamic are revealed; particularly, the presence of actin stress fibres in fibroblast (Ballestrem, C. 1998).

The Atomic Force Microscope

This technique has been used to map spatially and temporally a cell in division. The atomic force microscope (AFM), operated in force-mapping mode, can be used to measure the local elastic properties, or Young's modulus of a sample with a spatial resolution ~ 100 nm. The cell thickness has been mapped, but also the Young's modulus reflecting the cortical stiffness and eventually an additional active cortical tension. Surprisingly, the nascent furrow region begins stiffening ~100 s before that the onset of furrowing appears. As the furrow contracts to separate the both cells, its Young's modulus reaches 10.1 kPa, which is 10 times higher than the value measured for cell before division (Matzke, R. 2001).

The Optical Tweezers (Optical Trap)

Small latex beads, typically ~1-2 μm in diameter, can be trapped in a focused laser beam. The bead's potential energy is minimal at the centre of the beam. If the position of the trap is changed, the bead is placed in a higher potential energy. Thus, a force is applied to the bead and pushes back the bead in the beam centre. FN 7-10 fragment-coating beads adhering on NIH-3T3 fibroblast lamellipodium move rearward from the lamellipodium edge to the nucleus in connection with the actin rearward stream. A restraining force is then applied to these beads. The cellular actin cortex generates locally a force proportional to the restraining force. This mechanism is dependent on ligand binding site occupancy. This technique has been used to mimic the ECM rigidity and to highlight the coupling between adhesion via integrins and force generation (Choquet, D. 1997).

Magnetic Tweezers

Magnetic beads are previously coated with collagen. These beads adhere to the dorsal surface of cells spread on a cover-slip. Integrins mediate the binding. A permanent magnet creates a magnetic field gradient and consequently a vertical force is applied to beads. In response to constant force a local recruitment of F-actin to the bead/membrane adhesion sites occurs. It demonstrates clearly the coupling between actin cortex and forces (Glogauer, M. 1997).

Micro-Needles

A simple micro-needle could reveal a lot about the viscoelastic properties of spread cells cytoplasm and nucleus. RGD-coated micro-needle have been placed in contact with the dorsal side of a spread cell. Then, the micro-needle has been move and the eventual deformation of the nucleus observed. It has been shown that the nucleus can be deformed and elongated in the direction of pull. The closest to the nucleus the micro-needle is placed, the more local the nucleus deformation is. The mechanical coupling seems to connect directly discrete anchorage points together. Using drugs, which destabilise either MTs, IFs or MFs, the integrity of IFs appears sufficient to exert this mechanical connection with the nucleus. Actin MFs form a volume-filling gel that efficiently bears compression, but it does not have the strength to resist external tension, whereas the IFs network efficiently resists tension and hardens at high strains (Maniotis A.J. 1997).

The micro-needle can be bent against the surface on which the cell adheres. By translation of the microplate, a part of a lamellipodium can be pushed toward the cell nucleus in order to destroy the adhesion. In the second part of the lamellipodium (mechanically non-perturbed part), a reinforcement of the cell adhesion is observed in order to keep the balance of forces in the cell. The adhesion enhancement is demonstrated by the growth of the so called

focal contacts (FCs) in the direction of the applied force, behaving as force-sensors (Riveline, D. 2001).

Laser Tracking Micro-Rheology

The laser-tracking micro-rheology (LTM) allows for quantifying cytoskeletal mechanics. Viscoelastic shear moduli are inferred from the Brownian motion of particles embedded in the cytoskeleton. The kidney epithelial cell line (COS7) has numerous spherical lipid-storage granules that are ideal probes for non-invasive LTM. At low frequencies, lamellar regions (82 Pa) are more rigid than viscoelastic perinuclear regions (33 Pa), but spectra converge at high frequencies (Yamada, S. 2000).

1.3.2 Global Mechanical Assays with Non-Adherent Cells

The Micropipette Aspiration

A controlled depression is imposed in a capillary in order to aspirate the cell body. This technique has been successfully used to study the connection of the plasma membrane with the underlying cytoskeleton by pulling tethers from the plasma membrane (Hochmuth, R.M. 2002). The adhesion energy per unit area between lipid membrane and cytoskeleton is evaluated from the measurement to 0.13 $N.m^{-1}$ for neutrophils and 0.075-0.1 $N.m^{-1}$ for red cells (RBC). It is comparable. In contrast, the effective viscosity (viscous drag between lipid membrane and cytoskeleton) is ~10 times higher for RBC (0.034 $N.s.m^{-1}$) than for neutrophils (0.002 $N.s.m^{-1}$). The plasma membrane adapts to the underlying cytoskeletal shape by a "shrink wrapped" mechanism (Heidemann, S.R. 2004). The micropipette aspiration technique is appropriate to study neutrophils mechanics, because these cells are pushed in blood capillaries in the body.

The Optical Stretcher

A cell, a dielectric object, is placed between two opposed, non-focused laser beams. The total force acting on the cell is zero but the surface forces are additive, thus leading to a stretching of the object along the axis of the beams. The technique is well adapted to measure the mechanical properties of the plasma membrane and the underlying cytoskeleton. A typical relative deformation for fibroblasts is ~ 5.43 % along the beam axis and -2.25% in the perpendicular direction (Guck, J. 2001).

1.3.3 Global Mechanical Assays with Adherent Cells

Membrane mechanical Stretcher

Endothelial cells have been cultivated on elastic silicone membranes. Then membranes are stretched in one direction at 20% magnitude and 0.86 Hz. The two-dimensional cell assembly displays after 48 h, a clear orientation of cells and also actin stress fibres along the stretching axis. It shows a dynamic adaptation of cells to mechanical constraints (Shirinsky, V. 1989).
Osteoblasts are grown on RGD-peptide-functionalised silicone membrane. RGD is the following peptide: arginine-glycine-aspartic acid. It is an ECM-ligand for $\alpha_V\beta_3$ integrins. A dynamic uniaxial strain, 2% magnitude and 0.25 Hz, was applied to osteoblasts for 2 h. Cells

display more dense actin cytoskeleton and an up-regulation of α_V integrin expression. It indicates a reinforcement of cell adhesion (Cavalcanti, E.A 2002).

This collection of techniques to measure cell mechanical behaviour is not exhaustive. Some experimental set-up have been selected and presented.
All attempts to quantify cell mechanical behaviour present advantages and disadvantages. Some techniques are more suitable than other, if one cares about the biological relevance of measurements. The experiments should try to mimic biological situations. In this artificial environment, in which most parameters are fixed by the experimenter, physical phenomena can be qualitatively identified or even quantified.

The living environment of an animal cell is a tissue in which it experiences forces and in which it adheres to other cells or to ECM. The normal temperature in human tissues is 37°C. The aim of this work is to reproduce around a single cell an environment similar to the tissue and simultaneously to measure physical values, such as cell displacement and force, of this single living cell. The constraints to satisfy are: the control of temperature at 37°C, the control of the adhesion, the control of the force and/or the displacement and the control of the bioactive molecules in the solution around the cell. What should be the spatial geometry to choose? The adhesion of a cell in tissue is three dimensional (in the ECM, in stratified epithelium) or two dimensional (in endothelium, in simple epithelium, such as the pancreas). The simplest mechanical assay is a uniaxial stretching or compression. An interesting compromise is to allow a cell to adhere between two plates. First, the cell bridges the gap between the plates. It places the cell in a 'three dimensional-like' situation. Second, the plate can be used to apply displacement and force. A fibroblast from the PDL could be in such a situation. Between a tooth and the alveolar bone, a fibroblast could be compressed or stretched uniaxially. The two plates have to be designed as follows: one is rigid and the second flexible. If the flexible plate satisfies the Hooke's law, it can be easily used to apply forces, which are simply proportional to the deflexion. The measurement of the deflexion of the flexible plate and of the distance between the plates allows for measurement of force and displacement applied to the cell. The plates used are called microplates because of their dimensions ~ 5 µm thick and ~ 50 µm wide. Thoumine and al. used the microplate stretching technique to apply a sudden deformation to single fibroblast at room temperature (Thoumine, O. 1997). The analysis of picture sequence allows for plotting the variation of force and cell displacement as a function of time.

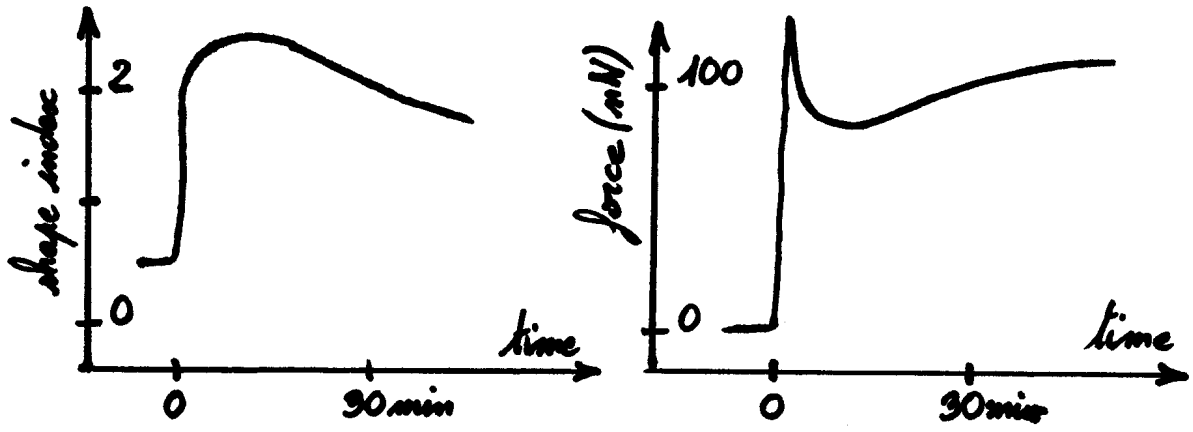

Figure 11: Mouse-embryonic-fibroblast displacement and force measured after a step-deformation.
The cell displacement is suddenly increased. In response, the cell adapts this displacement and force during in the course of the time. Adapted from Thoumine, O. et al (Thoumine, O. 1997).

In this work, the technique has been improved. A real-time measurement of force and cell displacement enables to maintain constant force or displacement. It is important because it allows, as we will see later, interpretation of measurements with the model of Kelvin. The mechanical assays are conducted at 37°C, temperature required for normal cell activity. Only two kind of adhesion have been explored: the ‘chemical adhesion’ (originally developed and used by Thoumine and al.) and the adhesion to fibronectin. Cells from three different cell-lines have been used: embryonic fibroblasts from mouse and rat and cancerous epithelial cells of human pancreas.

2 Description of Techniques of Single Cell Stretching and Protein Adsorption

The experimental set-up, based on a cantilever technique (Thoumine, O. 1997), allows a uniaxial mechanical stretching of a single cell. It has been implemented in order to achieve measurements under physiological conditions and defined physico-chemical environment moreover, it allows to generate real-time values of both cell displacement and force. Such a measurement enables a feed-back control, and therefore dynamic studies of cell mechanics. The cell is basically placed between two walls and adheres to them. As a wall is then moved, the cell experiences a stress and a strain. If the feed-back control is on, strain or stress can be controlled and applied to the cell. In response, the cell can match the non-fixed parameter, the stress or the strain. Additional techniques have been used for the preparation of these measurements: shaping of cantilever-glass plates at the micrometric scale, the quantification of cell-adhesion-protein adsorption on surfaces and the local adsorption on several micrometer-scale patches of cell-adhesion-proteins.

2.1 Experimental Set-up

The mechanical behaviour studies of an adherent single eukaryotic cell impose constraints. The original environment of eukaryotic cells is an assembly of cells, a tissue or at least a biological fluid. Biologists developed the technique of cell culture. In Petri dishes filled with suitable medium, maintained at 37°C in an atmosphere containing between 5 to 10% of CO_2, cells are growing in most cases as a two dimensional sheet on the surface. Cells adhere and grow on these plastic surfaces (in most case simply negatively charged), because cells secret themselves cell-adhesion proteins, which adsorb on the surface and then promote a stable attachment and spreading of cells. Proteins contained in the medium adsorb also on the surface. Mechanical measurements on a single cell have to be performed under the same conditions, called physiological conditions.
Briefly, in order to perform uniaxial mechanical deformation, a cell is placed between two bio-chemically functionalized walls – so-called “glass microplates”. One of the microplates is more elastic by two orders of magnitude; its binding generates a force proportional to its deflection. This microplate is used as a force sensor.

2.1.1 Uniaxial Mechanical Assay

The schematic of the complete setup is presented in the Figure 12. It is mounted on an anti-vibration table (Melles Griot, Carlsbad, CA, USA). An inverted optical microscope (Axiovert 135, Zeiss, Oberkochen, Germany) is used for the measurements. On its stage, two optimized microplate holders are mounted on top of an XY micro-translation stage (Physik Instrumente,

Karlsruhe, Germany) to allow positioning of the microplates. A low voltage piezoelectric translator (LVPZT) (Physik Instrumente, Karlsruhe, Germany) actualizes the position the rigid microplate, p_{rigid} (t), with 50 nm step resolution in the Y-direction. A controller achieves a closed-loop control of the LVPZT and an interface with the computer.

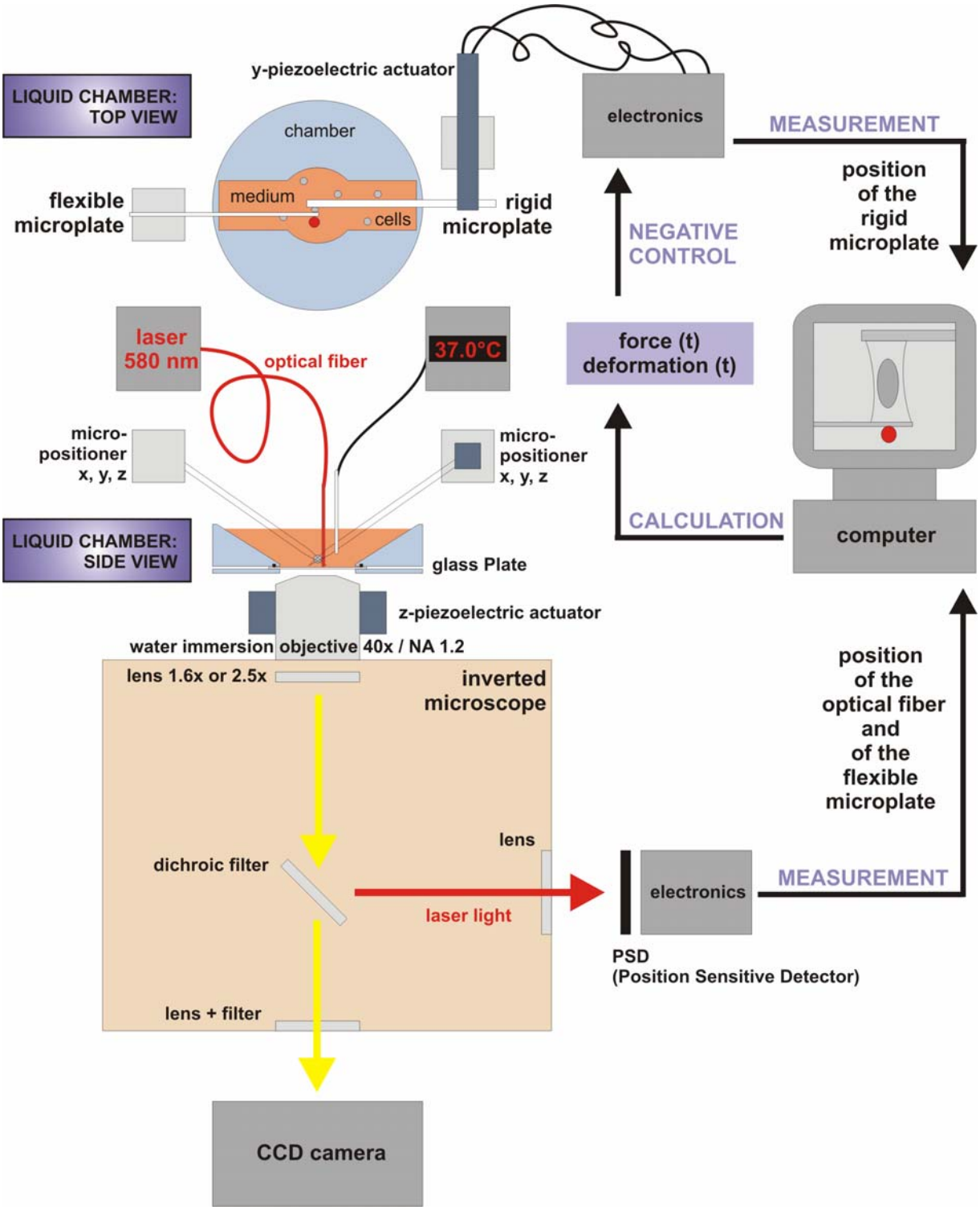

Figure 12: Schematic representation of the cell micromanipulation and measurement experimental setup
Top view and side of the liquid-chamber are drawn in the upper-left part of the representation. The inverted microscope is symbolised by a beige square. In the microscope, the dichroic filter initiates the feedback-control loop by reflecting the laser light on the PSD. The PSD signal is interpreted in displacement by the computer. Then, the computer actualises the position of the microplate according to the control on the value of interest (force or displacement). The updating of the value of interest can be achieved at a maximal frequency of 10 Hz, which is fast enough for studies of mechanics of a whole cell.

The position of the flexible microplate, $p_{flexible}$ (t), is monitored by detection of laser spot arising from the tip of an optical fibre (FS-SN 3224, Thorlabs, Newton, NJ, USA). The fibre is glued onto the flexible microplate tip with poly(di-methylsiloxane) (PDMS) (Sylgard® 184, Dow Corning, Midland, MI, USA). This is an optimal condition of stability. Some measurements have been made without gluing the optical fibre. It does not affect the quality of the measurement as long as the optical fibre to not move along the microplate. It has been checked. The optical fibre is prepared as follows. A 125 µm diameter optical fibre is etched in a 48 % hydrofluoric acid solution (Sigma-Aldrich, St. Louis, MO, USA) to a diameter of about 8 µm over a length of ~ 20 mm. The resulting fibre force constant is smaller than 1 10^{-4} $N.m^{-1}$. Such a low force constant does not interfere with the measurements of microplate deflection. A diode laser (~685 nm, HL6726MG, Thorlabs, Newton, NJ, USA) light is coupled to the optical fibre. The fibre tip shining the laser red light is imaged through the microscope using a water immersion objective (C-Apochromat 40x / 1.2 W, Zeiss, Oberkochen, Germany) and a 2.5 optovar magnifying lens mounted in the microscope. The final magnification is 100x. Pictures are taken with a CCD camera (1300 pixels x 1030 pixels) (AxioCam, Zeiss, Oberkochen, Germany). Fine focusing is obtained without risks of vibrations into the microscope by a second LVPZT (Pfoc, Physik Instrumente, Karlsruhe, Germany), which translates the objective in Z-direction. A dichroic filter (Edmund Scientific, Barrington, NJ, USA) placed on the light-path in the microscope, reflects the laser light onto a position sensitive photo diode (PSD) (S1300, Hamamatsu Photonics, Hamamatsu City, Shizuoka Pref., Japan). The PSD analogue signal is electronically intensified and converted to position. Values are recorded by a computer equipped with a signal acquisition board and LabView software (National Instruments, Austin, TX, USA).

The force and distance between microplates – the cell displacement – are defined as follows. The cell displacement D(t) is defined as the difference between the microplate position measured with respect to their respective initial position. If the rigid microplate is the microplate, which is translated with the LVPZT, the displacement is:

$$D(t) = [p_{rigid}(t) - p_{rigid}(t = 0)] - [p_{flexible}(t) - p_{flexible}(t = 0)] \quad \textbf{(eq. 1)}$$

The force, F(t), applied to the cell adhering between the tips of two microplates, and also reciprocally applied by the cell to the flexible microplate is given by:

$$F(t) = k_{flexible} \, . \, [p_{flexible}(t) - p_{flexible}(t = 0)] \quad \textbf{(eq. 2)}$$

wherein $k_{flexible}$ is the spring constant of the flexible microplate.

The force F(t) and cell displacement D(t) are calculated simultaneously each control interval $\tau_{control}$ by a LabView program. The program achieves a negative control. Each $\tau_{control}$, the measured value to be controlled X(t) is compared with the set value X_{set}. X(t) can be either the force F(t) or the cell displacement D(t). To reach the set value, the cell has to be stretched or pressed. To perform this, a microplate is moved by a step, called control step, $s_{control}$. The sign of the control step is defined according to the equation (eq. 3),

$$s_{control} = - \, sgn \, (X(t) - X_{set}) \, . \, abs \, (s_{control}) \quad \textbf{(eq. 3)}$$

Typical control values used during the measurements are: $\tau_{control}$ = 100 ms and $s_{control}$ = 50 nm. A typical control speed is 0.5 $\mu m.s^{-1}$. The control speed can be increased by increasing the control step size or decreased by increasing the control interval.

50 nm is the smallest step that the LVPZT can induce. The LVPZT is able to induce precise translations over a distance of 90 µm. The LabView program records values with a typical interval between 100 to 200 ms or slower.
An interesting way to measure cell mechanics is to design the computer control in such a way that either the cell deformation or the force is kept constant.

2.1.2 Enforcement of Measurements Under Physiological Conditions

The set-up is placed into a thermo-isolated chamber having a volume of ~ $1m^3$. Measurements take place in a plexiglass observation chamber placed on the microscope stage. It is filled with 30 ml of medium. The height of the medium on the top of the objective is ~ 2 cm. The temperature of the medium in the liquid chamber is maintained at 37 ± 0.1 °C by control of the temperature in the thermo-isolated chamber. All walls of the latter, except the 10 mm thick plexiglass front wall, are made of styrofoam. Heating wires are attached at 2 to 3 cm from the walls surrounding the microscope. Heating the thermo-isolated chamber causes temperature gradients across the microscope, which results in micrometric drift of the position of the microplates in the observation chamber. These temperature gradients were minimized by using two separate heating wires. One is attached against the back and the side walls of the thermo-isolated chamber and the second against the front wall. The power output of each heating wire is regulated by a temperature controller (Grado 901, Hengstler, Aldingen, Germany), which is connected to a temperature sensor (PT100, Conrad Electronic, Hirschau, Germany). The accuracy of the temperature sensor is ± 0.1 °C. In the liquid chamber, microplates are orientated along the axis front to back. One microplate holder is mounted on the microscope stage before the objective and the second, after the objective. Two temperature sensors are bind to the both microplate holders symmetrically with respect to the objective. The result is a minimal drift of the microplates: less than 1 µm during 10 hours as demonstrated in Figure 13. At t = 0, the microplates are attached to the microplate holders, positioned in the focal plane of the objective. The thermo-isolated chamber, the liquid chamber and the medium were pre-warmed.

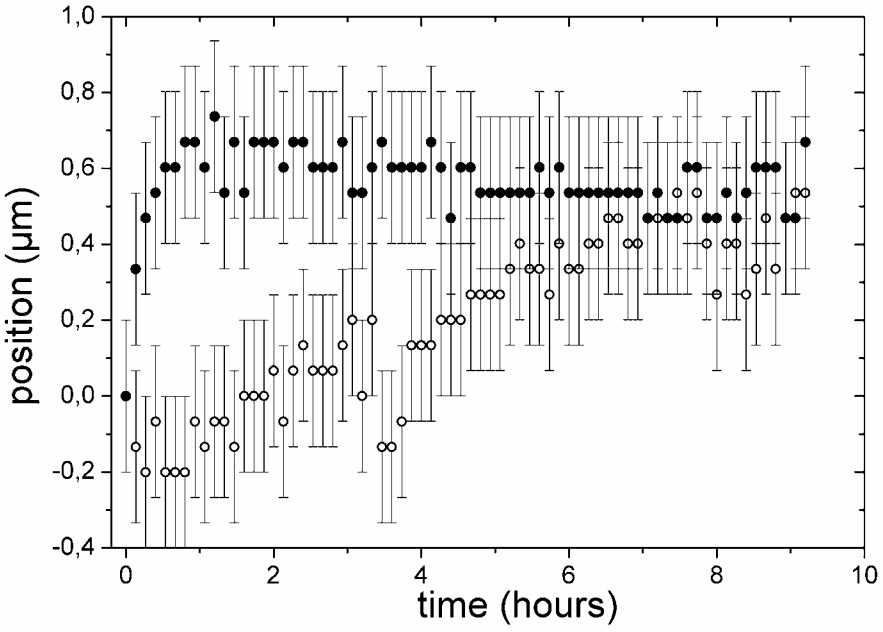

Figure 13: Microplate drift after mounting as a function of time
The graph presents the position of the microplates as a function of time, after they have been mounted into the temperature controlled chamber. The open circles represent the rigid microplate and the black filled circle the flexible one.

During the first hour, the flexible microplate drifts by ~ 0.7 μm (black filled circles) and then the position stay constant. The rigid microplate (open circles) drifts by ~ 0.7 μm in the first 4 hours after mounting microplates. These values are obtained only if the arms of the microplate holders are perpendicular to the greatest temperature, which is along the axis front to back. In this orientation, cell deformation occurs along a plane of constant temperature. When the orientation of the microplate holders is rotated by 90°, that is, with the LVPZT translation parallel to the temperature gradient, the drift is one order of magnitude larger. The mechanical drift proved to be erratic if only one heating wire is used to serve the entire chamber. All experiments begin when the microplate position is stabilized. In the Figure 13, the behaviour of the flexible microplate shows the typical thermalization behaviour of the both microplates. The thermalization behaviour is characterized by fast and oriented position change of less than 1 μm during the first hour after microplate mounting and later by a stabilized position with accuracy of 0.1 μm. Stability occurs one hour after mounting. This has been observed, but not systematically recorded.

In the thermo-isolated chamber, the CO_2 percentage is maintained at a value between 5 and 10% using an electromagnetic valve. Opening and closing of the valve are controlled by a LabView program.

A flexible tube (inside diameter 0.13 mm) connects the liquid chamber to a flexible-tube pump (Ismatec, Glattbrugg, Switzerland) placed outside of the thermo-isolated chamber. This system allows exchanges of warmed medium. No mechanical oscillations of the microplate or optical fibre positions are observed.

2.2 Fabrication of Microplates

2.2.1 Microplates Tips Shaping

The fabrication of the rigid and the flexible microplate is achieved as follows. 0.2 x 1.0 x 100.0 mm^3 borosilicate ribbon pieces (VitroCom, Mountain Lakes, NJ, USA) are used to shape microplates. A ribbon is pulled apart with a laser micropipette puller (P-2000, Sutter Instrument, Novato, CA, USA). It results a set of two asymmetric microplates due the settings of the puller parameters. Each microplate is terminated by a micro-tip, as demonstrated in the optical micrographs of the Figure 14 (b) and (c). The micro-tips are identical for both microplates. In a set, the microplate asymmetry origins only in one parameter, the length of the tip (Figure 14 (a)). For a rigid microplate, the tip length equals ~ 1 mm. In contrast, the tip length equals ~ 10 mm for a flexible microplate. The tip retains the original planar surface of the ribbon (Figure 14 (b)) and a constant width and thickness respectively ~ 20-60 µm and ~ 5 µm, depending on the parameters used for pulling. For each experiment, a new set of microplates is used. The force dependent bending of the flexible microplate is linear over the working range. The force constants of the flexible and rigid microplates, respectively $k_{flexible}$ and k_{rigid}, differ by a factor of at least ~ 100 (the calibration procedure is outlined in section 2.2.2.). Thus the possible bending of the rigid microplate is negligible in comparison to bending of the flexible microplate. The flexible microplate follows the Hooke's law and is used as force sensor. The region of interests for cell adhesion (ROI) located upstream of the micro-tip (Figure 14 (a)).

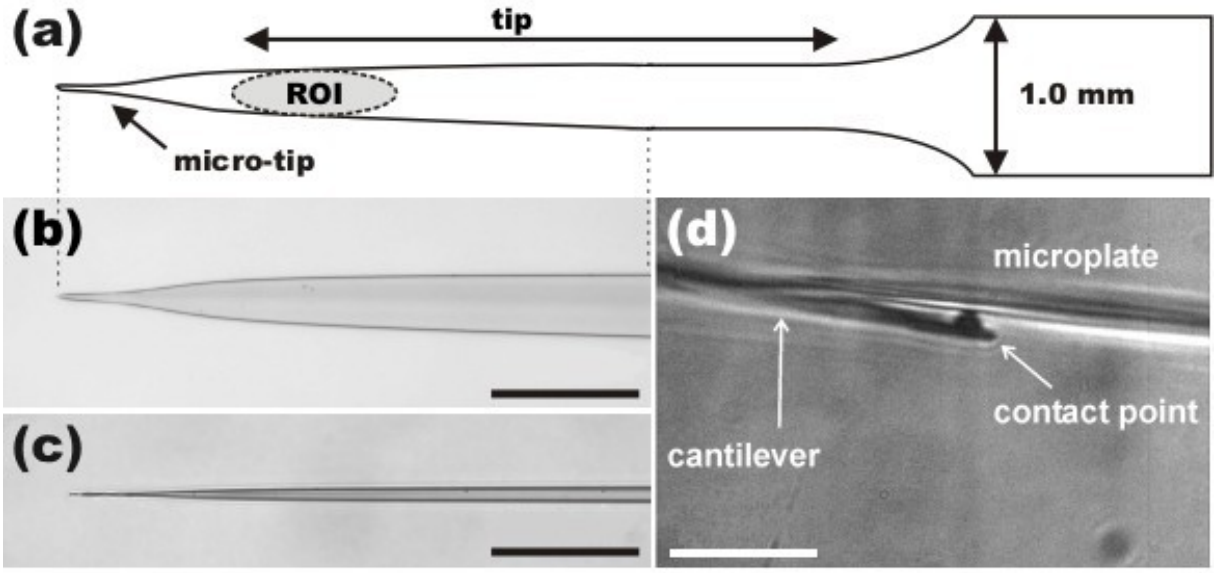

Figure 14: Microplate shaping.
(a) Schematic representation of a microplate; Micro-tip, tip and region of interest for cell adhesion (ROI) are indicated. (b) and (c) are optical micrographs of the top and side view of microplate tip respectively; bar = 100 µm. (d) Calibration of a flexible microplate with a scanning force microscope cantilever of known stiffness. The cantilever contacts the microplate at the cantilever ROI; bar = 100 µm.

2.2.2 Calibration of Microplates

The flexible microplate is calibrated against a Si_3N_4 scanning force cantilever (SFC) (Figure 14 (d)) with a force constant k_{SFC} of 0.06 $N.m^{-1}$ ± 5 % (Nanosensors. Neuchatel, Switzerland). The microplate is fixed in the microplate holder and displaced by 1 µm steps using the

LVPZT. $D_{flexible}$ is the reached displacement. Each step induces a bending of the SFC. The optical fibre is placed against the SFC and allows a measurement of the bending. Displacements are monitored and recorded. For small displacements $d_{flexible}$ and d_{SFC} microplate and SFC are linear and the microplate is characterized by a force constant $k_{flexible}$. The balance of forces is written in the (eq. 4).

$$K_{flexible} \cdot d_{flexible} = k_{SFC} \cdot d_{SFC} \qquad \textbf{(eq. 4)}$$

The stiffness of the flexible microplate is adjusted to $k_{flexible} = 10^{-3}$ to 10^{-2} $N.m^{-1}$ by adjusting the length of its tip. The value $k_{flexible}$ is adapted in function of the cell line and the force working range.

2.2.3 Functionalization of the Glass Microplates

The glass microplates were first cleaned in a 1:1 stochiometric ratio of H_2SO_4 and H_2O_2 for 30 minutes and rinsed extensively with distilled water. First, microplates were incubated in 94% acidic methanol (1 mM acetic acid in methanol), 5% H_2O and 1 % (3-aminopropyl)-triethoxysilane at room temperature for 30 min (Stenger, D.A. 1992). Then they were rinsed three times in methanol and finally they were backed in an oven at 100°C for 10 min. The NH_2-functionalized glass microplates (product of the previous step) were immersed in a 2 % glutaraldehyde solution in distilled water for 30 min at room temperature and rinsed in distilled water. Finally, the now CHO-functionalized glass microplates were incubated in a 10 $\mu g.ml^{-1}$ fibronectin (FN) solution in phosphate buffer saline (PBS) for 30 min, causing FN to covalently link to them.
After such a protein coating, a cell recognizes the microplates as a potential surface for adhesion and spreading. FN is a cell adhesive ligand from the ECM. It binds specifically to integrins, transmembrane adhesion receptors.
All chemicals are from Sigma-Aldrich, St. Louis, MO, USA.

2.3 Cell Lines and Cell Culture

Swiss 3T3 mouse fibroblasts, rat embryonic fibroblasts (REF), human pancreatic cancer cells (Panc-1) are cultured in Dulbecco's Modified Eagle Medium (DMEM) supplemented with 2 mM L-glutamine and 10 % fetal bovine serum (FBS) at 37°C in an atmosphere containing 10% CO_2. Swiss 3T3 mouse fibroblasts transfected with GFP-actin transfected under the same conditions with the same medium supplemented with 1 $mg.ml^{-1}$ of geneticin.
To obtain a cell suspension, cells were rinsed with PBS. Adherent cells are detached from the culture petri dishes by 0.05 % trypsin (enzyme hydrolyzing the ECM proteins) and 0.53 mM ethylendiaminotetra-acetic acid (EDTA) (Ca^{2+} scavengers) treatment for 1 to 2 minutes (or shorter if cells get detached). Then the trypsin solution containing the rounded cells is diluted in DMEM 1% (by volume) FBS. For the studies involving lysophosphatidic acid (LPA) or sphingosylphosphorylcholine (SPC), an aqueous solution of 1% (by weight) Bovine Serum Albumin (BSA) essentially fatty acid free is used instead of FBS. FBS contains LPA and SPC. The new solution is centrifuged for 10 minutes at 1000 rpm and finally cells are re-suspended in DMEM in absence of FBS.
These substances were purchased from Invitrogen, Carlsbad, CA, USA except the geneticin, which was purchased from Calbiochem, San Diego, CA, USA and the BSA, essentially fatty acid free, which was purchased from Sigma-Aldrich, St. Louis, MO, USA.

3T3 Swiss mouse fibroblasts and 3T3 swiss mouse fibroblasts transfected with GFP-actin are a gift from Dr. B. Wehrle-Haller, University of Geneva, Switzerland. Panc-1 and AGS cell lines are a gift of PD Dr. T. Seufferlein, University of Ulm, Germany.

2.4 Micro-Manipulation of Cells

2.4.1 Positioning of a Cell between the Microplates

The liquid chamber is filled in advance with 30 ml of DMEM warmed up to 45°C and supplemented with 2 mM L-glutamine. Immediately after FN-coating, both (rigid and flexible) microplates are mounted in holders and their tips are positioned parallel to each other in the liquid chamber in the focus plane of a 10 times magnification objective. A third CHO-functionalized glass microplate is also positioned near the both microplates. In the filled liquid chamber, the optical fibre is glued to the flexible microplate with PDMS. A film of mineral oil (Sigma-Aldrich, St. Louis, MO, USA) is spread on the medium surface to prevent undesirable drying of proteins present in DMEM at the interface liquid-air. Without the use of oil, a thin and opaque film occurs. It disturbs the observation and the measurement.

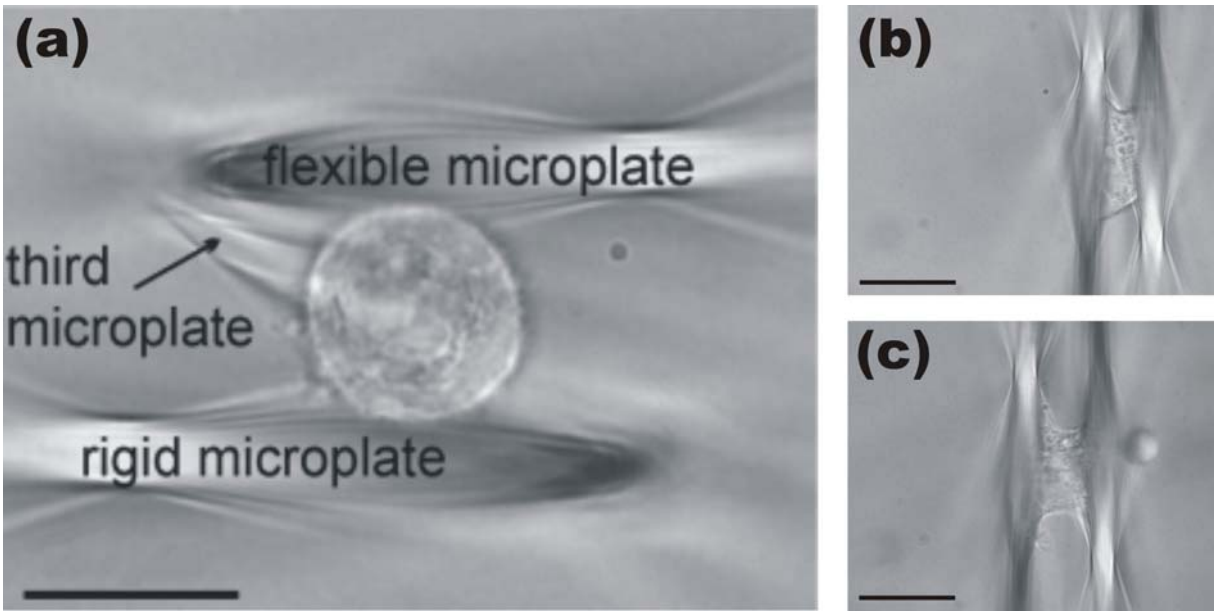

Figure 15: Positioning of a cell in between microplates tips.
Gravitational force points perpendicular to the image plane. (a) The cell is held by the third microplate at the centre of symmetry of the both bio-functionalized microplates, but without touching them; bar = 20 µm. (b) the cell, slightly compressed between the two parallel microplates, spreads on them; the third microplate has been removed upon building of a sufficiently strong cell adhesion; such an adhesion occurs in few minutes; bar = 20 µm. (c) the compression on the cell is released; the optical fibre is placed against the force sensor, if it did not have been done before; bar = 20 µm.

Approximately 100 µL of a highly diluted cell suspension is gently injected in proximity to the tips of the microplates in the liquid-chamber. Cells sink to the bottom of the liquid chamber, which is a thin (0.13 – 0.17 mm) cover slip (Menzel-Glaeser, Braunschweig, Germany). The cover slip has been pre-coated with BSA by incubation with a 1% (by weight) BSA aqueous solution for 15 min in order to prevent early adhesion of cells. The micro-tip of the third microplate is placed in contact with a cell seating on the cover slip. In less than one minute a weak adhesion is established allowing the positioning of the cell between both parallel microplates by the micromanipulation of the third microplate. Because the contact area is small and because the adhesion is chemical, this adhesion can be qualified of weak adhesion in comparison with the adhesion on FN. The disposition of microplates is shown on the Figure 15. At this step of the preparation, the distance from the cell to the FN-coated microplates is ~ 0.5 µm. The next step is to let the cell spread on the microplates. The rigid microplate is pushed against the cell using the piezoelectric actuator. This displacement brings

the cell also in contact with the flexible microplate. Under weak compression, the round cell takes an oval shape. A symmetry and synchronized contact is established on the both microplates. Due to the symmetry of the both microplate tips (accepted the length), the cell senses two identical potential areas for adhesion and spreads in a symmetrical way. This area is called ROI in the Figure 14 (a). The cell spreading starts immediately after the contact with the FN-coated microplates. After ~ 5 minutes the cell adhesion to the rigid and flexible microplates is strong enough to allow a gently withdraw of the third microplate and the vanishing of the compression. This micromanipulation is the most difficult step of the measurement preparation. Contacts between microplates, even transient, have to be avoided; they lead to microplate displacements and consequently cell stretching. Such stretching conditions the cell and influences the subsequent cell response. In order to keep the same cell conditioning over all experiments, a special care has been given to this step of the preparation. After 10 to 15 additional minutes given to the system to stabilize and depending on the purposes of the measurement, proteins and bio-chemicals can be added in the liquid chamber using the flexible-tube pump.
The pumping of 1 to 1.5 ml in and out of the liquid chamber (total volume of 30 ml) is possible without disturbing mechanically the system (the cell, the microplates and the optical fibre). Thus dissolved bio-chemicals, drugs… can be injected slowly. For example, FBS or the addition of LPA and/or SPC dissolved in DMEM.

2.4.2 What Kind of Measurements can be achieved?

Depending on the purpose of the measurement, the system could be mechanically excited in various manners. The feedback control allows for setting of force or displacement of the system as constant. A displacement or a force can be maintained to a constant value and the relaxation or response of the system observed e.g., under constant displacement, the differential equation from the Kelvin model can be analytically solved, as it will be discuss in section 3.1. A periodic mechanical excitation can be applied in order to probe the system mechanical property changes versus time (see section 3.6). More generally, the frequency response of the system can be explored.

If the optical fibre is glued to the force sensor before the cell adheres to the microplates, the PSD signal can be recorded during the spreading. The force generated by cell spreading can be measured as a function of time (see section 3.5).

2.5 Photolithography and Micro-Channels

In order to obtain micrometric patches of adsorbed cell-adhesion proteins, micro-channels have been fabricated in polydimethylsiloxane (PDMS) layers. The technique based on the work of Cuvelier, D. et al (Cuvelier, D. 2003).

2.5.1 Fabrication of Masks

The following preparation has been conducted in a clean-room. The water used was distilled water.
49 x 49 x 1 mm^3 glass plates (Neolab-Migge, Heidelberg, Germany) were vertically placed for 30 min in an ultrasonic bath in a 10% Extran (Merck, Darmstadt, Germany) aqueous solution. Dusts present in the solution are let to sediment overnight. Then, glass plates are intensively washed with water, and subsequently with isopropanol. A layer of thickness > 100 µm of chrome is sputtered on a glass plate using a sputtering machine (MED020, BAL-TEC AG, Balzers, Principality of Liechtenstein). Finally one sample is spin-coated on the chrome with 500 µl of AZ1505 photo-resist (MicroChemicals, Ulm, Germany) using the following parameters: 550 rpm for 7s and 3500 rpm for 25s. The sample is now ready to be exposed in the mask writer (DWL 66, Heidelberg Instruments, Heidelberg, Germany). The following pattern is drawn: 10 parallel lines 5 µm in width and 5 cm in length separated by 250 µm. From the middle of each line, 10 disks are drawn in one direction and 10 in the other each 250 µm. 5 series of 10 lines are drawn in parallel with respectively non disk, disks of 20, 40, 60 and 80 µm in diameter. After developing, the sample is dept in a chrome-etching-solution (Merck, Darmstadt, Germany) for ~ 1 min. The sample is washed with acetone in order to remove the non-exposed photo-resist. The mask is now ready for use. The mask presents parallel slits in the chrome layer. They are the previously drawn structures.

2.5.2 Fabrication of Moulds

The following preparation has been also conducted in a clean-room. The water used was distilled water.
With the mask prepared, the mould is fabricated. A 49 x 49 x 1 mm^3 glass plate is cleaning as in section 2.5.1. Then, it is spin-coated with 1000 µl of the negative photo-resist SU8-2 (Microchem Corp, Newton MA, USA). A 5-7 µm SU8-layer is obtained on the glass plate with the parameters: 500 rpm for 5s and 1000 rpm for 30s. The sample is pre-backed at 65°C for 3 min and at 95°C for 3 min; illuminated with UV through the prepared mask using a mask-aligner (MJB3, Karl Suss München, Germany). After, the sample is backed at 65°C for 3 min and at 95°C for 1 min. The sample is developed with the solution mr-DeV600 (Microchem Corp, Newton MA, USA) and washed intensively 3 times in water. Finally, the sample is hard-backed at 150°C for 30 min. The structures drawn in the section 2.5.1 are obtained now as 5-7 µm high parallel barriers and posts. This is a mould.

2.5.3 Fabrication of Micro-channels

The mould is used to fabricate the micro-channels. In the 10 cm petri-dishes, two pieces of microscope slides are placed as spacers. ~ 3-4 ml of liquid PDMS are poured between the spacer. The mould prepared in section 2.5.2 is pressed gently against the spacers.

A ~ 1 mm layer of PDMS is formed between the petri-dish and the mould. The petri-dish is placed at 65°C during several hours. The PDMS hardens and can be peeled off. The 5-7 µm deep micro-channels are obtained. Obviously they have the structure, which has been draw in section 2.5.3.

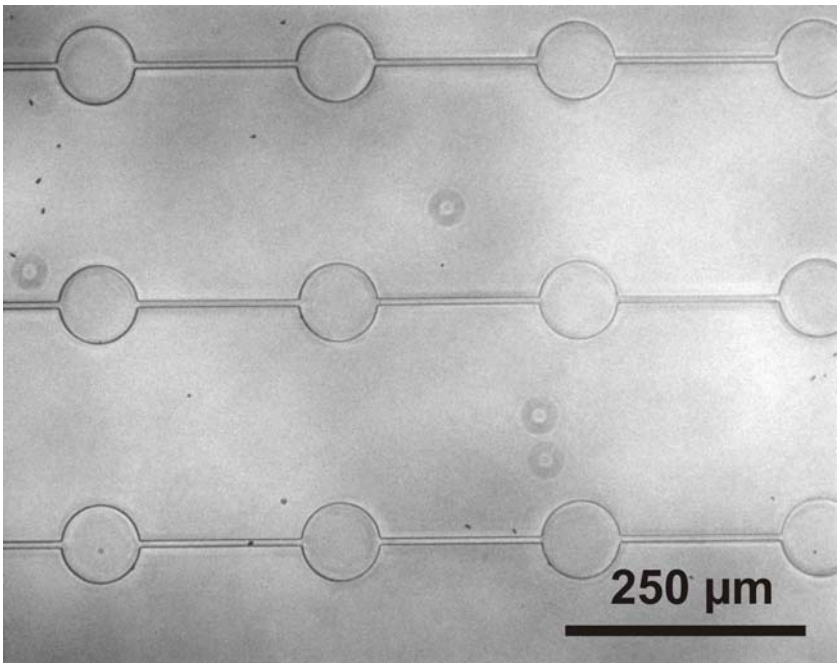

Figure 16: Micro-channels in PDMS.
This micrograph presents 3 micro-channels separated by 250 µm. The disks have a diameter of 60 µm and are separated of 250 µm.

2.5.4 Protein Adsorption with Micro-Channels

The structured PDMS layer is exposed to hydrogen plasma (100-E, TePla, Feldkirchen, Germany) for ~ 4 min. It results that the surface looses its hydrophobicity and can be wetted. It is then incubated with a 1% (weight/weight) BSA solution for 30 min and washed with distilled water. CHO-functionalised cover-slip or microplates are prepared as in section 2.2.3. The PDMS layer is brought in contact with the surface and sticks to it. The BSA proteins adsorb to the surface beside the channels. The micro-channels are closed except at the both extremities. By capillarity a protein-solution flows into the micro-channel and proteins locally adsorb on the surface. Later results will be presented.

3 Cell Mechanics, Adhesion and Kelvin Model

If most of materials obey Hooke's law in a defined range of stress and strain, only few biological tissues do. The measurements presented in this work and other measurements support that cells can obviously be considered neither as Hookean elastic bodies, nor nonviscous fluids. Cells are a closed volume containing cytofilaments (polymers of proteins) and organelles. The cytosol, fluid reach in proteins, pads the remaining free volume. In a first approach, neglecting the cell contractile activity, generated by the assembly of cytofilaments and motor-proteins, the minimal description of a cell mechanics has to include at least the property of viscoelasticity. Cell viscoelasticity appears clearly in stress relaxation, if a strain is suddenly applied and maintained; identically, in the creep response (displacement), if a stress is applied and maintained. Hysteresis occurring during a loading/unloading cycle is also an evidence of viscoelasticity. Such a mechanical behaviour has been pointed out at the sub-cellular scale. For example, magnetic beads coated with FN or collagen bind on the surface of endothelial cells spread on a cover-slip. Trans-membrane proteins, called integrins, connect the beads to the cytoskeleton through the cell membrane. The sample is placed in a magnetic-field gradient. Thus, a force can be applied on the beads and consequently a local force on the cytoskeleton. The bead displacement allowed by the cell is typically a creep response (Bausch, A.R. 1998). Simple mechanical models combine dashpots with a coefficient of viscosity η and springs with a spring constant μ allows a good description of the force and displacement changes as a function of the time (Fung, Y.C. 1993).
After a brief description of these models, various uniaxial mechanical assays on living single cells are presented and commented. The cell adhesion cannot be neglected. Some simple experiments show its importance.

3.1 The Kelvin Model

A suitable mechanical model in the case of a uniaxial deformation of viscoelastic samples is the Kelvin model. A Kelvin body is composed of a spring built in parallel with a Maxwell body. This last kind of mechanical body comprise a dashpot and a spring in series. A Kelvin body is depicted in the Figure 17.

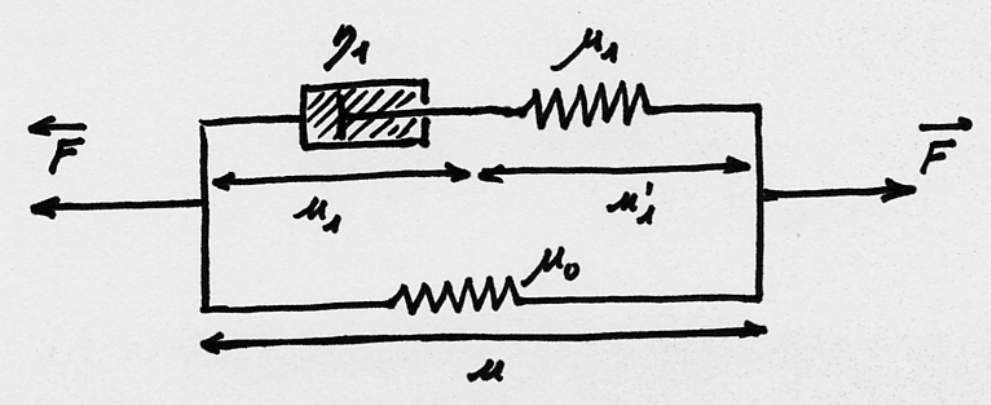

Figure 17: Schematic representation of the Kelvin body.
The Kelvin body is composed of two springs and a dashpot mounted as shown by the representation.

Four equations allow the mathematical description of its mechanics. First we define the values F is the force applied on the Kelvin body and u, its displacement. F_0 is the force applied on the spring built in parallel and F_1 the one applied on the Maxwell body. F is the sum of these forces. The displacement u is also the displacement of the Maxwell body, so that it can be written as the sum of the displacement u_1 of the dashpot and u_1' of the spring.

$$F = F_0 + F_1 \qquad \text{(eq. 5)}$$

$$u = u_1 + u_1' \qquad \text{(eq. 6)}$$

The forces F_0 and F_1 can be written as follow:

$$F_0 = \mu_0 u \qquad \text{(eq. 7)}$$

$$F_1 = \mu_1 u_1' = \eta_1 \dot{u}_1 \qquad \text{(eq. 8)}$$

Inserting equations (eq. 5), (eq. 7) in (eq. 8), u_1' and $\dot{u}_1$ can be written as function of F and u :

$$u_1' = \frac{F_1}{\mu_1} = \frac{F - \mu_0 u}{\mu_1} \qquad \text{(eq. 9)}$$

$$\dot{u}_1 = \frac{F_1}{\eta_1} = \frac{F - \mu_0 u}{\eta_1} \qquad \text{(eq. 10)}$$

The equation (eq. 6) and (eq. 9) can be derived with respect to the time. One obtains:

$$\dot{u} = \dot{u}_1 + \dot{u}'_1 = \dot{u}_1 + \frac{\dot{F} - \mu_0 \dot{u}}{\mu_1} \qquad \text{(eq. 11)}$$

Finally, (eq. 10) can be inserted in (eq. 11):

$$\dot{u} = \frac{F - \mu_0 u}{\eta_1} + \frac{\dot{F} - \mu_0 \dot{u}}{\mu_1} \qquad \text{(eq. 12)}$$

(eq. 12) contains only the Kelvin-Body displacement, the force applied on this body, their first derivatives with respect to the time and the Kelvin-Body parameters. The equation can be reorganised in order to separate displacement and force.

$$F + \tau_\varepsilon \dot{F} = \mu_0 \left(u + \tau_\sigma \dot{u}\right) \qquad \text{(eq. 13)}$$

where $\tau_\varepsilon = \frac{\eta_1}{\mu_1}$, $\tau_\sigma = \eta_1 \frac{\mu_0 + \mu_1}{\mu_0 \mu_1}$ (eq. 14)

The physical significance of these two parameters will appear clearly, as the solutions will be fund. Solutions of the equation (eq. 13) can be fund for two particular cases, which can be easily experimentally achieved. The two cases correspond to mechanical assay during them force or displacement are maintained constant. Mathematically, force or displacement can be written with the help of the Heaviside step function $H(t)$: $F(t) = H(t)$ and $u(t) = H(t)$. The output functions, solutions of the equation (eq. 13) for input step-functions, are respectively named: creep function $c(t)$ and relaxation function $k(t)$. After Laplace transformation of the equation (eq. 13), the Laplace transform function of $u(t)$ or $F(t)$ can be calculated. The reverse Laplace transform operation leads to the relaxation function and the creep function written below.

$$u(t) = H(t) \qquad k(t) = \frac{F(t)}{u(0)} = \mu_0 \left[1 - \left(1 - \frac{\tau_\sigma}{\tau_\varepsilon}\right) e^{-t/\tau_\varepsilon}\right] H(t) \qquad \text{(eq. 15)}$$

$$F(t) = H(t) \qquad c(t) = \frac{u(t)}{F(0)} = \frac{1}{\mu_0}\left[1 - \left(1 - \frac{\tau_\varepsilon}{\tau_\sigma}\right) e^{-t/\tau_\sigma}\right] H(t) \qquad \text{(eq. 16)}$$

Using the equations (eq. 14), the ratio $\tau_\sigma / \tau_\varepsilon$ appears to be superior to one or equals one, as μ_1 vanishes (Maxwell body):

$$\frac{\tau_\sigma}{\tau_\varepsilon} = 1 + \frac{\mu_1}{\mu_0} \geq 1 \qquad \text{(eq. 17)}$$

This implicates two remarks. First, the value at t = 0 and at $t \to \infty$ of the both functions depend only on μ_0 and μ_1. Second, the constant of time of the exponential function is proportional to η_1. $u(0)$ is the displacement value applied under constant displacement. $F(0)$ is the force value applied under constant force. The initiation conditions connect the both value:

$$\tau_\varepsilon \, F(0) = \mu_0 \, \tau_\sigma \, u(0) \quad \text{or} \quad \frac{F(0)}{u(0)} = \mu_0 + \mu_1 \qquad \text{(eq. 18)}$$

restrictions of time	relaxation function
$t > 0$	$k(t) = \frac{F(t)}{u(0)} = \frac{1}{E}\frac{\sigma(t)-\sigma(0)}{\varepsilon(0)} = \mu_0 + \mu_1 e^{-t/\tau_\varepsilon}$
$0 < t << \tau_\varepsilon \le \tau_\sigma$	$k(t) \approx \mu_0 + \mu_1 - \frac{\mu_1^2}{\eta_1} t$
$t \to \infty$	$k(t) \approx \mu_0$

Table 2: Relaxation function and its approximations.

restrictions of time	creep function
$t > 0$	$c(t) = \frac{u(t)}{F(0)} = E\frac{\varepsilon(t)}{\sigma(0)} = \frac{1}{\mu_0}\left(1 - \frac{\mu_1}{\mu_0+\mu_1}\right) e^{-t/\tau_\sigma}$
$0 < t << \tau_\varepsilon \le \tau_\sigma$	$c(t) \approx \frac{1}{\mu_0+\mu_1} + \left(\frac{1}{1-\mu_0/\mu_1}\right)^2 \frac{1}{\eta_1} t$
$t \to \infty$	$c(t) \approx \frac{1}{\mu_0}$

Table 3: Creep function and its approximations.

τ_σ is the time constant of displacement relaxation under constant force. τ_ε is the time constant of force relaxation under constant displacement. As $t \to \infty$, creep function and relaxation function converge respectively to $1 / \mu_0$ and μ_0 (see Table 2 and Table 3). μ_0 appears as the relaxed spring constant.

The pair of functions stress-strain (σ(t), ε(t)) is also solution of the equation (eq. 13).
If S is the constant section of the deformed object, the strain and stress are defined by the following equations:

$$\varepsilon(t) = \frac{u(t)-u(0)}{u(0)} \qquad \sigma(t) = \frac{F(t)}{S} \tag{eq. 19}$$

(eq. 7) combined with (eq. 19), one obtains the equation coupling stress and strain:

$$\varepsilon(t) = \frac{F(t)-F(0)}{\mu\, u(0)} = \frac{S}{u(0)}\frac{\left(\sigma(t)-\sigma(0)\right)}{\mu} \tag{eq. 20}$$

$$E = \frac{S}{u(0)}\frac{1}{\mu} = \frac{\sigma(t)}{\varepsilon(t)} \tag{eq. 21}$$

where E is the elastic modulus.

It follows that:

$$\sigma(t) + \tau_\varepsilon \dot{\sigma}(t) = E\left[\varepsilon(t) + \tau_\sigma\, \dot{\varepsilon}(t)\right] \tag{eq. 22}$$

3.2 Cell Adhesion and Cell Mechanics

A very simple experiment has been performed in order to observe the influence of the cell adhesion on its mechanical properties of a single cell. A rat embryonic fibroblast (REF52) has been used for this measurement. The cell adheres between two surfaces, which have been functionalised differently. The Young's modulus of the cell has been evaluated at the proximity of both kinds of surface. This measurement of the elasticity in two parts of the same cell allows for ruling out the unavoidable variations of measured values in different cells.

3.2.1 Results

Cells are injected in the liquid-chamber. They sink on the bottom, coated with bovine serum albumin (BSA). Because of such a coating, the cell does not adhere immediately. A flexible microplate is brought in contact with the cell, pressing it gently against the liquid-chamber bottom. After 1-2 min, the microplate is rotated of 90 degrees and placed close to a vertical surface (Figure 19, (a) and (b) on the left). Because the microplate is CHO-functionalised, membrane-proteins bind covalently to the microplate. The cell spreading is not at all or weakly controlled by the cell: the cell takes a typical half-sphere-like shape. The etched optical fibre has been glued on the microplate. All these micromanipulations require 5-10 min. The vertical wall is a glass plate coated with fibronectin (FN), by 30 min incubation in a solution at 10 $\mu g.ml^{-1}$.

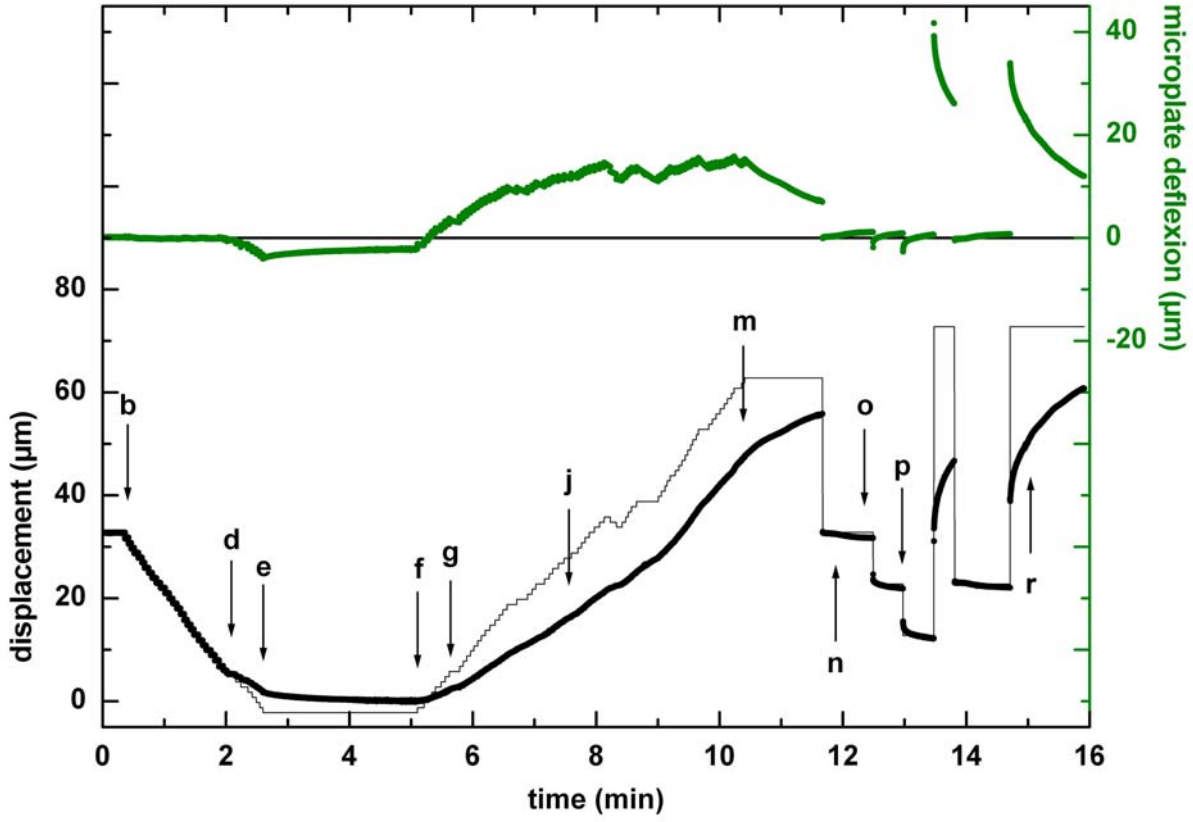

Figure 18: Stretching of a REF52 cell adhering on surfaces differently functionalised.
The positional changes of the flexible-microplate position are plotted as a function of time (solid line). The cell displacement (black curve) and the flexible-microplate deflexion – proportional to the force generated by the cell – (green curve) are also plotted as a function of time. The letters indicated the time, at which micrographs have been taken. These letters correspond with the letters in Figure 19.

With the help of the piezoelectric transducer, the flexible microplate is translated step by step in the direction of the wall (Figure 19, (b)-(d)). As the cell touches the wall, it deforms slightly (Figure 19, (e)). To obtain a good adhesion, the cell is pressed further against the wall (Figure 19, (f)). Cell displacement (black) and the microplate deflexion (green) have been measured during all these steps. It can be read in the Figure 18. In this plot, the zero-force and the zero-displacement are set to be the measured values at t = 5.3 min. Until the time t = 2 min, the microplate position (thin black line) and the distance microplate-wall (thick black line) (which is the cell displacement after contact of the cell with the wall) are superposed (Figure 18). At the time 2.1 min, the cell touches the wall. The following compression of the cell appears clearly: the microplate position and cell displacement values do not decrease at the same rate (between t = 2.1 and 2.6 min). The compression is maintained for 2 min.

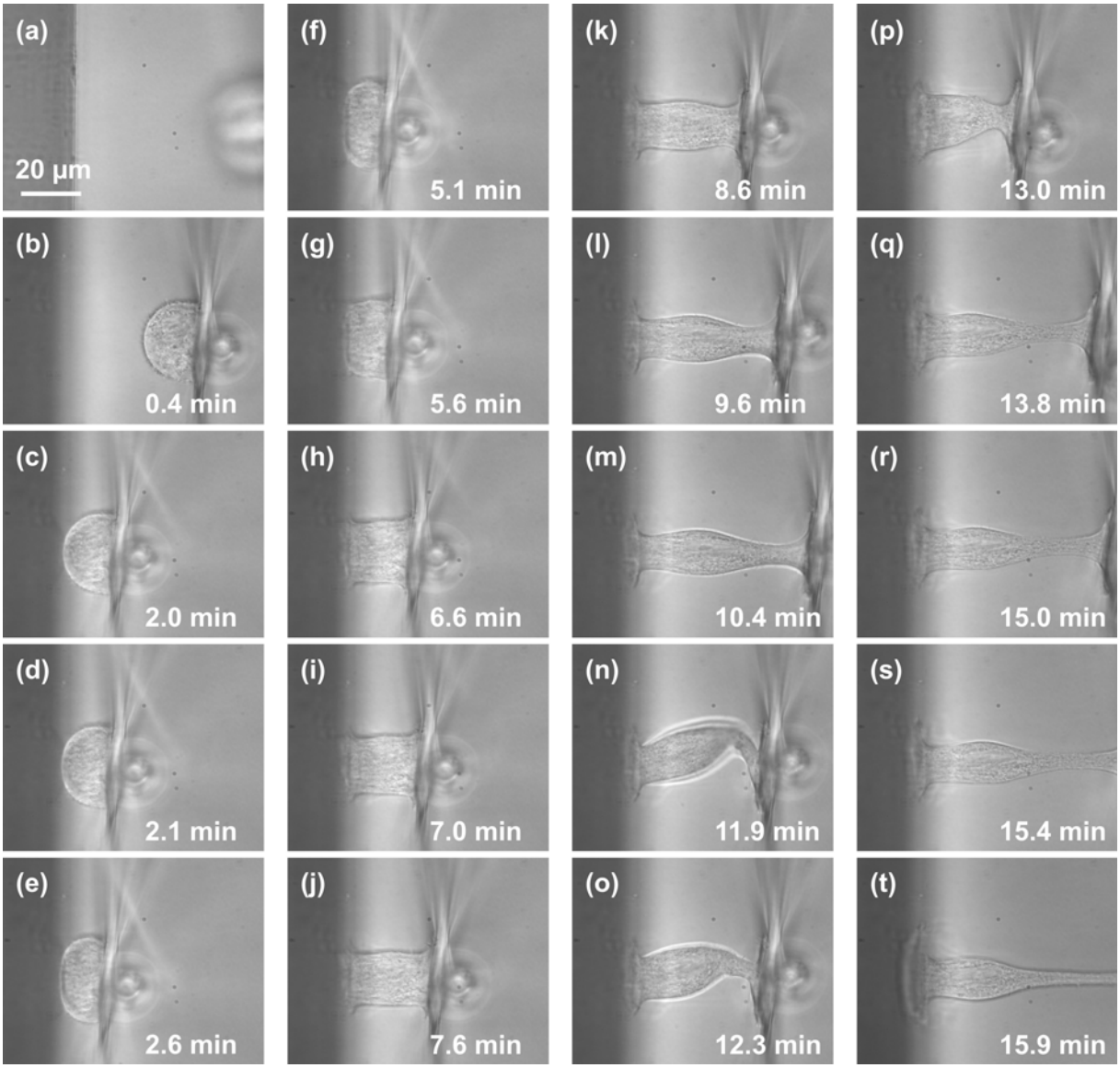

Figure 19: Micrographs taken during the stretching of a REF52 cell adhering on two different surfaces.
Focus on (a) the bottom of the liquid-chamber and (b) the cell. On the left, the glass plate coated with FN (called wall in the text). On the right, the CHO-functionalised microplate. (c)-(f), the cell is pressed against the FN-coated surface. (g)-(m) progressive stretching of the cell. (n)-(p) steps back of the microplate. The cell is bent. (q)-(t) sudden stretching steps.

After this period, the microplate is translated by 1 µm step far away from the wall. The cell is stretched. Its shape is cylinder-like. The corresponding diameter decreases slightly with time, but it is constant along the stretching axis from the wall to the microplate (Figure 19, (g)-(j)).

At the time t = 8.6 min, the diameter is not constant anymore (Figure 19, (k)). It decreases at proximity of the microplate surface. It still decreases as the microplate is translated further (Figure 19, (l)-(m)). Despite of the changes in shape, the cell displays a mechanical resistance. The microplate deflexion, which is proportional to the generated force, saturates at ~ 15 µm. The constant force of the microplate is unfortunately missing. Considering other calibration measurements, it can be evaluated at 0.01 $N.m^{-1}$. At the time t = 11.7 min, the microplate is suddenly stepped back of 30 µm. Surprisingly, the cell is bent! The bending occurs in the region of smaller diameter (Figure 19, (n)). Slowly the cell recovers a cylinder-like shape, but the region of smaller diameter remained, even if the microplate is translated of 10 µm more in the direction of the wall (Figure 19, (o), (p)). It is interesting to notice that the adhesion area of the cell did not change during the measurement. As the displacement is increased, the lamellipodium-like process of the cell on the surface is depleted in cytosol. It is refilled as the displacement is reduced. This is obvious in Figure 19, (p) on the microplate. To test the adhesion, two jumps of respectively 60 µm (t = 13.5 min) and 50 µm (t = 14.7 min) are applied to the cell. The adhesion was not destroyed, even if the cell was elongated of 60 µm. In the part of the cell of smaller diameter, this last one becomes even smaller. The cell elongation occurs mainly in this part of the cell. At the times t = 11.7, 12.5, 13.0 min, three sudden translation of the microplate, in the direction of the wall, have been made. If the second and the third steps back show an exponential decrease of the cell displacement with respectively the time constants τ = 0.12 and 0.08 min, the first one inducing the cell bending is not exponential.

3.2.2 Discussion

The apparent elastic modulus can be evaluated using the micrographs (f)-(j) (Figure 19). The diameter is constant from one side to the other side of the cell. The Table 4 summarises the calculations of the cell's elastic modulus. It increases slightly as the displacement increases demonstrating a slight hardening of the cell. It seems that the cell hardens, but without the error, it could be speculative to affirm it. In the considered range of displacements, the cell displays an elastic modulus of ~ 340 Pa in average.. This value is a bit low in comparison with the evaluation at 0.6-1 10^3 Pa of the elastic modulus of 3T3 fibroblasts (Thoumine, O. 1997). Because the spring constant of the microplate could not be measured, it is not possible to explain this difference by the variation of mechanical properties between cell types or by an under estimation of the spring constant of the microplate. Typically, variations of the spring-constant value, in a set of microplates pulled with the same parameters (or slightly adjusted if it is required), is in the range of a factor 2-4.

micrograph	l [µm]	d [µm]	$\Delta l / l$	S [μm^2]	F [nN]	σ [Pa]	E [Pa]
f	11.9	29.8	0.0	698	0	0	-
g	14.2	26.2	0.2	539	27	50	250
h	21.0	20.0	0.8	314	91	289	361
i	23.6	19.7	1.0	305	100	328	328
j	27.4	17.3	1.3	235	123	523	402

Table 4: Evaluation of the Young's modulus of a REF52 cell.
Different geometric parameters have been measured on the micrographs (f), (g), (h), (i) and (j) in Figure 19. l, d, $\Delta l / l$, S, F, σ, E are respectively cell displacement, diameter, strain, cross-section surface, force, stress and elastic modulus. The error on the cell displacement value is ± 0.5 µm; diameter, ± 0.5 µm; strain, ± 1 µm; surface, ± 50 μm^2; for force, stress and elastic modulus, the errors are unknown, because the spring constant of the microplate could not be measured.

In Figure 19, in the micrograph (k)-(m), the cell nucleus can be localised by a slightly bigger diameter close to the middle distance between microplate and wall. Two different regions can be distinguished in this cell: the left part (part 1) between the wall and the nucleus and the right part (part 2) between the cell nucleus and the microplate. In part 1 the cytoskeleton is based on an adhesion to FN, whereas in part 2 it is based on a chemical adhesion. The plan parallel to the wall crossing the centre of the nucleus is chosen has boundary between part 1 and 2. The cell can be modelled as two pieces of different materials (1 and 2) juxtaposed between two walls.

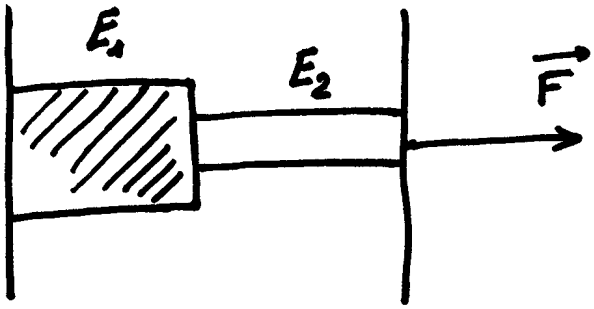

Figure 20: Schematic representation of the mechanical model of the deformed REF52 cell.

Using this rough model, the micrographs (j)-(m) (Figure 19) can be used to compare the elastic modulus of the part 1 and 2. At a time t, the force is constant:

$$F = \sigma_i S_i = \varepsilon_i E_i S_i = \frac{\Delta l_i}{l_i} E_i S_i = cte \qquad \text{(eq. 23)}$$

wherein: $I = 1$ or 2 for respectively the part 1 and 2
ε_i , σ_i , Δl_i , l_i , E_i are respectively the strain, the stress, the elongation, the length and the Young's modulus of the material *i*.

Finally, the ratio of the elastic modulus of the both material equals:

$$\frac{E_2}{E_1} = \frac{l_2}{\Delta l_2} \frac{\Delta l_1}{l_1} \frac{S_1}{S_2} \qquad \text{(eq. 24)}$$

micrograph	l_1 [µm]	l_2 [µm]	Δl_1 [µm]	Δl_2 [µm]	d_1 [µm]	d_2 [µm]	S_1 [µm^2]	S_2 [µm^2]	$\Delta l_1 / l_1$	$\Delta l_2 / l_2$	E_2 / E_1
j	14.1	13.2	-	-	17.3	17.3	235	235	0.00	0.00	-
k	17.6	18.9	3.5	5.7	15.0	12.8	176	128	0.25	0.45	0.75
l	21.7	27.0	7.6	13.8	13.1	8.6	135	58	0.55	1.05	1.22
m	25.8	33.1	11.4	19.9	11.8	6.4	109	32	0.80	1.50	1.82

Table 5: Ratio of elastic moduli of the both cell parts.
Different geometric parameters have been measured on the micrographs (j),(k),(l) and (m) in Figure 19 for the two part of the cell. The two parts are defined by the position of the nucleus. L_i, Δl_i, d_i, S_i, $\Delta l_i / l_i$, E_i are respectively the displacement, elongation, diameter, cross-section surface, strain and elastic modulus of the part I of the cell. The error on the cell displacement value is ± 0.5 µm; elongation, diameter, ± 0.5 µm; surface, ± 50 µm^2; strain, ± 1 µm.

The part 2 displays a strain almost 2 times greater than the part 1, for each micrograph. The ratio E_2 / E_1 increases with the global elongation of the cell. A hardening of the part 2 is

observed in comparison to the part 1. It could be explain by a lack of cytoskeletal organisation in the part 2 in comparison with the part 1, because of the absence of FN.
As the microplate is suddenly translated toward the wall, the cell undergoes buckling (Figure 19, micrograph (n)). The critical force of buckling F_c (Euler force) has been reached. It is obvious: the cell is bent. The expression of this critical force for a beam is the following (Howard, J. 2001, p. 104):

$$F_c = \pi^2 \frac{EI}{L^2} = \frac{\pi^3}{4} E \frac{r^4}{L^2} \qquad \text{(eq. 25)}$$

with $$I = \frac{\pi}{4} r^4 \qquad \text{(eq. 26)}$$

wherein: I is the second moment of inertia
E is the elastic modulus
L is the length of the beam
r is the radius of the beam

Using the values of the Table 5, measured for in the micrograph (m) before that the buckling occurs, the Euler force can be evaluated for the part 1 and 2. The ratio of the both forces is:

$$\frac{F_c(2)}{F_c(1)} = \left(\frac{r_2}{r_1}\right)^4 \left(\frac{L_1}{L_2}\right)^2 \frac{E_2}{E_1} \approx 0.1$$

It follows that even if the part 2 is intrinsically harder than the part 1, it is ~ 10 easier to bend the part 2 of the cell instead of the part 1. It occurs as demonstrated in the micrograph (n), Figure 19.
To summarise, as the cell is homogeneously deformed, its elastic modulus increases slightly. As a certain deformation is reached, an asymmetry occurs in cell shape. From this time-point, the cell mechanics can be reasonably described by a model composed of two juxtaposed pieces of different materials strongly tighten together. It seems that the adhesion on FN induces a different cytoskeletal organisation as the chemical adhesion. The cellular material appears softer at proximity of the FN, but, at the same time, the cell lateral deformation is smaller in this region of the cell as in the other side. It results, that the cell body is much more preserved against deformation close to the FN adhesion surface than to the chemical-adhesion surface. It is well known that a cell builds its cytoskeletal scaffold on the base of its adhesion to its environment. For example, depending on the FN-sub-units adsorbed on a surface, the cell motility can be switched on or off (Moyano, J.V. 2003). Cells are able to sense the rigidity of the substrate through the integrin bind and clustering (Lo, C.-M. 2000). It can be hypothesised, that the chemical adhesion does not allows or reduces the lateral movement in the plasma membrane of trans-membrane proteins, such as integrins. For this reason, the cytoskeleton could fail to sense the stress and/or to structure in order to sustain stress. The signalling originating from the adhesion on FN is probably missing or partly missing. The cytoskeletal dynamic is consequently down regulated.

3.3 Mechanics of Mouse Embryonic Fibroblasts

Fibroblasts are among those cells, which are mechanically the most active after muscle cells. This is due to their functions in CTs (protein secretion, fibre formation and tissues repair). Fibroblast's mechanical activity is supported by the actin cytoskeleton (Revenu, C. 2004). Used commonly as model-cells in biology, a lot of knowledge has been collected about fibroblasts. By applying uniaxial stretching to a single cell, it is hoped to understand more the regulation of cell contractility, which as been observed in cell spreading or crawling on flat surfaces (Cramer, L.P. 1997; Döbereiner, H.-G. 2004; Dubin-Thaler, B.J. 2004; Lo, C.-M. 2000; Verkhovsky, A.B. 1999). A Swiss 3T3 mouse embryonic fibroblast (Swiss 3T3) has been placed between the two microplates and let to adhere on them as described in section 2.4.1. A displacement Heaviside function-like is applied to the cell.

3.3.1 Results

Cell displacement is control during this measurement. The control acts at a rate of 0.5 $\mu m.s^{-1}$. The cell regulates the displacement rate. Over this measurement, the displacement rate is almost constant at 0.23-0.29 $\mu m.s^{-1}$ (Table 6). The displacement is increased or decreased between the three plateau-values 0, 15 and 30 µm (Figure 21, black curve). Five displacements steps have been applied to the cell. First the displacement is increased linearly to 15 µm, maintained for ~ 8 min and finally brought down to the initial displacement for 6 min. The initial displacement is set as zero-displacement in Figure 21. It equals 7 µm.

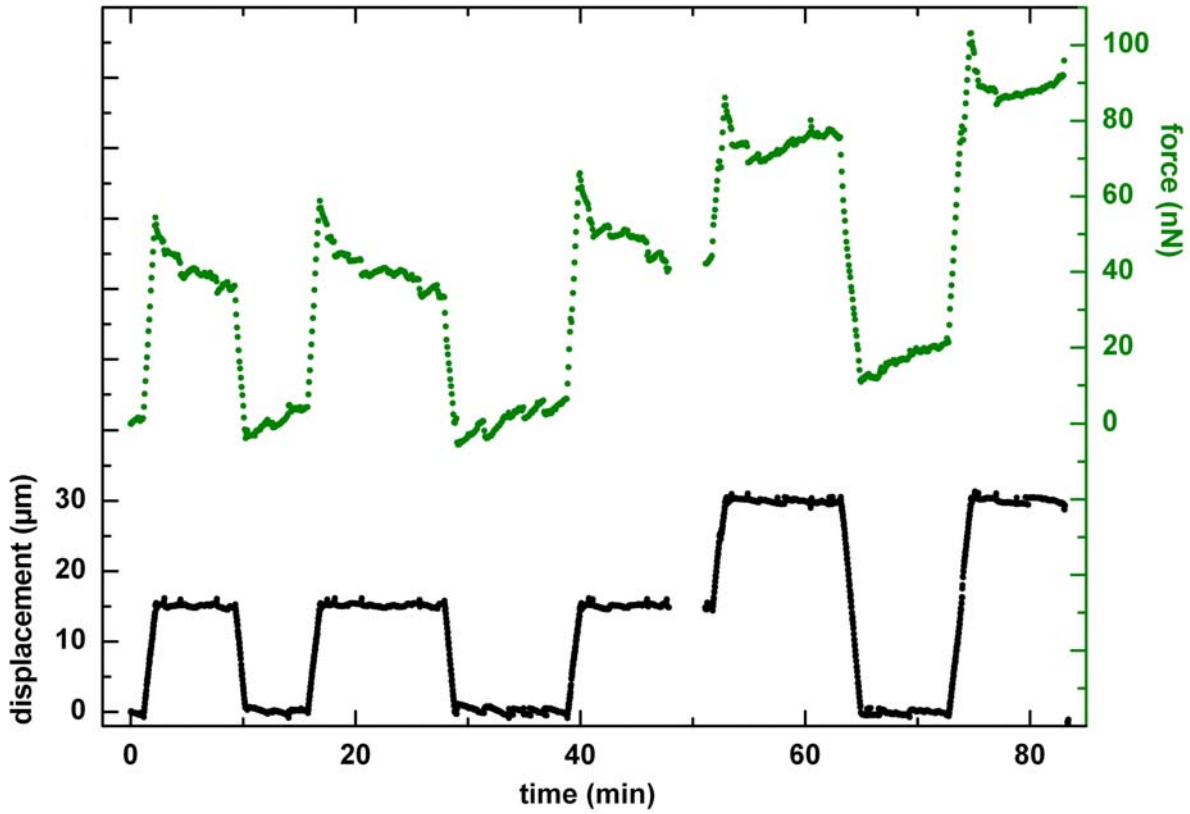

Figure 21: Mechanical assay with a Swiss 3T3 cell.
The measurement is a control displacement measurement. The set displacement is plotted in black. The force generated by the cell in response to the assessed displacement is plotted in green as a function of time.

Second, the displacement is again increased to 15 µm, maintained for ~ 12 min and reset to the zero-displacement for 10 min. The third displacement cycle is composed of an increase of 15 µm, maintained for ~ 12 min, followed by an increased to 30 µm, maintained for ~ 10 min and finally brought down to zero-displacement. The last cycle is limited to an increase to 30 µm, maintained for ~ 10 min. The cell generates a force in response to the imposed displacement. This force is plotted as function of the time in Figure 21, green curve. As the displacement is linearly increased or decreased, the cell response appears obviously elastic (Figure 21). An effective loading/unloading spring constant can be calculated (Table 6). The cell appears more deformable, more elastic, during unloading than during the loading. At higher displacement, this effective spring constant is reduced. If the displacement is constant, the force decreases in the course of the time. According to the Kelvin model, the force relaxation should be observed at constant displacement. In fact, the relaxation function can be efficiently used to fit the force decreases. μ_0, μ_1 and η_1, the three parameters of the Kelvin model (Table 2), are obtained. Their values are listed in the Table 6. Interestingly, as the 30 µm displacement is maintained (cycle 4 and 5), the force decreases (relaxation) first and then increases higher than the plateau value of the relaxation. The cell is probably trying to contract, working against the displacement control. This behaviour has not been observed at 15 µm displacement.

	Loading / unloading parameters			**Kelvin model parameters**				
cycle	**plateau value**	**rate**	**spring constant**	μ_0	μ_1	τ_ε	η_1	$-\mu_1^2/\eta_1$
	[µm]	[µm.s^{-1}]	[10^{-3} N.m^{-1}]	[N.m^{-1}]	[N.m^{-1}]	[min]	[10^3 N.s.m^{-1}]	[N.m^{-1}.s^{-1}]
1	15	0.22 / -0.25	3.7 / 2.6	1670	790	2.68	127	-4.9
2	15	0.23 / -0.28	3.7 / 1.8	1720	1040	2.46	154	-7.0
3	15	0.22 / -	3.8 / -	2320	980	0.84	50	-19.2
4	30	0.22 / -0.29	2.4 / 1.9	1860	410	1.06	26	-6.5
5	30	0.26 / -	2.5 / -	2320	550	0.64	21	-14.4

Table 6: Viscoelastic parameters of a Swiss 3T3cell.
The initial displacement equals 7.0 ± 0.5 µm. The error on the plateau value is ± 0.5 µm; rate, ± 0.01 µm.s^{-1}; loading/unloading spring constant, ± 0.1 10^{-3} N.m^{-1}; spring constants, ± 10 N.m^{-1}; spring constants, ± 25 N.m^{-1}; time constant, ± 0.05 min; coefficient of viscosity, ± 5 10^3 N.s.m^{-1}

3.3.2 Discussion

The loading/unloading effective spring-constant cannot be compared to the parameters μ_0 and μ_1, because these three parameters are effective parameters and have definitively different definitions. The loading/unloading spring constant reflects the cell elastic response in a dynamic regime: the cell is stretched at a constant rate and it has to respond to an increase of stress and strain simultaneously. If, at same displacement variation, the loading/unloading spring constant decreases, the force variation has to decrease too: it means that the cell does not resist to the deformation. As the displacement plateau-value is doubled (30 µm instead of 15 µm), if the cell reacts identically, the loading/unloading spring constant should keep the same value. Indeed it decreases. The peak-force is 35% smaller than expected: the cell resists

less at 30 µm displacement than at 15 µm displacement. Two interpretations are possible. It could be that cross-link-bridges of the cytoskeleton statistically rupture, because the constant rate is maintained longer. It could be also that the cell actively allows deformation to limit the stress increase. In contrast to the loading/unloading spring constant, the parameters μ_0 and μ_1 are calculated at constant strain: the cell is free to adapt to stress, which can be achieved by controlling the contraction activity of motor-proteins such as myosin or by formation of protein-filaments. A hypothesis to interpret results is to consider, that the cell experimenting a constant strain tries to stabilise the stress value efficiently. According to the equations in the Table 2, the peak-force value is $(\mu_0 + \mu_1)\, u(0)$. $U(0)$ is imposed. The parameter μ_1 decreases of a factor ~ 2 at the cycle 4 and 5 in comparison with the first cycles 1, 2 and 3. It limits the increase of $\mu_0 + \mu_1$, thus the high of the peak force. μ_0 increases slightly with the repetition of identical cycles, but does not change significantly as the displacement is doubled. It indicates a small stiffening of the cell under repetition of mechanical cycles. Interestingly, for the cycle 4, the first stretching from 15 µm to 30 µm, the parameter μ_1 takes a value almost equal to the values for the cycle 2, the second stretching from 0 µm to 15 µm, the same amplitude (15 µm) as the cycle 4 (Table 6). During the cycles 3 and 5, the parameter μ_1 increases similarly of 20%. At short times, the relaxation function is a linear function of the time with the slope - μ_1^2 / η_1 (Table 2). The absolute value of this slope increases (Table 6), when a mechanical stimulation is repeated. It shows maybe, the history-dependence of the cell's mechanical behaviour. The cell hardens, as it experiences a new strain value for a second time. The apparent viscosity η_1 drops significantly during the measurement. It is efficient way to obtain a fast relaxation of the force. At higher strain, the cell generates a force after the relaxation plateau has been reached. There is probably a balance between the strain and the stress that a cell can undergo. As the strain is doubled, the cell minimises the peak-force and then the cytoskeleton reorganises. The force does not stabilise at the plateau value defined by the relaxation function: it force increases again. The cell contracts in order to adapt the force. This would lead to interpret the peak-force and the following relaxation as a passive behaviour, comparable to the behaviour of a gel, and the contraction as a cell-activated active behaviour.

At this point, an interesting question to ask is: do the Kelvin parameters represent active or passive cytoskeletal mechanisms? All cross-linkers and motor-proteins sense a force applied quickly. It is known that molecular bounds between proteins break more efficiently, if the force is small and applied at low loading rate. Typically, for streptavidin-biotin, force < 100 pN and rate < 100 $pN.s^{-1}$ (Merckel, R. 1999). A typical loading rate, for this measurement, is 830 $pN.s^{-1}$. The number of cytoskeletal cross-links is difficult to evaluate. An evaluation of the number of myosin copies in neutrophils gives the number of ~ 100 10^6 myosin-heads bound to the cytoskeleton per cell, considering 200 kDa per head (White, J.R. 1983). For a force of 100 nN, the force per bound is ~ 10^{-3} pN. Using these values, the assembly cross-linkers and motor-protein on actin filaments would be in a regime of low force, but high loading rate. Consequently, the cytoskeletal cross-linkers and motor-proteins offer likely an immediate resistance to fast displacement and produce the peak force. The parameter μ_0 may origin in this passive mechanism. About the myosin, another interesting point is that it has been demonstrated *in vitro* that the non-muscle myosin (NMM) (present in non-muscle cell) are motor-protein, which can eventually work at a surprisingly high duty ratio. This duty ratio, depending on ADP and actin filaments concentrations, could reach the value of 0.8. It means that NMM motor-proteins could spend ~ 80% of the duration of an ATP-hydrolysis cycle bound to actin filaments (Kovács, M. 2003; Wang, F. 2003). As a comparison the duty ratio of muscle myosin is 0.035-0.14 under physiological conditions. This property of the NMM motor-proteins can be an advantage to sustain forces. At constant actin concentration, an increase of the ADP concentration in the actin cortex turns NMM motor-proteins into cross-linker-behaving-like proteins. It would result in a stiffening of the actin cytoskeleton. Cell might use this mechanism to switch the actin-cytoskeletal state from dynamic to passive.

Consequently, the variations of the parameters μ_0 and μ_1 may origin in active stiffening of actomyosin complexes trigger by the cell through adjusting of ADP concentration.
The cell mechanical behaviour is definitely highly regulated. All the studies about cell crawling and spreading on a surface demonstrate it. Between the microplate, relaxation and contraction of a cell have been demonstrated under a simple stretching step (Thoumine, O. 1997). The cell was free to adapt displacement and force. The present measurement gives new insights in cell mechanics. First the viscoelastic behaviour of cell is confirmed, but in addition, the parameters of the Kelvin model can be evaluated under constant displacement. Second, it seems that the contraction event depend on the strain applied. It was not observed during the cycle 2 in comparison the cycle 4 and 5 where it occurs obviously. The correlation between the parameters and the underlying cytoskeletal structure are still difficult to understand. The use of drugs against the cytoskeleton organisation and dynamic, and the ATP-depletion of the cell in correlation with the parameters of the Kelvin model should give a better comprehension of their significance.

3.4 Energy Consumption of a Cell Sustaining a Constant Force

After the measurement at constant displacement, a measurement at constant force, i.e. constant stress has been conducted.

3.4.1 Results

Figure 22 represents a typical stretching experiment of a single Swiss 3T3 cell, in which a constant stress is applied. This stress is applied with a rate of ~ 80 Pa.min^{-1} corresponding to a pulling rate of 3.2 nN.min^{-1} until a plateau at 500 Pa, corresponding to a force of 20 nN, is reached. During the first 5 minutes, the applied stress elongates the cell to ε ~ 4.5. The cell then contracts at a constant speed of about v = 0.3 µm.min^{-1}. This results in partial neutralization of cell shape deformation back to ε ~ 1.2.

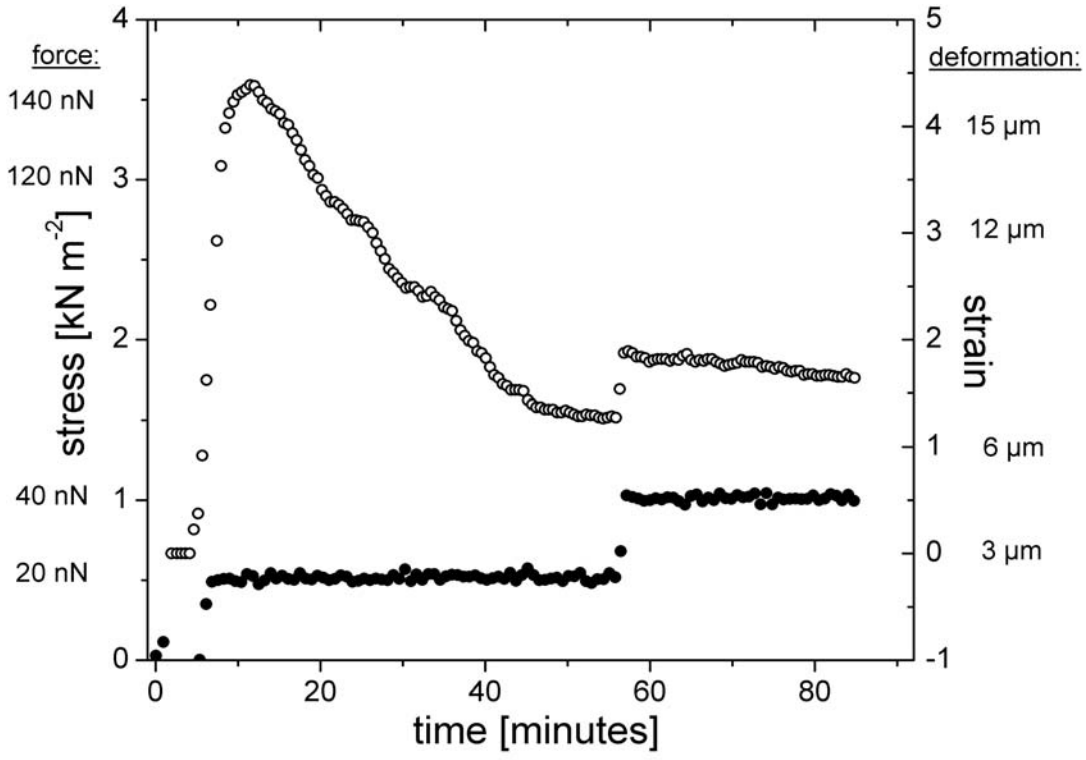

Figure 22: Constant force measurement with a Swiss 3T3 cell.
Cell strain (open circles, right scale), when a constant stress (filled circles, left scale) is applied. The strain of the cell indicates an initial passive response followed by an active contraction. Doubling the stress at 58 min. indicates stiffening of the cell represented by reduced plasticity. Corresponding force and deformation values are shown. Stress is applied with a pulling rate of approximately 80 Pa.min^{-1} which corresponds to 3.2 nN.min^{-1}.

At t = 58 min, the applied stress is doubled to 1,000 Pa. Calculating the stiffness at this moment as the applied force divided by the maximum deformation gives 6.7 mN.m^{-1} in comparison to 1.5 mN.m^{-1} after the first pull. The speed of the subsequent cell contraction is v = 0.03 µm.min^{-1}, a factor of 10 smaller than after the initial pull. The maximum contraction power of the cell, $P_{max} = F$ x v, for a load of 20 nN is about P_{max} = 100 x 10^{-18} W or 25,000 $k_BT.s^{-1}$ at 300 K. The doubled load of 40 nN gives a contraction power about 5 times smaller. These cell parameters are summarized in Table 7.

Stress [Pa]	Force [nN]	Cell Elasticity [mN/m]	Contraction Speed [μm/min.]	Max. Contraction Power x 10^{-18} [W]
500	20	1.5	0.3	100
1000	40	6.7	0.03	20

Table 7: Cell response to sequential stress application.
The pulling rate equals 80 Pa.min^{-1}

3.4.2 Discussion

The cell contraction speed (between 5 and 0.5 nm.s^{-1}) is relatively slow compared to the speed of molecular motors like kinesin or myosin, but it is comparable to protein-filament polymerization rates (Howard, J. 2001) or the typical speed of cell motion (Peckham, M. 2001; Bray, D. 2001 p.23). The cell contractive power is 100 x 10^{-18} W, corresponding to about 2,500 ATP molecules/s of the order of 10 k_BT of energy each. A single molecular motor generates a maximum force of approximately 1 pN against a stiff load (Finer, J.T. 1994; Block, S.M. 1995) and moves with a step size of roughly 10 nm per ATP. Here, the assumed motor performs a step every two seconds or slower – a situation close to stalling condition. To resist the imposed force, about 10^4 motors would be necessary, consistent with an ATP consumption of 5,000 molecules/s, leading to a reasonable efficiency of about 50 % of the molecular contractile machinery. A single cell contains about 2,000 Mitochondria with 10^4 to 10^5 ATP-synthases each. An ATP-synthase like the F1 is capable of producing up to 600 ATP/s, giving a total production of about 10^{10} ATP-molecules/s per cell, thus only a very small fraction of the order of 10^{-5} of the cell metabolism is used for contraction.

The data further indicate that active contraction is generated about 12 min. after uniaxial application of external load. It could be interpreted by the fact that oriented F-actin stress bundles, primarily responsible for cell contraction, must be formed first.

3.5 Activation of Cell Contraction

The aim of this measurement is to understand the influence on the cell's mechanical behaviour between the microplates of the presence of serum in the medium. The serum is necessary to induce the cell growth in culture. The serum, more precisely foetal bovine serum (FBS), contains proteins and polypeptides such as albumin (40-80 $mg.ml^{-1}$), cell-adhesion ligands, such as fibronectin (1-10 $\mu g.\ ml^{-1}$). It contains also protease inhibitors, growth-factors such as the epidermal growth factor (EGF), the platelet-derived growth factor (PDGF) (1-100 $ng.\ ml^{-1}$), amino acids, lipids, as such lysophosphatidic acid (LPA), carbohydrates, iron, zinc, hormones, vitamins… (Freshney, R.I. 2000). FBS induces cell contractility and the formation of actin stress fibres (Nobe, H. 2003). Some of serum compounds for example the EGF, PDGF and LPA have been shown to induce reorganisation of the actin cytoskeleton, the formation of stress fibres, in connection with adhesion reorganisation and motor-protein activity (Seufferlein, T. 1994, Tangkijvanich, P. 2002).

3.5.1 Results

During this measurement no control of either displacement or force has been enhanced. The position of a flexible microplate has been shifted stepwise in order to stretch the cell (from the right to the left in the micrograph Figure 23) until an ultimate displacement of 55 µm. After, the microplate has been droved back to the initial position. The resulting cell displacement and force generated by the cell have been monitored (Figure 24). The microplates are coated with FN following the protocol given in the section 2.2.3. The cell used is a rat embryonic fibroblast (REF52). The liquid-chamber is filled with serum free medium (DMEM and L-glutamine).

Cells have been kept in suspension in serum free medium during at least 1 hour at 4°C. About 100 µl of cell suspension are injected close to the microplates. A cell is placed between both microplates and pressed gently between them. The cell builds adhesion on the FN-coated surfaces. After 5 min, the negative force is vanished. During the first 10 min, force and displacement are almost constant (Figure 24, (a)). The force increases slowly to 0.8 nN at a rate of 0.03 $nN.min^{-1}$. The displacement decreases to -0.8 µm at a rate of -0.04 $\mu m.min^{-1}$ simultaneously. Each steps of the flexible microplate are listed in Table 8. In the same table, the amplitude of force and displacement changes, induced by the step, is indicated.

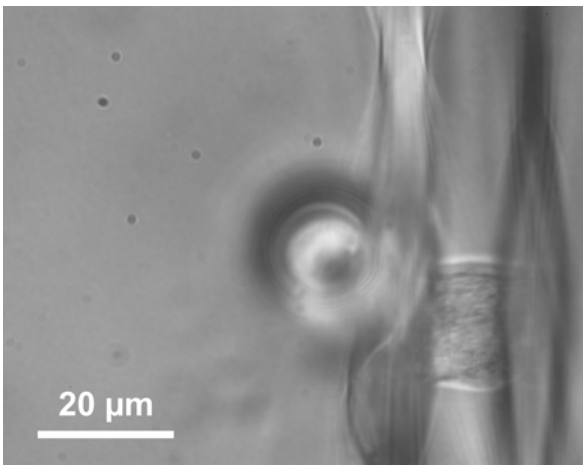

Figure 23: Micrograph of the REF52 cell.
On the right side: the rigid microplate. The PDMS droplet, which glues the optical fibre to the flexible microplate, appears as a sphere almost at the centre of the micrograph. FBS has not been added yet.

10 steps have been achieved. 5 steps translate the flexible microplate away from the cell. It infers an increase of the force (Figure 24, I). During 20 min, the cell experiences no mechanical perturbation. After that, 5 steps place the microplate in the initial position (Figure 24, (d)). At the time t = 10.8 min, in serum free medium, the flexible microplate is suddenly moved of 5 µm (step 1). The cell is stretched. The force jumps instantaneously to 4 nN and then relaxes to 1.4 nN over 5 min. After an initial jump, the cell displacement relaxes to 3.7 µm. At the end of the relaxation, the cell displacement is 4.5 µm. The cell did not resist to the imposed 5 µm displacement (Figure 24, (b)). At t ~ 15 min, FBS is gently added in the liquid-

chamber in sufficient amount to obtain a final concentration of 5%. At t = 16 min, the cell displacement decreases suddenly at a rate of -20 µm.min^{-1} during the first 6 seconds (Figure 24, (b)). This rate drops gradually to -0.30 µm.min^{-1} at t = 20 min.

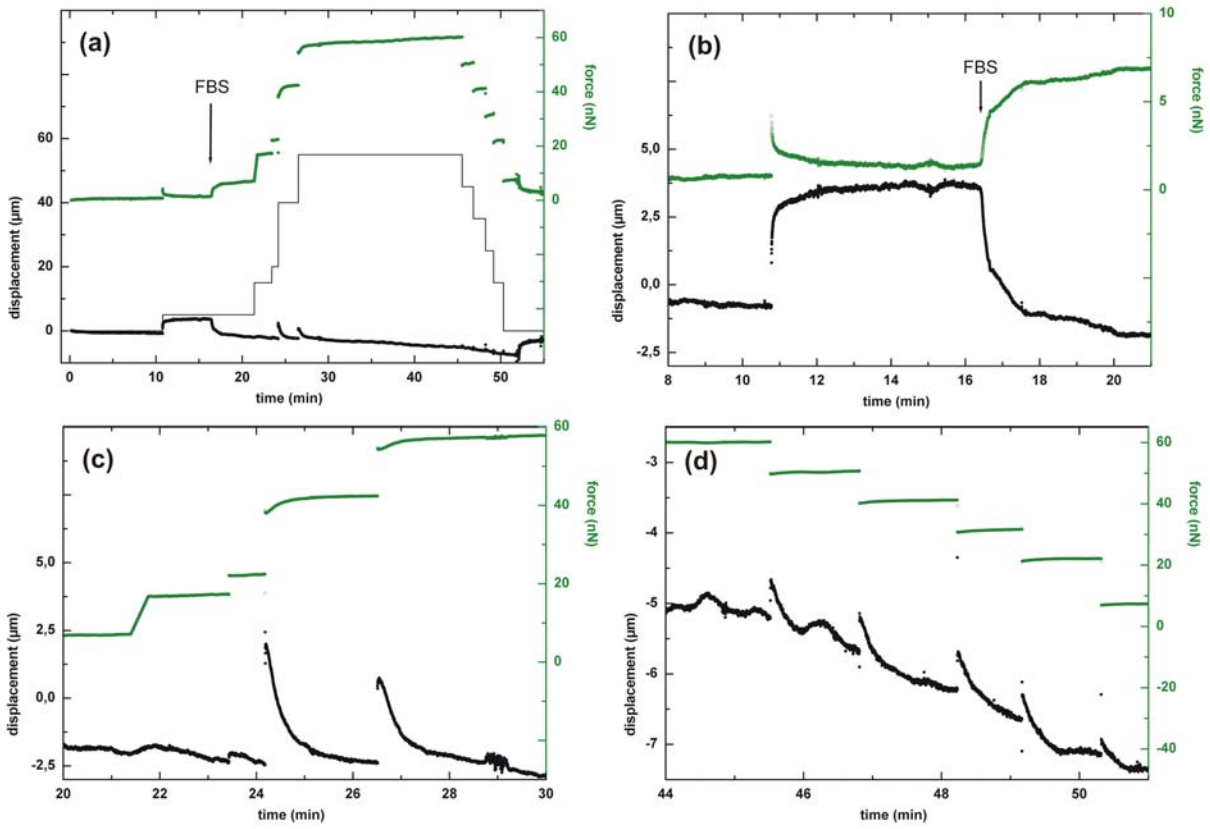

Figure 24: Stretching and spreading of a REF52 cell.
(a) Force (green plot) and cell displacement (black plot) measured as a function of time during the stretching of a REF cell. The stepwise changes of the flexible-microplate position are plotted as black solid-line. (b) Focus in the plot (a) from t = 8 min to 21 min: the FBS-mediated contraction of the cell can be observed after addition of FBS at t = 16 min. (c) Focus in the plot (a) from t = 20 min to 30 min: the flexible microplate is moved in order to increase the force; the cell's mechanical behaviour strongly depends on the rate, at which the microplate is translated. (d) Focus in the plot (a) from t = 44 min to 51 min: the flexible microplate is moved back to the initial position.

Step number	time [min]	microplate displacement [µm]	variation of force [nN]	variation of cell displacement [µm]	time constant [min]
1	10.8	5	3.4	4.5	-
addition of FBS	16.0	0	4.7	-4.9	0.38
2	21.4	10	9.7	0.3	-
3	23.5	5	4.7	0.3	-
4	24.2	20	15.7	4.5	0.34
5	26.5	15	12.2	3.1	0.40
6	45.5	-10	-10.5	0.5	0.42
7	46.8	-10	-10.5	0.6	0.30
8	48.2	-10	-10.5	0.5	0.38
9	49.1	-10	-10.3	0.5	0.28
10	50.3	-15	-15.2	0.2	0.17

Table 8: Analysis of each loading and unloading step.
For each displacement step of the flexible microplate, the correspondent variation of the force and cell displacement. If the cell displacement decreases exponentially, the corresponding time constant is given. FBS-mediated variations, occurring after its addition, are also indicated.

At t = 18 min, cell-generated force and cell displacement reach a temporary plateau. The FBS-mediated variation of cell displacement and force are respectively -4.9 µm and 4.7 nN. At t = 21.4 min step 2 begins: the microplate is moved of 10 µm at a rate of 30 µm.min^{-1}. The force increases linearly at a rate of 26.5 nN.min^{-1}, but surprisingly the cell displacement does not increase significantly (Figure 24, I). Even if the force variation is 9.7 nN, only a bulge of 0.3 µm is detected in the displacement as the force increases. In contrast, a sudden 5 µm step (step 3) induces a clear jump of 0.3 µm in displacement and 4.7 nN in force (Figure 24 I). Step 4 is a 20 µm step. Cell displacement and force jump respectively of 4.5 µm and 15.7 nN. During the first 2 seconds after the step, the force is decreases and the displacement relaxes to a higher plateau. After these few seconds, the cell displacement decreases exponentially with a constant of time τ = 0.35 min. Force and cell displacement reach stable values, respectively to 36.2 nN and -2.4 µm Cell mechanical behaviour is similar for step 5, a step of 15 µm. A few seconds after the sudden deformation, the cell displacement drops exponentially with a time constant τ = 0.37 min (Figure 25).

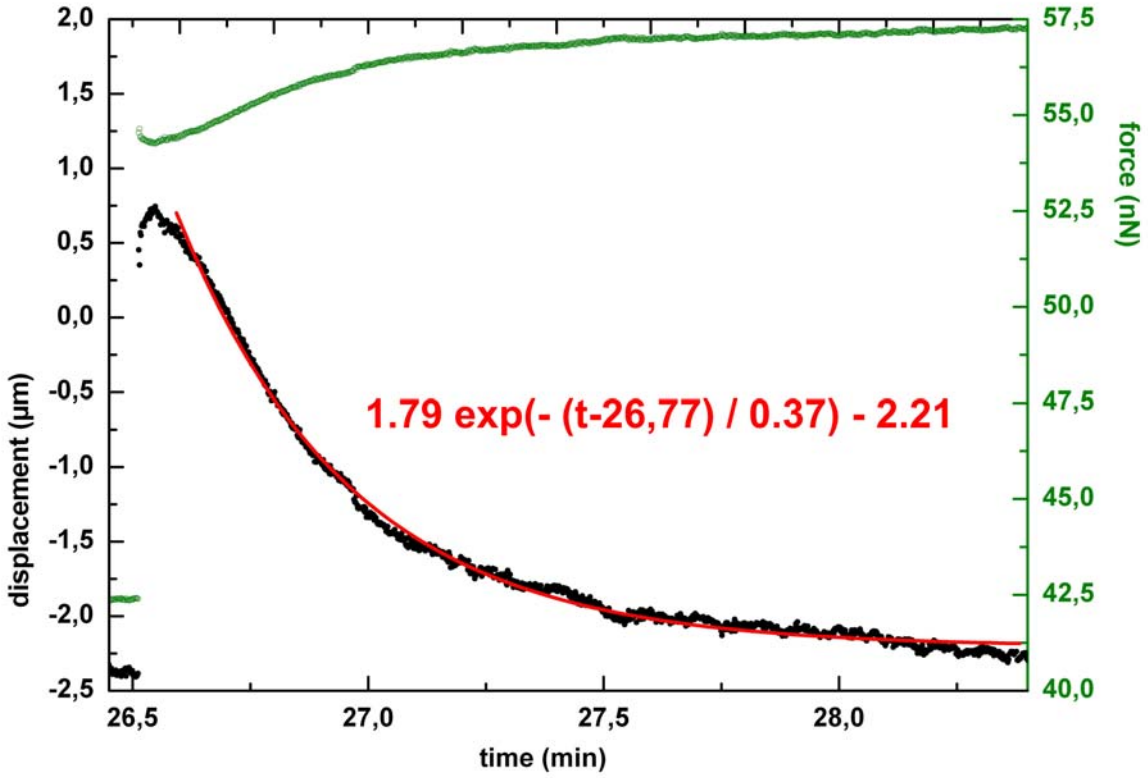

Figure 25: Focus on the step number 5 from Figure 24 (a) and (c).
Plots of the force (green) and the displacement (black) of the REF52 cell, after a sudden microplate translation of 15 µm. The fit function of the cell displacement is drawn as a solid red line.

After step 5, the position of the flexible microplate is not changed during ~ 20 min. During this period, the cell displacement decreases with a rate of -0.16 µm.min^{-1}. Symmetrically, the force increases with a rate of 0.16 nN.min^{-1}. The cell displays an apparent spring constant of 1 10^{-3} N.m^{-1}. After this period without mechanical perturbation of the cell, in 5 steps, the flexible microplate is translated to the initial position (Figure 24, (d)). The 4 first steps are 10 µm steps and the 5th, 15 µm. For each of these steps, the cell behaviour is similar. Variations of force and cell displacement are the same for the 10 µm steps: respectively -10.5 nN and 0.5 µm. The displacement decreases exponentially with a time constant of 0.23 min in average. A trend is superposed to the exponential decreases. This trend is roughly linear and causes a decrease of the displacement at a rate of -0.39 µm.min^{-1}.

3.5.2 Discussion

The first interesting point in this measurement is the coupling between cell mechanics and biochemical signal, for instance the signalling from FBS. The second piece of information is that the cell's mechanical response depends on rate and amplitude of simulations. The Kelvin model is not very useful to interpret this measurement, because neither the force, nor the cell displacement is kept constant. Two phenomena are superposed in this measurement. One is cell spreading and the second is cell contractile activity. The cell-generated force has consequently two potential origins. It seems to be possible to separate the effects of both mechanisms, because they act at different time scales. As a reference scale, a REF52 cell flattens on a FN-coated surface in ~ 30 min. The adhesion area does not increase further, only reorganisation occurs. As a cell spreads on the both microplates simultaneously, the cell-microplate adhesion area increases. For example, epithelial cells, such as panc-1 cells, present a limited spreading and the cell ends in a relatively stable state in which the cell adopts a catenoid-like shape. In contrast fibroblasts do not stop to spread on uniformed FN-coated microplates. In the final state, the fibroblast is like a 1 µm thick film gluing the microplates together. Mechanical assays, in such a case, give only weak information about cell mechanics. Adhesion rupture occurs before measurable deformation.
The cytoskeletal architecture of a spread cell and its adhesion to a surface are developed in response to the substrate mechanical properties, the presence and kind of cell-adhesion ligands and their density on the surface (Polte, T.R. 2004). Cell-adhesion ligands of FN can induce cell migration, but the entire FN molecule does not (Moyano, J.V. 2003). Interestingly, the formation of anchorage points is coupled to the force applied on the early bound integrins. If a force is applied, the formation of adhesion complexes is triggered (vinculin is recruited). An external force acts as a signal to strengthen cell adhesion (Galbraith, C.G. 2002). In comparison to a surface, a cell, spreading between the microplates, senses in additional a stress or/and a strain as the adhesion is built due to the defined distance between microplate. It suggests that the cell adhesion could be somehow favoured, if the spreading occurs between two microplates.
First, we comment the FBS-mediated contraction. The cell does not offer resistance to 5 µm deformation in serum free medium. The addition of FBS influence considerably and almost immediately the cell behaviour: suddenly the cell is able to contract. This contraction is sharp: it occurs at an initial rate of -20 $\mu m.min^{-1}$. In 2-3 min, the 5 µm displacement have been vanished. The cell contractility and consequently the cell generated forces origin in the cell's actomyosin machinery (Hörner, B. 1988). For example, the amoeba *Dictyostelium discoideum* is in biology a model-system to study multicellular morphogenesis. The following experiment has been done: mutant amoebae of lacking myosin II have been mixed with wild type amoebae. If the cell-cell contacts are not affected, mutant amoebae cannot resist to mechanical forces produced in the cell assembly and they accumulate at the periphery of the cell aggregate, where the stress is reduced (Shelden, E. 1995). Fibroblasts are also able of contractility. The serum-dependent contractility of cells has been observed in 'fibroblast fibres'. Fibroblast fibres have been formed by growing 3T3 Swiss fibroblasts in collagen. After 3-5 days incubation, such a fibre has been mounted between two posts. One post is fixed and the second is glue on a force transducer. The force generated by the sample is 3 times larger in presence of 30% serum than in serum free medium. The dose-response relationship for serum and force of these samples appears to be linear (Obara, K. 1995; Nobe, H. 2003). The FBS-mediated contraction observed in this measurement is attributed to the activation by FBS of cell contractility.
Second, now that the cell contractility is activated, is it possible to distinguish between spreading and uniaxial contraction in response to deformation? Spreading occurs during the measurement: the diameter of the cylinder-like cell increases with the time. In Figure 24 (a),

the cell displacement presents a slight decreasing trend. At the time t = 50 min, the cell displacement is about 7.5 µm smaller than at the commencement of the measurement. The spreading occurs almost linearly at low rate ~ 0.15 µm.min^{-1}. As the cell displacement varies exponentially during this measurement, a plateau is in 2-3 min. During this period, the spreading generates only a negligible decrease of the displacement (0.5 µm). Nevertheless, it should not be forgotten, that the cell is spreading and it influences probably the dynamic of its mechanical behaviour, even if the mechanical assay are achieved at a time scale smaller than the spreading time scale. As the force is vanished (Figure 24 (d)), the cell displacement decreases faster: remaining cellular strain is decreasing. In Figure 24 (c) and Table 8, effects of steps increasing the force are listed. The cell deforms of 0.3 µm, slightly and progressively, as the force is linearly increased under the slope of 10 µm. Abrupt steps induce force and displacement jumps: the cell behaves as an elastic material. Suddenly placed in a state in which stress and strain are increased, the cell contracts in order to annihilate exponentially the strain. As the stress is decreased stepwise (Figure 24 (d) and Table 8), the cell is expected to display an elastic behaviour, but in fact, the cell presents stiffening. The cell displacement does not decrease, but increases slightly (~ 0.5 µm) and than relaxes. A translation of the flexible microplate induces a proportional cell displacement, if the force variation is positive (see Table 8). In contrast, if the force variation is negative, the cell first resists to the sudden compression and after takes advantage of it to probably reorganise its cytoskeleton and then continues to spread. The characteristic time, at which the displacement relaxes, is 0.23 min in average. It could be interpreted as the time that the cell needs to reorganise after the mechanical perturbations. This time constant is ~ 1.4 times smaller than the time constant measured after an increase of the force. It seems, that cells adapt by cytoskeletal reorganisation faster after a load decrease than after an increase.

3.6 Influence of the Control Rate on Measurements

In the previous section, it has been shown, that the mechanical response of a cell depends on the rate at which a cell deformation is applied. A jump of several µm of the microplate position in 100 ms results in jumps of the force and displacement values, whereas a translation at constant rate induces an increase of the force at a constant rate also, but almost no cell displacement. Is it possible to establish a relationship rate-cell mechanical behaviour? Different rates have been tried, in order to address this question.

3.6.1 Results

A human pancreas cancer cell (Panc-1) has been used for this measurement in medium with serum. The control rate has been varied in the range of 0.25 to 2 $\mu m.s^{-1}$. As a comparison, a jump is achieved at a rate on the order of 100 $\mu m.s^{-1}$. The force set-value is 250 nN. The force increases to this value and then immediately decreased to the zero-force. This cycle is repeated 4 times for each of the following control rates: 0.25, 0.5, 1.0 and 2.0 $\mu m.s^{-1}$. To increase the control rate, the control step is increased. The control time-lapse is kept constant at 100 ms, except for the lower rate, which has been achieved with a control time-lapse of 200 ms and a control step of 0.05 µm – the smallest step that the piezoelectric transducer can make. Increase of force and displacement are linear function of the time. Their decrease is only partly linear.

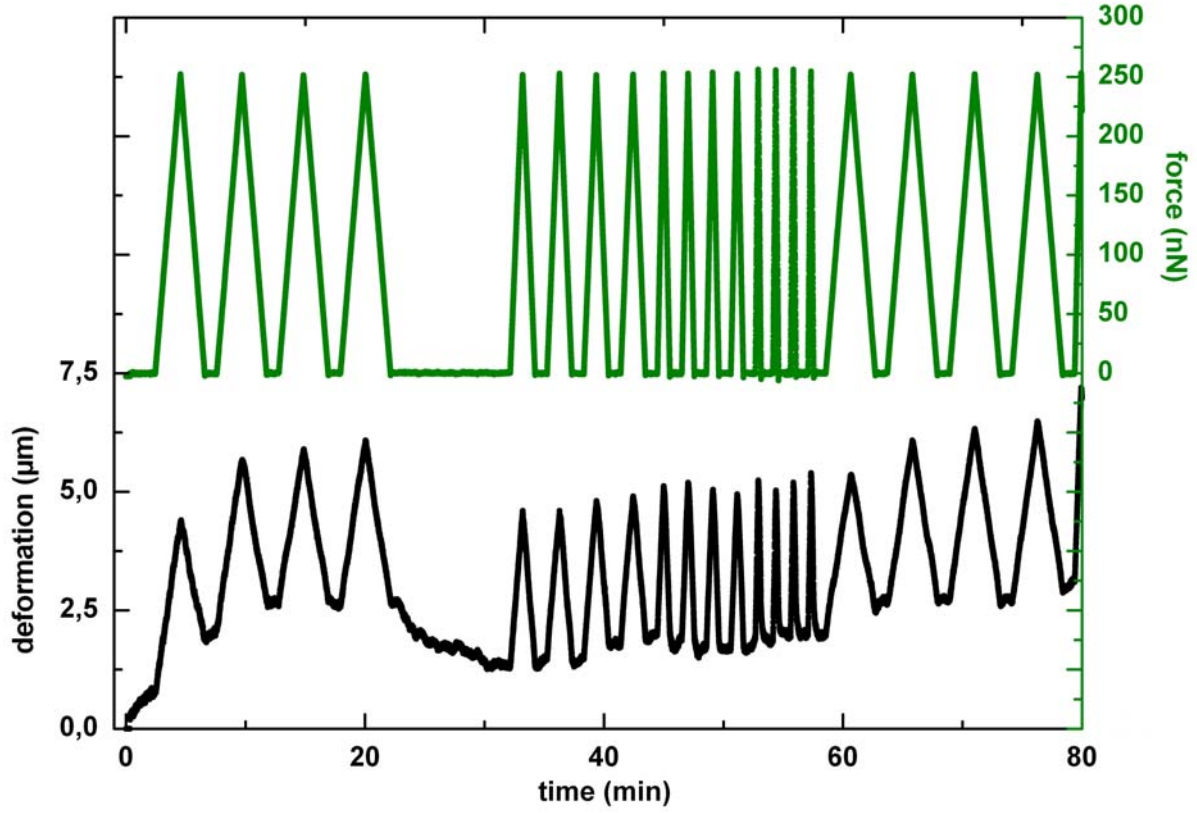

Figure 26: Periodic stretching of a Panc-1 cell at different rates.
The force (green curve) is controlled during this measurement. Triangle-like force cycles are repeated and applied at different control rates (0.25, 0.5, 1.0 and 2.0 $\mu m.s^{-1}$, and 0.25 $\mu m.s^{-1}$ again). For each rate, the cycle is repeated four times. The cell displacement is plotted as a function of time (black curve).

This looks like a hysteresis loop in a force-displacement graph. The linearity during the stretching is used to measure force rate and displacement rate, which result both from the reaction of the cell to the control rate. The Figure 26 presents the recording of force (green) and cell displacement (black) as a function of time.

3.6.2 Discussion

The Figure 27, (a) shows variation with the time of the control rate (open circles). The displacement rate is proportional to the control rate. It represents ~ 10% of the control rate.

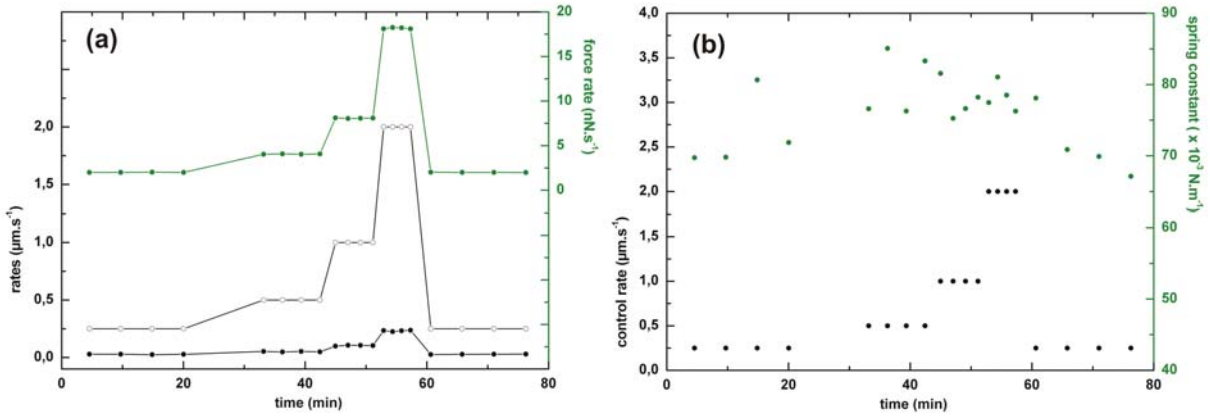

Figure 27: Force rate, displacement rate and cell spring constant at different control rates for a Panc-1 cell. *(a) Control (open circles), cell displacement (black filled circles) and force (green filled circles) rates measured for each cycle are plotted as function of time. (b) Control rate (black filled circles) and loading/unloading spring constant (green filled circles) also as a function of time.*

This shows the resistance of the cell to a deformation: only 10% of the control step is converted in an effective cell displacement. The rest of 90% is converted in bending of the microplate, so in force generation. A loading/unloading spring constant can be defined as the ratio of force rate to cell displacement rate. The value is plotted in the Figure 27, (b). At the same rate, variations of 5% of this value occur accidentally due to the cell. The dependence of the loading/unloading spring constant on the control rate in the range of rate explored is very weak. It can be considered that mechanical properties of panc-1 cells are not dramatically influence by the control rate in the range of 0.25 to 2 µm.s^{-1}.This appears to be cell-type dependent. For example, in the section 3.3, Table 6, for a REF52 cell, the control step in converted at 50% in cell displacement and not 10% as for the panc-1 cells.

In the next chapter, the panc-1 cell mechanics will be studied in more details and under different conditions.

4 Coupling between Serum, Bioactive Lipids, and Mechanics of Human Pancreas Cancer Cells

This chapter focuses on human pancreas cancer cells (panc-1) and their mechanical behaviour. Connections will be established between mechanical behaviour of panc-1 cells and biochemical signaling. Serum and two bioactive lipids, lysophosphatidic acid (LPA) and sphingosylphosphorylcholine (SPC) influence the cell mechanics.

The cell line named Panc-1 has been established after 73 passages from a pancreatic carcinoma of ductal origin from a 56-year-old Caucasian male. Therefore the cell line origins from an epithelium. Cells in Petri dishes present effectively an epithelial morphology. A basic observation in phase contrast of cell cultures reveals some cell-population characteristics. Cells favour cell-cell contacts leading to the formation of cell islands and cells do not spread as much as fibroblasts do: Panc-1 cells keep a certain volume on the surface, whereas fibroblasts flatten more building an actin stress fibres-based scaffold under tension. Panc-1 cells have been transformed *in vivo*, because they are cancerous cells and also *in vitro,* because of these 73 passages, nevertheless they kept properties from the original pancreatic duct cells: first they tend to establish cell-cell contact and second, they mainly express keratin pair K8/K18, but lack vimentin – human pancreatic cells express keratins K7, K8, K18 and K19 (Micoulet, A. 2003). In comparison to fibroblasts, the cytoskeleton of epithelial cells contains a new component: an assembly of keratin proteins. Keratins belong to the third kind of cytoskeletal filaments, named intermediate filaments (IFs), besides MTs and actin filaments. The expression of IFs, and specially keratin filaments, in cells is strongly cell-type-dependent. For example, embryonic fibroblasts contain vimentin IFs, but no keratin. Panc-1 cells express only keratin, but no vimentin. The epithelial cell line PtK2 established from a kidney of a normal adult male potoroo contains a vimentin assembly and a keratin assembly (Yoon, K.H. 2001). The IF-proteins are classified into five distinct types. Type I and II are the keratin family. The type-III-IF-proteins include in particular vimentin, desmin. Expressed only in neurons, the type IV is composed of neurofilament subunits. Finally, the nuclear IF-proteins lamin A, C, B1 and B2 compose the type-V group. The 10-12 nm diameter of IFs place them between actin filament and microtubule. The elementary unit of IFs is a rod-like dimer: ~ 45 nm long and ~ 2-3 nm thin. The dimerisation occurs through interaction between two α-helical peptidic chains oriented in parallel and intertwined in a coiled-coil rod. An acidic type-I keratin and a basic type-II keratin assemble in a heteromeric unit, whereas two vimentin copies associate in a homomeric unit. *In vitro* studies have shown that the IF assembly takes place in a three-step process (Chang, L. 2004). Tetramer formation is the first assembly step. Lateral interactions play an important role at this step – *in viv*o, the tetramers are the smallest soluble so far detected.
A sudden increase of ionic strength initiates polymerisation of vimentin *in vitro* – similarly to actin polymerisation. In less than 2 sec, tetramers assemble in larger hole-cylinder-like object, named units-length filaments: ~ 60 nm long and 16 nm in diameter (Hermann, H. 1999; Strelkov, S.V. 2003). These units-length filaments aggregate longitudinally in longer filaments of same diameter. After 10 min, the population of 100 nm filaments is dominant. At

one hour time-point, vimentin filaments are several μm long and their diameter decreased to ~ 11 nm. The diameter reduction is supposed to be a consequence of a lateral rearrangement of subunits leading to radial compaction.
Keratins (40-70 kD) are expressed in an organ and/or cell-type specific manner in epithelial cells, and are the major structural protein in these cells. Keratins constitute the largest group of IF building proteins. Type-I keratins (K9 to K20) are acid, whereas type-II keratins (K1 to K8) are relatively basic. All epithelial cells express in a 1:1 molar ratio type I keratins and type II keratins. For example, mouse pancreatic acinar cells express K8, K18 and K19 such that the amount of K8 copies equals the amount of K18 and K19 copies. For example, in cultured human colonic HT29 tumour cells, keratins K8, K18 and K19 represent 5% of the total cellular protein (Chou C.F., 1993) and 0.3% of the total tissue protein content in mouse pancreas (Zhong B. 2004). This abundance is correlated with keratin function. Keratins protect epithelial cells from mechanical and non-mechanical forms of injury. Tissue-specific injury of mouse pancreas, for example, induces over-expression of keratins reaching a maximum 2 days after the injury and is maintained at this level. Pancreatic tissue recovery occurs in 10 days after the injury (Zhong B. 2004). What is happening at the scale of an epithelial cell during tissue injury? The tissue-specific injury in question is a pancreatitis artificially induced by injections of a drug named caerulein. Pancreatitis is consisting in a premature activation of digestive enzymes in the pancreas. Enzymes start digesting the pancreas itself. Histological sections show important turnover in the tissue structure. Lesions appear and result in a local generation of forces applied to cells. The keratin cytoskeleton acts as a mechanical scaffold: it distributes and balances these forces and thus protects cells. The same happens in the skin. Keratin K4 and K15 assemble to form the keratin cytofilaments. Cytoskeletons of neighbour cells are connected together by strong cell-cell junctions called desmosomes. Thus, a keratin scaffold is built through the whole epithelium and protects it from mechanical trauma (Fuchs, E. 1998).
In the cytoplasma, keratin solubility is highly dynamic and varies profoundly depending on the keratin pair and the physiologic state of the cell (mitosis, cell stress…). Simple epithelial keratins K8/K18 pairs are among the most soluble: approximately 5% is soluble at basal conditions. Phosphorylation plays an important role in regulating keratin solubility, and differences occur in site-specific phosphorylation depending on the soluble versus cytoskeletal partitioning of the keratin (Omary, M. B. 1998 and Coulombe, P.A. 2002).

Rheological properties of the pair wise assembly of keratin I and II in solution have been characterised *in vitro* (Ma, L. 1999; Yamada, S. 2002). 1 $mg.ml^{-1}$ suspensions of polymerised vimentin or polymerized K4/K15 keratin raintain a constant elastic and viscous modulus, respectively G' ~ 2-4 Pa and G'' ~ G/10, until a 10% strain is reached. The phase shift is small: $\delta \sim 8\text{-}10°$ indicating that the suspensions behave as viscoelastic solid. For a strain superior at 10%, keratin-suspension storage modulus drops down. It becomes smaller than the loss modulus for a strain of 300%. The keratin suspension displays then liquid-like properties. As a comparison, for actin gel G' ~ 1 Pa and a phase shift of ~ 25 degrees. The cell cortex *in vivo* displays G' ~ 100 Pa and a phase shift of ~ 10-15 degrees (Ma, L. 1999).

Are there interactions between IFs, MTs and actin filaments?
In REF52 cells, a protein named plectin (~ 500 kD) has been shown to decorate and associate with vimentin IFs. Immunoelectron microscopy has evidenced that plectin cross-bridges between IFs themselves, IFs and MTs, IFs and actin filament, and even IFs and myosin filaments (Svitkina, T.M., 1996). Without detailed explanations, it should be mention that the vimentin IFs are interacting with MTs via kinesin and dynein motor-proteins, whereas keratin-IFs interact with the actin-filaments (Chang, L. 2004).

After an introduction about the IFs, briefly, the bioactive lipids LPA and SPC will be now introduced.
LPA and SPC are both potent mitogen factors. LPA is not present at significant concentration in blood plasma, whereas SPC occurs naturally in it.
LPA is a water-soluble glycerophospholipid generated and released by activated cells, notably platelets (blood clotting), fibroblasts and leukocytes. It is therefore considered to be a mediator in wound healing and tissue regeneration. Among the biological responses to LPA are platelet aggregation, induction of cell growth, smooth muscle contraction, actin stress-fibre formation, focal-adhesion assembly and many others (Cremers, B. 2003). LPA is present at elevated levels in ascites and plasma of ovarian cancer patients, and may contribute to the progression of certain types of human cancer (Fang, X. 2000).
SPC is also involved in numerous biological processes, including proliferation, cell migration and wound healing. SPC levels are increased in blood and malignant ascites of patients with ovarian cancer. Thus, SPC could have an important function in cancer biology, in particular in metastasis, as SPC can stimulate cell migration (Boguslawski G., 2000). Interestingly in Panc-1 cells, SPC induces keratin cytofilaments reorganisation (Micoulet, A. 2003). The effect on keratin assembly is concentration-dependent and time-dependent. At 10 µM SPC concentration and after 45 minutes incubation, the keratin-reorganisation is complete.

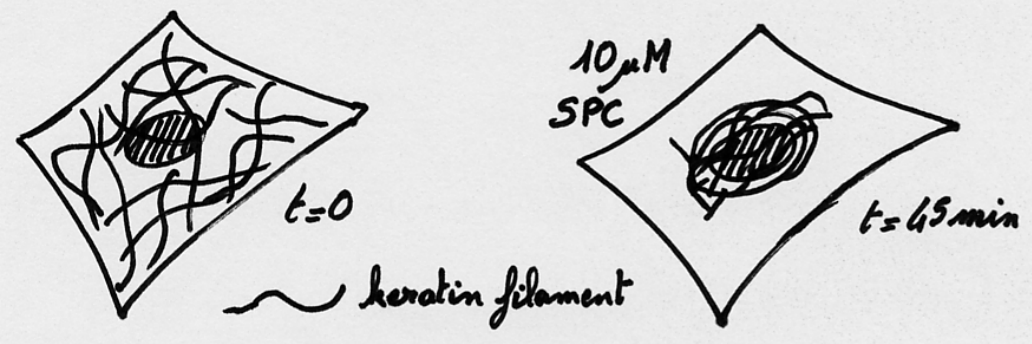

Figure 28: Schematic representation of the keratin K8/K18 reorganisation in the presence of SPC.
45 min incubation at 10 µM are sufficient to obtain the complete keratin reorganisation induced by SPC. Adapted from Micoulet, A. 2003

The keratin cytoskeleton initially spread through the cytoplasm is, after SPC treatment, reorganized in a ring-like structure around the cell nucleus. SPC induces keratin phosphorylation, which is already known to be connected with keratin assembly turnover. Effect of SPC on keratin is largely independent of the other cytoskeleton components, actin filaments and MTs. The cell pre-incubation with drugs affecting actin and tubulin polymerisation do not block or modify keratin reorganisation by SPC. The following drugs have been tested: cytochalasin D (which favours actin depolymerisation), jasplakinolide (which favours actin polymerisation), nacodazole (which disrupts MTs) and taxol (which stabilize MTs). SPC exerts its effect on keratin assembly independently of other major cytoskeletal components. The SPC-mediated keratin reorganisation required metabolic energy.

Because of the specific SPC-mediated reorganisation of keratin in panc-1 cell, the characterisation of cellular mechanical properties in absence and in presence of SPC is interesting. Does the keratin reorganisation change the cell viscoelasticity? LPA reorganise the actin cytoskeleton, but not the keratin cytoskeleton. Does it affect the cell viscoelasticity? These questions have been addressed by uniaxial stretching of panc-1 cell in serum free medium, in presence of serum, in presence of SPC, in presence of LPA and finally in presence of LPA and SPC.

4.1 Mechanical Behaviour of Human Pancreas Cancer Cells in Serum Free Medium

The aim of this measurement is to understand the influence on the cell's mechanical behaviour of the presence of serum in the medium. The serum or precisely foetal bovine serum (FBS) contains proteins and polypeptides such as albumin (40-80 $mg.ml^{-1}$), FN (1-10 $\mu g.\ ml^{-1}$), a cell-adhesion ligand. It contains also protease inhibitors, growth-factors (1-100 $ng.\ ml^{-1}$), amino acids, lipids such LPA (several nM), carbohydrates, iron, zinc, hormones, vitamins… (Freshney, R.I. 2000). FBS induces cell contractility and the formation of actin stress fibres (Nobe, H. 2003).

4.1.1 Results

Panc-1 cells have been kept in serum-free suspension for two hours. Serum-free means, that the medium contains DMEM and L-glutamine, but no FBS.

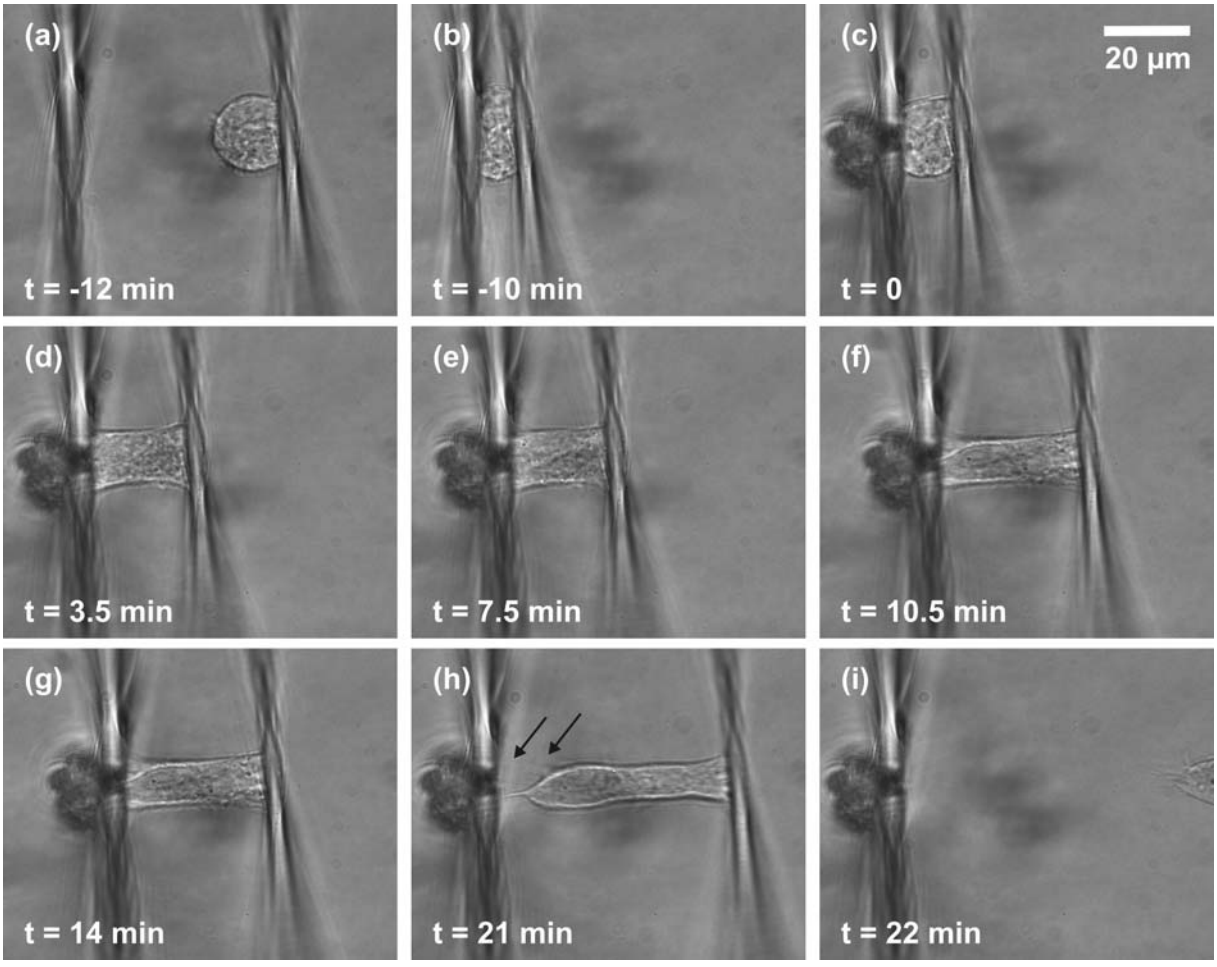

Figure 29: Stretching of a Panc-1 cell chemically bound to the microplates in serum free medium.
The cell displacement has been controlled during this measurement. (a) Both, rigid (right) and flexible (left) microplates place parallel to each other. The Panc-1 cell adheres already on the rigid microplate. (b) The cell is pressed between the microplates in order to obtain adhesion. (c) Applied forces are vanished. The initial cell displacement equals ~ 10 µm. The optical fibre has been placed in contact with the flexible microplate. (d) and (e) 10 µm displacement with respect to the initial position. (f) and (g) 20 µm displacement with respect to the initial position. (h) Rupture of cell adhesion. The black arrows indicate tethers, pulled out of the plasma membrane. It indicates that adhesion protein-complexes break likely in the cell. (i) Unloaded flexible microplate (zero-force).

In suspension, the lack of adhesion, the absence of growth factors and certain bioactive lipid such LPA, which are usually added in the culture medium with the addition of FBS, induce the down regulation of actin polymerisation and cell contractility (Seufferlein, T. 1994; Ren, X.-D., 1999). The liquid-chamber is filled with serum-free medium during the measurement. Microplates are previously functionalized with amino-silane and then with glutaraldehyde (see section 2.2.3). On such microplates, the cell adherence is not a biological adhesion. Integrins do not find any ECM ligands to bind. Cell adhesion to the microplates occurs through the formation of covalent bounds. Aldehyde groups react with the amino-groups present in the trans-membrane proteins (for example, the side chains of the amino-acids lysine and arginine are terminated with amino groups). The rigid microplate is gently pressed on a cell, which was on the liquid-chamber bottom. A cell-microplate contact is established. Cells do not spread or not too fast on this kind of surface. More than 30 min after the first contact with the microplate, the cell did not spread more. After careful micromanipulation, both microplates are set as shown in the micrograph (a), Figure 29. As fast as possible, the cell is pressed between the microplates in order to obtain adherence on the flexible microplate (Figure 29, (b)). This compression is maintained during 10 min. At t = 0, the compression is vanished and the measurement begins (Figure 29, (c)). The force equals the zero-force (Figure 30). The mechanical assay consists in a step-like increase of the cell displacement. The displacement is increased or decreased at a constant rate until the displacement reached the set-value. The control rate is 0.5 $\mu m.s^{-1}$. Under this control, the cell imposes the displacement rate, which appears to be constant during displacement variations (Table 9) at 0.25 $\mu m.s^{-1}$ in average.

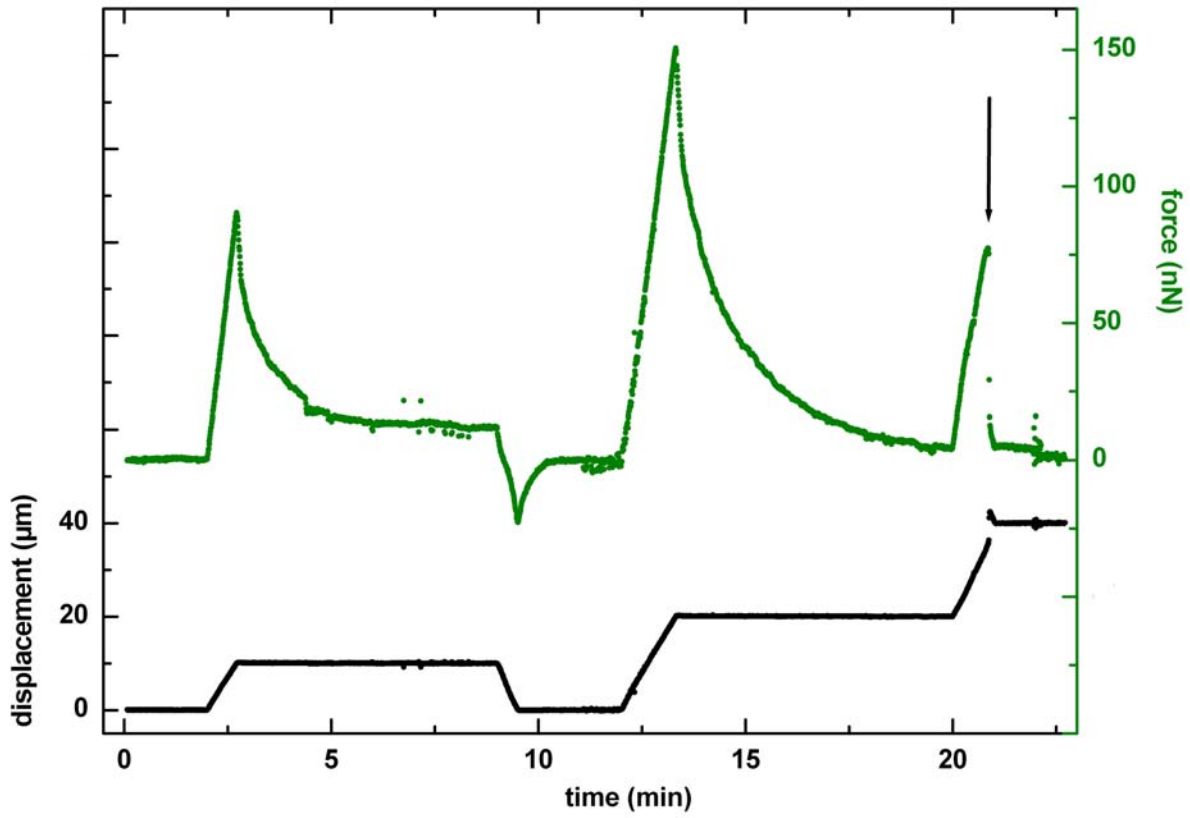

Figure 30: Stretching of a Panc-1 cell chemically bound to the microplates in serum free medium
Recording of cell generated force (blue) and cell displacement (black) under uniaxial controlled displacement. The rupture of cell adhesion is marked with a black arrow.

During the loading and unloading, the apparent linearity allows the definition of a loading/unloading spring-constant. Spring constant and displacement rate values are listed in Table 9. The displacement variations are the following (black curve in Figure 30). First, the initial distance between microplates is maintained at ~ 11.5 µm: this cell state defines the zero-displacement. In the course of time, the set-displacement takes successively the following values: 10, 0, 20 and 40 µm. The zero-displacement value is maintained ~ 2 min, whereas displacements at 10 and 20 µm are maintained for ~ 6 min. The displacement at 40 µm is not reached, because a rupture of the adhesion on the flexible microplate occurs at the time 21 min, before the set-value of 40 µm has been reached (black arrow in Figure 30 and micrograph (h) in Figure 29). Between the microplates, the cell takes a cylinder-like shape. The cylinder diameter can be evaluated with help of the micrographs (d)-(g), Figure 29. At initial displacement, 10 µm and 20 µm displacement, the diameter equals respectively 19 ± 2 µm, 14 ± 1 µm and 11 ± 1 µm. The cell-generated force is plotted in blue in Figure 30. During loading, the force increases linearly with the time. As the displacement is maintained constant, the force drops: the cell displays a stress relaxation. After the 10 µm displacement (until t ~ 9 min), the cell has to be pressed (negative force) in order to reach and to maintain the zero-displacement, which has been set. The negative peak-force reaches ~ -22 nN and then the cellular stress relaxes to the zero-force. When the force value is stable (t ~ 12 min), a 20 µm displacement is applied to the cell. As previously, the cell behaviour is elastic until the set displacement is reached and then the force relaxes.

The absolute force values given in nN are not known very accurately for this measurement, because the flexible microplate could not be calibrated. The spring-constant used to calculate the force is the mean value of force-sensors pulled with the same parameters. However, the variation of the force during this measurement can be exactly compared. The comparison of absolute value with other measurement or reference values has to be done with precaution.

	Loading / unloading parameters		**Kelvin model parameters**			
displacement	**rate**	**spring constant**	μ_0	μ_1	$\tau_\varepsilon = \eta_1 / \mu_1$	η_1
[µm]	[µm.s^{-1}]	[x 10^{-3} N.m^{-1}]	[N.m^{-1}]	[N.m^{-1}]	[min]	[10^3 N.s.m^{-1}]
10	0.23	9.0	570	2480	0.890	132
0	-0.35	3.8	14	1090	0.285	18.6
20	0.25	8.0	183	3300	1.430	283
(40)	0.29	5.2	-	-	-	-

Table 9: Viscoelastic parameters of a Panc-1 cell chemically bound to microplates in serum free medium.
The parameters are calculated by fitting data points with the relaxation function of the Kelvin mechanical model. The initial cell displacement equals 11.5 ± 0.5 µm. The error on the displacement is ± 0.5 µm; rate, ± 0.02 µm.s^{-1}; loading/unloading spring constant, ± 0.05 N.m^{-1}; spring constant μ_0, ± 10 N.m^{-1}; spring constant μ_1, ± 15 N.m^{-1}; time constant, ± 0.005 min; coefficient of viscosity, 10 10^3 N.s.m^{-1}

4.1.2 Discussion

For the 10 µm and 20 µm displacement steps, the set-displacement has been reached respectively in ~ 42 s and ~ 82 s. The displacement rate equals 0.25 µm.s^{-1} in average. It

increases slightly as the displacement increases. The displacement rate of cell compression equals -0.35 µm.s^{-1}. The loading/unloading spring constant in compression state is ~ 2 times smaller than in stretching state. This indicates that the 0.05 µm control step (made each 100 ms) is ~ 2 times more efficient to induce cell deformation, if the cell is compressed, than if it is stretched. This shows that the cell resists to stretching in comparison to small compression. This spring constant is also decreasing slightly with increase of the displacement plateau. Relaxations of the force occur over intervals longer than 5 min in both cases. The performed displacement steps can be considered as an experimental approximation of Heaviside step function of displacement. The force relaxation can be efficiently fitted using the relaxation function of the Kelvin model. The resulting viscoelastic coefficients μ_0, μ_1, η_1 are given in Table 9. The parameter μ_0 is much smaller than μ_1. One deduces that the spring mount in parallel in the Kelvin body is negligible in this case: panc-1 cells in serum free medium behave almost as a Maxwell body in stretching regime. The parameter μ_1 increases of a factor ~ 1.4, as the displacement step is doubled, whereas the parameter μ_0 decreases of a factor ~ 3.0. The viscosity coefficient η_1 increases of a factor ~ 2.1 under the same conditions. Panc-1 cells appear to become stiffer and more viscous as the cell displacement is increased. The more the cell is deformed, the more difficult it is to deform it. This could be a demonstration of mechanism of protection against mechanical injuries. It has been shown that in pancreatic cells the keratin cytoskeleton achieves this role of mechanical protection in living tissue (Zhong B. 2004).

It is now interesting to compare these parameters with those characteristic for fibroblasts obtained in the section 3.3, Table 6. In both case, the adhesion is chemical. This kind of adhesion may perturb the actin cytoskeleton organisation. But, the fact that the cell contracts between the microplates, when adhering on such surfaces and that the use of drugs such as cytochalasin D inhibits the contractility (Thoumine, O. 1997) demonstrate, that the actin cytoskeleton definitely contributes to the mechanical response, despite the chemical adhesion. We can compare: on one side, the mechanical response of a fibroblast in medium with serum and on the other side, the mechanical response of an epithelial cell (panc-1) in serum free medium. In serum-free medium, a down regulation of the actin-cytoskeleton activity is expected (Nobe, H. 2003). For the interpretation, one could model the both cells as follow. The fibroblast's mechanical behaviour is dominated by the actin cytoskeleton, whereas the epithelial-cell's mechanical behaviour is composed of the keratin cytoskeleton and a "weak" actin cytoskeleton. As the displacement plateau-value is increased, the parameter values differ on three points: μ_0 increases slightly in fibroblasts, but it decreases in epithelial cells; μ_1 and η_1 decreases in fibroblasts, but it increases in epithelial cell. One could make the following interpretation: μ_0 represent mainly the mechanical resistance produced by the actin cytoskeleton, but μ_1 and η_1 reflect chiefly the IFs cytoskeleton (vimentin IFs in fibroblasts and keratin IFs in epithelial cells).

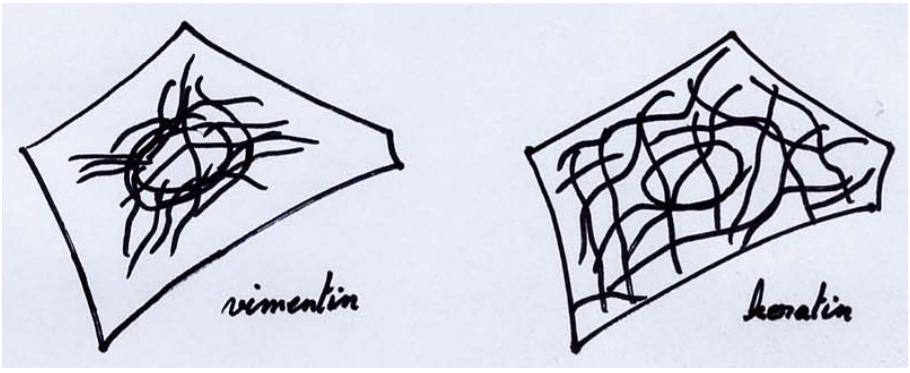

Figure 31: Schematic representation of vimentin and keratin assemblies in epithelial cell.
Potoroo kidney cell, PtK2 epithelial-like express vimentin in keratin. The cytoplasmic distribution of these IFs is different. Inspired from Yoon, K.H. 2001

The treatment with cytochalasin D – it is believed to act via the binding of cytochalasin to actin monomers and consequently prevent polymerisation – reduces the peak-force value (Thoumine, O. 1997). According to the Kelvin model, the peak-force is proportional to $\mu_0 + \mu_1$ (Table 2). This remark comforts the link between μ_0 and actin cytoskeleton. How about the parameters μ_1 and η_1? Fibroblasts have a vimentin cytoskeleton, whereas panc-1 cells have a keratin cytoskeleton. The assemblies of vimentin and keratin are different in a cell. The vimentin filaments spread from the nucleus to the cell membrane, but their density is much higher close to the nucleus. The keratin filaments spread everywhere in the cytoplasm at the same density (Figure 31) (Yoon, K.H. 2001). Because of a difference in assembly architecture, the mechanical properties should be also different. One can hypothesise that the keratin cytoskeleton, because of its repartition in the cell, is able to have a greater contribution than the vimentin cytoskeleton to the cell's mechanical behaviour. This hypothesis allows for understanding that the parameter μ_1 increases in epithelial cells, but decreases slightly in fibroblasts, and respectively, that the parameter η_1 increases in epithelial cells, but decreases in fibroblasts.

In compression, the relaxation time constant is smaller than in stretching. It could be due to the cell nucleus, which displays a higher elastic modulus than the cytoplasm and for this reason could accelerate the relaxation after compression. In endothelial cells, the elastic modulus of the nucleus is evaluated to 5000 Pa, which is 10 times greater than the cytoplasm (Caille, N. 2002). The elastic modulus of the whole cell is evaluated to ~ 20 Pa in compression, which is much smaller.

Finally, the elastic moduli and viscosity of the panc-1 cell can be evaluated. The ratio $S / u(0)$ equals 24.7 µm, 7.2 µm and 3.0 µm (error: ± 1 µm), respectively at 11.5 µm, 21.5 µm and 31.5 µm total displacement. Under 10 µm displacement, it is found that the corresponding elastic moduli to the parameters μ_0, μ_1, η_1 are respectively ~ 80 10^6 Pa, ~ 350 10^6 Pa and ~ 20 10^9 Pa.s. Under 20 µm displacement, respectively ~ 60 10^6 Pa, ~ 1100 10^6 Pa and 100 10^9 Pa.s. Both elastic moduli are ~ 100-1000 times larger than elastic moduli and viscosity of embryonic fibroblasts, evaluated to respectively ~ 1 10^3 Pa and ~ 1 10^4 Pa.s (Thoumine, O. 1997). It is consistent with the presence of the keratin cytoskeleton in epithelial cells. As a comparison, such high values of viscosity are reached in warm asphalt (~ 1 10^3 Pa.s) or in incandescent lava (~ 1-10^6 10^6 Pa.s).

4.2 Mechanical Behaviour of Human Pancreas Cancer Cells in Presence of Serum

In order to have a reference measurement, the mechanical properties of a panc-1 cells have been tested in culture medium, meaning DMEM supplemented with 1% L-glutamine and 10% serum (FBS). As described in the section 2.4.1, the micro-manipulation to place the cell between the microplates has been performed in serum free medium. 10 min after the cell has been in contact with the both microplates, serum (FBS) has been added in order to obtain a medium at 10% FBS in the liquid-chamber. A period of 75 min elapses, before the commencement of the monitoring at the time t = 0 (Figure 32). During this time lapse, the optical fibre has been positioned (after the cell has been placed between the microplates for this measurement) and the cell adheres on the FN-coated microplates.

4.2.1 Results

The measurement has been performed under control of cell displacement. The imposed changes of cell displacement are plotted as a function of time in Figure 32 (black curve). The cell response can be read as the generated force also plotted as a function of time in this figure (green curve). A series of 2.5 µm displacement steps have been accomplished at a control rate of 0.5 µm.s^{-1}. Each ~ 12 min, the cell displacement is increased of 2.5 µm.

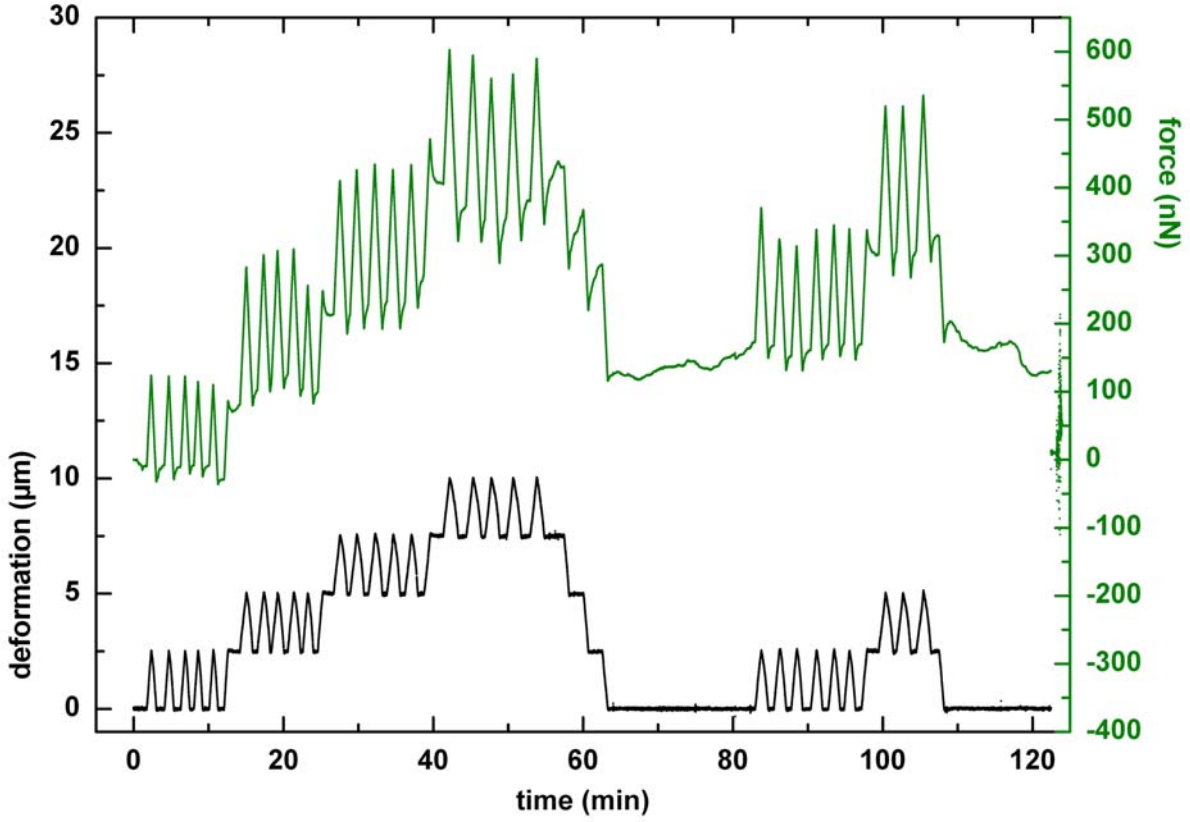

Figure 32: Mechanical assay of a Panc-1 cell in culture medium.
This plot presents a mechanical assay of a Panc-1 cell. A periodic mechanical excitation of a period of ~ 2-3 min is superposed to an increasing trend of the displacement (black curve). The mechanical response of the cell is given as the generated force (green curve). At constant rate displacement, the cell behaviour is elastic. At constant displacement, the force behaves as the relaxation function described by the Kelvin model. It highlights the viscosity of the cell. The errors on the values are ± 5 nN and ± 0.5 µm respectively for the force values and the displacement values.

This stepwise increase occurs 3 times at t = 12.5, 25.0 and 40.0 min, at this last time, it reaches 7.5 µm. Then, the cell displacement is decreased to the initial displacement (zero displacement in Figure 32) in three steps back (at t ~ 60 min). After a resting period of 20 min, at t = 98 min, a 2.5 µm step has been made and maintained for 10 min. A periodic displacement is superposed to this displacement-trend. The cell displacement increases linearly of 2.5 µm more and then drops to the present trend-value as the 2.5 µm additional displacement has been reached. These displacement cycles occurs each 2-3 min. They can be considered as a regular evaluation of the cell's mechanical properties over time. The cell displacement rate, which is imposed by the cell in reaction to the control rate, is constant during this measurement. In average, it equals ~ 0.065 $\mu m.s^{-1}$. In Figure 33, the generated force is plotted as function of the cell displacement. Each displacement cycles display a hysteresis. This hysteresis increases as the displacement-trend increases (Figure 33). The first five cycles (from 0 the 2.5 µm) present a good reproducibility. The series of cycles at other displacement plateau values present eventually a small force-offset, but the shape of the hysteresis loop is well conserved from cycle to cycle. After the resting period, the force is shifted of ~ 100 nN higher. For each cycle, the force increase is almost always linear, whereas the force decrease is partly linear. The force decreases first faster than it increased as a function of the displacement. After, it decreases almost as it increased before (Figure 33). After the time t = 110 min, cell adhesion deteriorate suddenly until it ruptures.

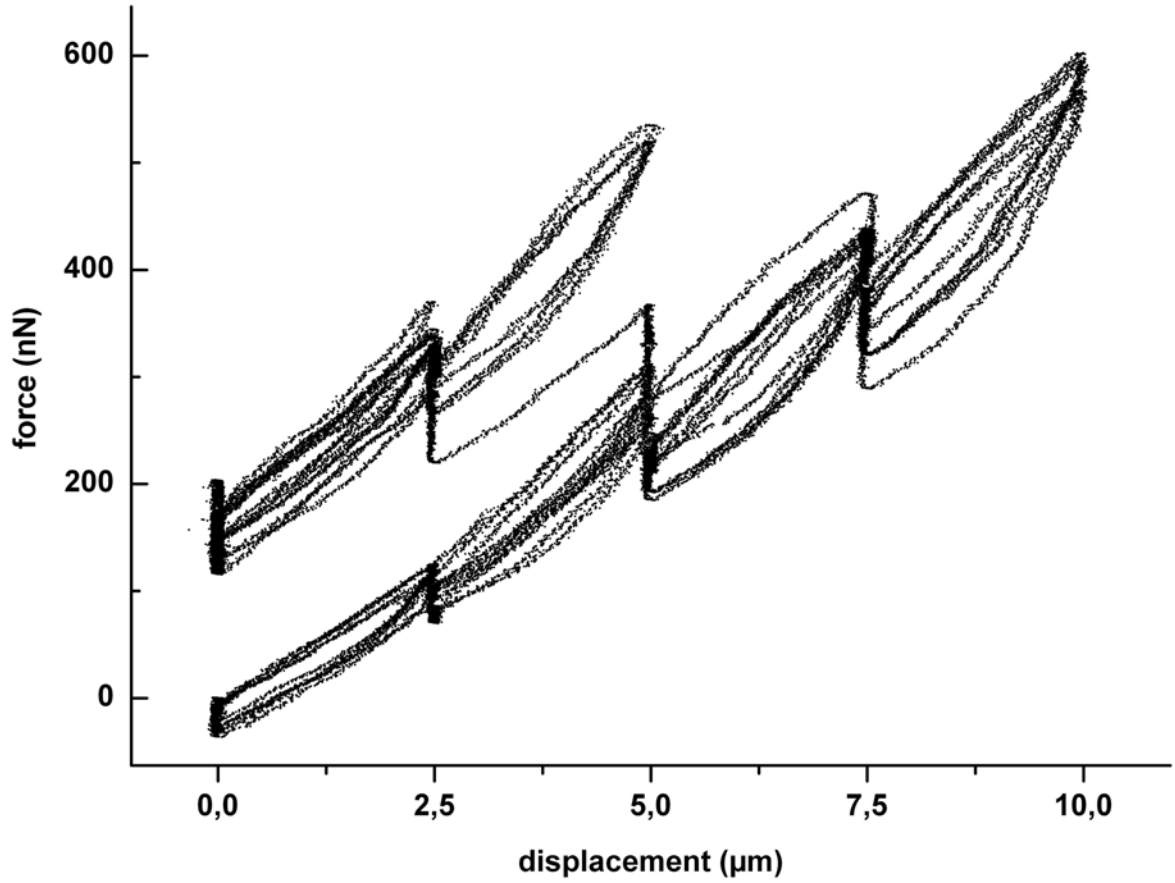

Figure 33: Force-displacement curves of a Panc-1 cell in culture medium.
Each displacement cycles of the previous measurement is visible in the graph as a hysteretic loop. The time runs along the curves clockwise. Hysteretic loops demonstrate the viscosity of the cell. The shape of the loops is well conserved as the cell undergoes equivalent displacement cycles. Small force offsets occurs during the same displacement series. A greater one (~ 200 nN) occurs as the cell is placed again under the initial displacement. It indicates a strong change in the cell activity and/or spreading even if an increase or a decrease of the adhesion area on the microplate has not been observed.

4.2.2 Discussion

To quantify the cell's mechanical properties in the course of time, the force-displacement linear relationship (which occurs as the displacement increases) is used to define a loading/unloading effective spring constant characteristic of the cell at a certain time. The results of this calculation are plotted in Figure 34.

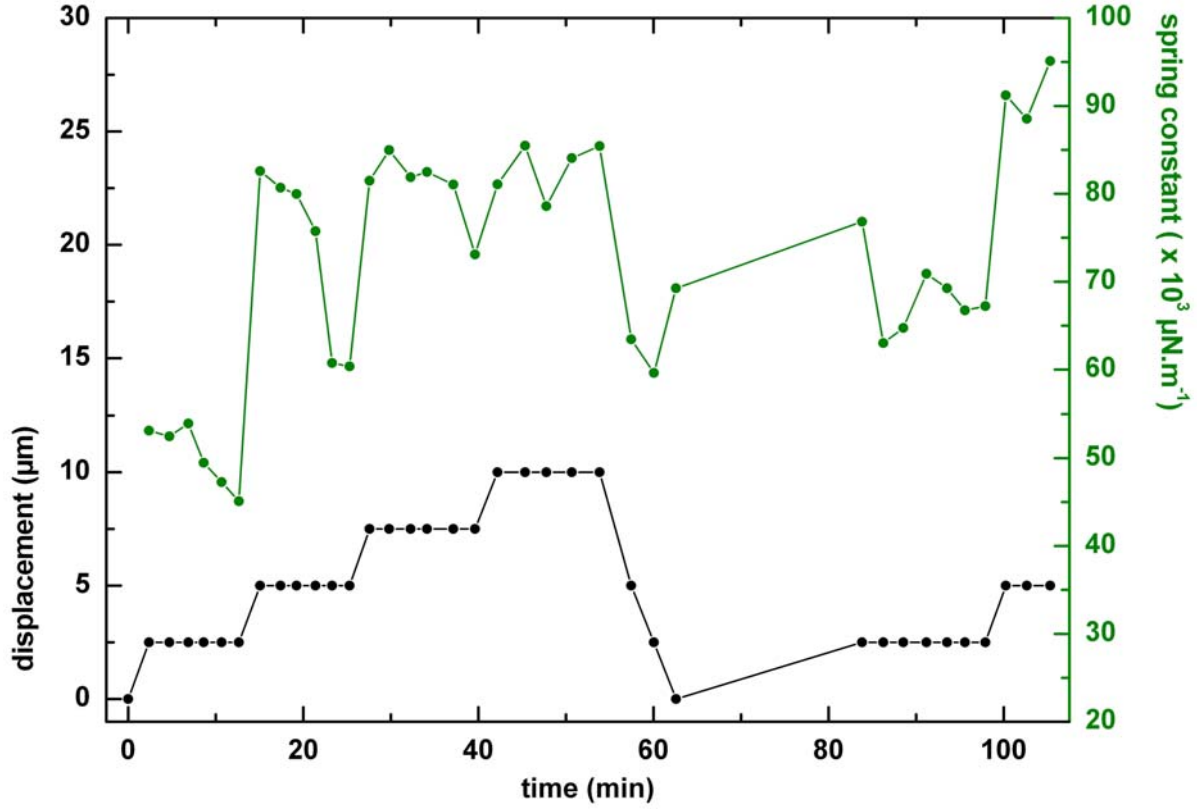

Figure 34: Peak-displacement and effective spring constant as a function of time.
The peak-displacement (black curve) and the effective spring-constant of the cell (green curve)are plotted as function of time. The errors on the values are ± 5 10 ^{3} µN.m^{-1} and 0.5 µm respectively for the spring-constant values and the peak-displacement values.

The changes of the loading/unloading spring-constant present a trend of stiffening over the displacement cycles in comparison with the first five cycles. In average, the spring constant is evaluated at ~ 50 10^{-3} N.m^{-1} during the first 10 min of the measurement. It rises to ~ 80 10^{-3} N.m^{-1} from the time t = 12 min to t = 58 min, as the displacement is over 2.5 µm and increases punctually until 10 µm. After a 20 min resting-period, comparable values increased respectively to ~ 67 10^{-3} and ~ 90 10^{-3} N.m^{-1}. It seems that the progressively increasing displacement (or strain) induces a stiffening of the cell, but stiffening is not only proportional to displacement. As the cell is allowed to settle for a period of time, it appears more difficult to stretch it again until a strained state that the cell experiences already. It shows clearly the history-dependence, which occurs frequently in biomechanics. During the resting period the cell cytoskeleton reorganises to adapt to the new biophysical state, so that the stretched cell after t = 80 min and at the beginning of the measurement is not the same system. In Figure 33, the small force-offsets occurring during a cycle series can be interpreted as a preconditioning of the system. By repeated cycles, a steady state can be eventually reached. This phenomenon is well known in biomechanics of tissue (Fung, Y.C. 1993, p.262).
At the times t = 12.5, 25.0, 40.0 and 98.0 min, the cell displays a relaxation behaviour. Because the displacement-trend is kept constant at a new value, the relaxation function of the

Kelvin model can be used to fit the force curve. According to the equation (eq. 15), the data have been fitted with an exponential-decay function. All the results are summarised in the Table 10.

	loading / unloading parameters			Kelvin model parameters			
time	**displacement (plateau value)**	**rate**	**spring constant**	μ_0	μ_1	$\tau_\varepsilon = \eta_1/\mu_1$	η_1
[min]	[µm]	[µm.s^{-1}]	[x10^{-3} N.m^{-1}]	[N.m^{-1}]	[N.m^{-1}]	[min]	[10^3 N.s.m^{-1}]
12.5	2.5	0.082	~ 80	4800	810	0.151	7.3
25.0	5	0.063	~ 80	12250	2100	0.182	22.7
40.0	7.5	0.052	~ 80	20550	3550	0.230	49.0
98.0	2.5	0.058	~ 90	20350	1800	0.360	37.8

Table 10: Parameters calculated according to the Kelvin model
The initial displacement equals 12.3 ± 0.5 µm. The error on the displacement is ± 0.5 µm; rate, ± 0.002 µm.s^{-1}; loading/unloading spring constant, ± 0.05 N.m^{-1}; spring constant μ_0 and μ_1, ± 50 N.m^{-1}; time constant, ± 0.002 min; coefficient of viscosity, 2 10^3 N.s.m^{-1}.

This analysis confirms the stiffening of the cell and the history-dependent behaviour of cell. The parameters μ_0 and μ_1 increase significantly with the displacement: between 2.5 µm to 7.5 µm plateau-value of displacement, the both parameters increase of a factor ~ 4.3. The cell hardens in response to stretching. All parameters depend on the cell history. H_1 is ~ 5 times higher, μ_0 ~ 4 times and μ_1 ~ 2 times, when the 2.5 µm plateau-value is reached for the second time. The loading/unloading effective spring constant, plotted in Figure 34, cannot be compared to the parameters μ_0 and μ_1, because both are effective parameters and have definitively different definitions, as we mention already. It reflects the cell elasticity in a dynamic regime.
It is interesting to compare parameters found, on one side, in presence of serum on FN and, on the other side, in absence of serum with chemical adhesion (section 4.1). Obviously, it is respectively a "more biologic" environment for the cell in comparison with a "less biologic" environment. It seems that in this range of deformation, the loading/unloading spring constant does not vary significantly, but it is ~ 10 times higher than in absence of serum (Table 6, and Table 9).

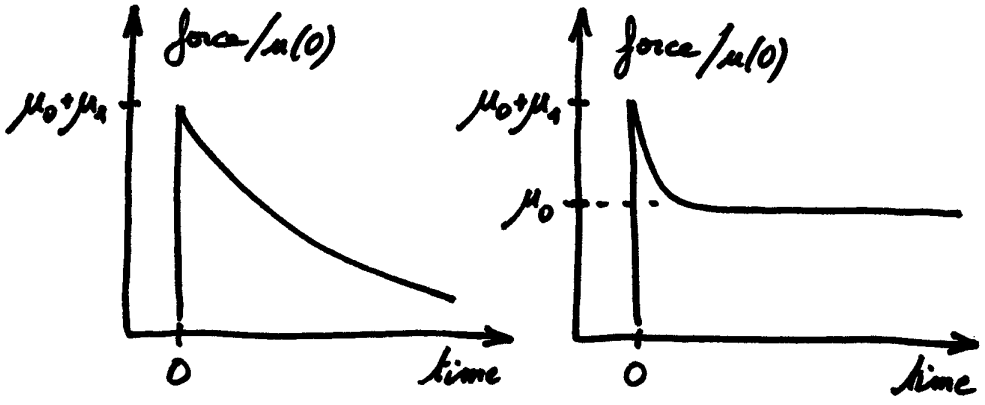

Figure 35: Representation of the relaxation function with conditions on the parameters.
The representation allows for comparison of relaxation function depending on the parameter values.

It shows that the cell develops a stronger resistance to deformation in presence of serum, possibly because of a serum-mediated activity of the actin cytoskeleton. The apparent cell viscosity increases disregarding in presence or the absence of serum under stretching, but it is much higher in absence of serum. Values of μ_1 are comparable (2500-3500 $N.m^{-1}$ at 7.5-10 µm displacement) in absence or in presence of serum. It comforts the hypothesis, that μ_1 may reflect chiefly the mechanical properties of keratin cytoskeleton which is not expected to be directly influenced by the serum. Unfortunately, the exact value of the microplate's spring-constant is not measured, but evaluated for the measurement in absence of serum, as explained in section 4.1, so these results have to be confirmed.
Nevertheless, it is possible to compare exactly the cell behaviour with and without serum. The parameters μ_1/μ_0 and τ_ε do not depend on rescaling through the spring-constant of the flexible microplate. They can be used for comparison without doubts. $\mu_1/\mu_0 \sim 0.1$ in presence of serum and $\mu_1/\mu_0 >> 1$ in its absence. τ_ε is smaller in presence of serum of about a factor 10. These both changes can be directly attributed to the serum coupled with adhesion on FN. It is coherent with the serum-mediated contractility of cell. The case with τ_ε small and $\mu_1/\mu_0 << 1$ correspond to a system, which can sustain forces and can stabilise them fast (Figure 35).

4.3 Mechanical Behaviour of Human Pancreas Cancer Cells in Presence of Sphingosylphosphorylcholine

In order to measure a value characteristic of the mechanical properties of human pancreas cancer cells (panc-1 cells) as a function of time under addition of SPC, a periodic mechanical excitation is applied to a single cell adhering between two microplates coated with FN. A cycle is composed of a mechanical loading followed by unloading and a rest period. During a cycle, the cell resists to progressive deformation. It results, that the cell is linearly loaded until the maximal value (several hundreds of nanonewtons). This linearity of the force and displacement changes allows definition of a loading/unloading spring constant, which is a measure of its elastic modulus under constant loading and displacement rates. Both rates are fixed by the cell in response to the control rate. This response is not depending on the control rate (section 3.6). Each cycle can be considered as a periodic punctual characterisation of the cell's mechanical properties.

4.3.1 Results

Figure 36 shows the displacement imposed on the panc-1 cell as a function of time (black curve) and the simultaneous measurement of resultant force (the cell's mechanical response) also as a function of time (green curve). The preparation of the cell before recording is shown in details in Figure 37 (a) – (d).

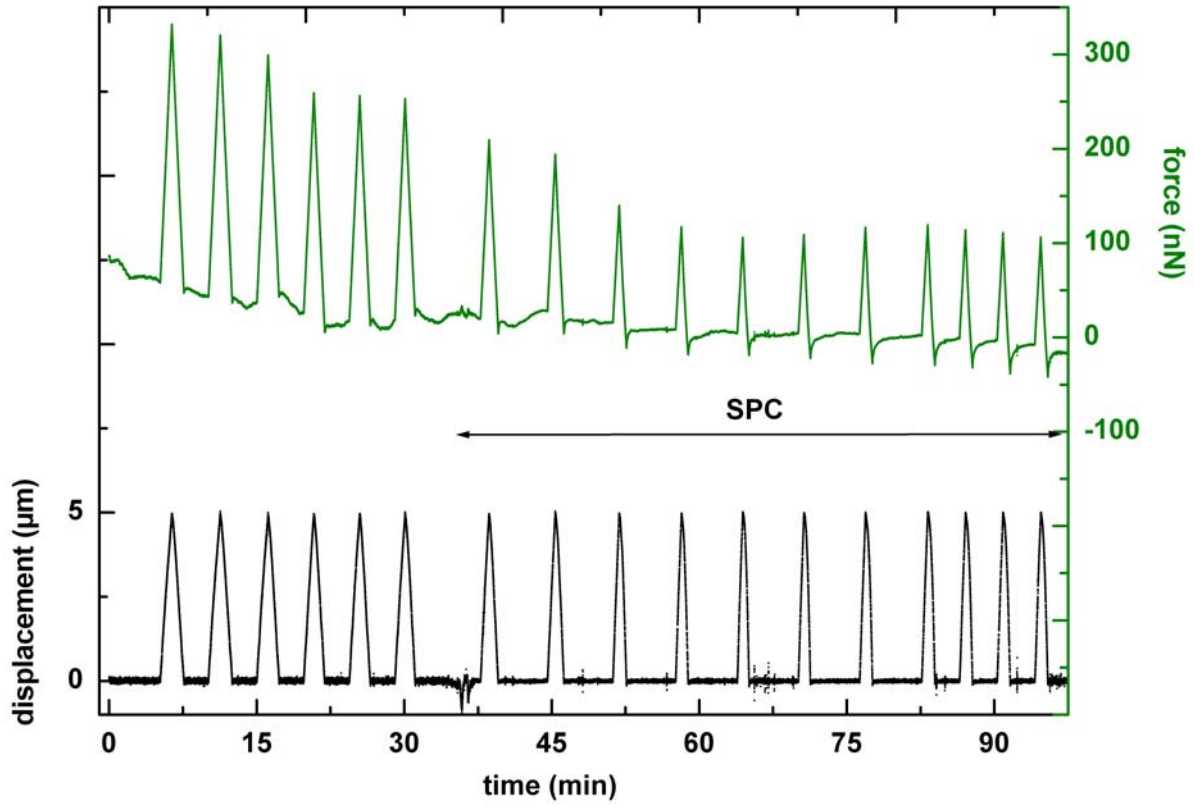

Figure 36: SPC effects on a panc-1 cell under controlled periodic displacement.
A uniaxial 5 µm amplitude and periodic displacement (black curve) is imposed to a cell with respect to the initial displacement. Cell response is recorded as the generated force (green curve) versus time. 35 minutes after the beginning of the recording 10 µM SPC is added in the liquid chamber.

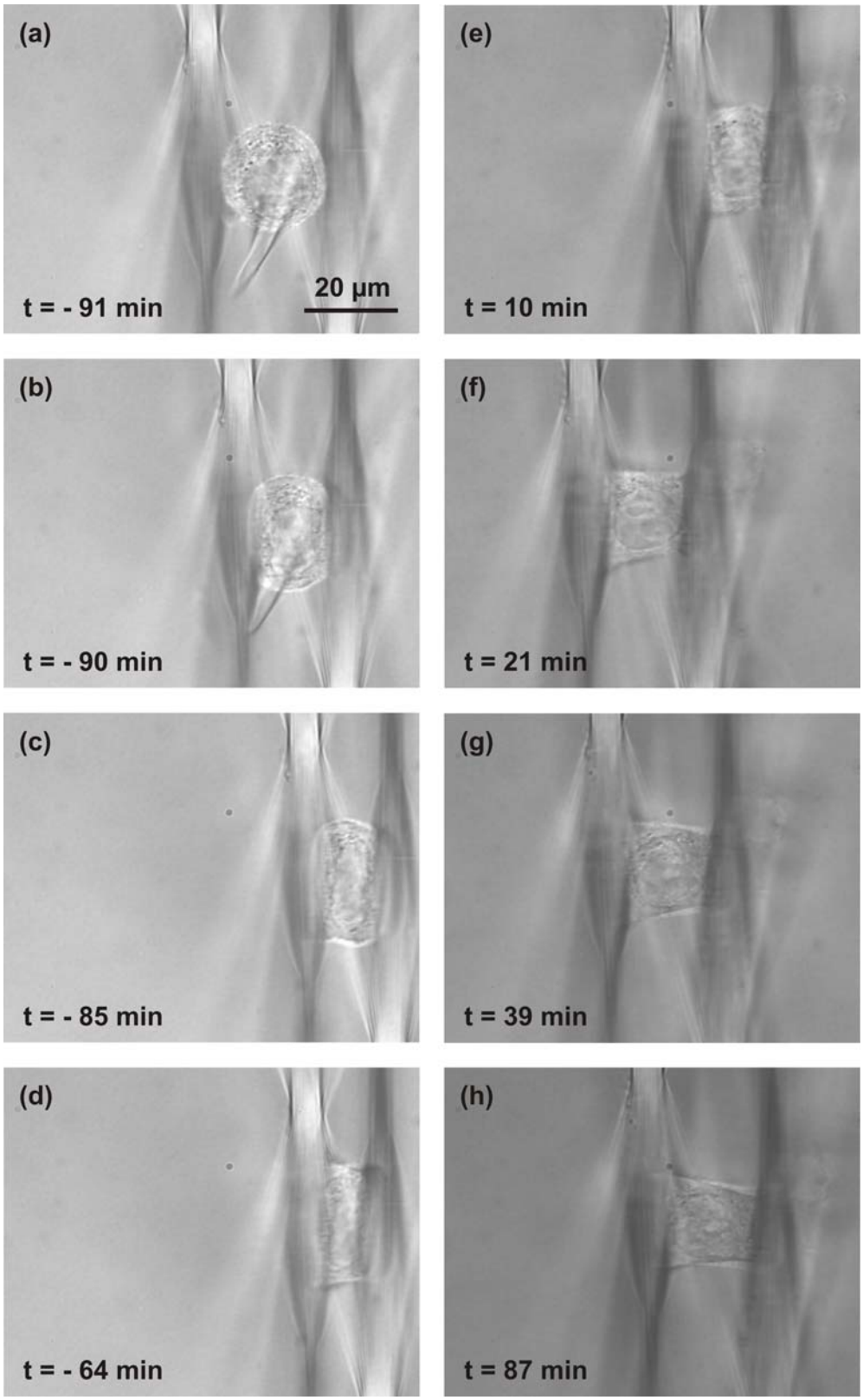

Figure 37: Micrographs of the preparation and of the measurement with a Panc-1 cell
Times are given regarding to the beginning of recording (t = 0). (a) with help of a third microplate, a cell is placed between rigid (left) and "force sensor" (right) microplates. (b) the cell is slightly pressed between the microplates. (c) the third microplate has been withdrawn. (d) the cell spreads on the microplates; The rigid microplate is moved back to set the force almost to zero: the initial displacement is then defined. (e) cell initial displacement at the end of the first displacement cycle – rest period. (f),(g),(h) are maximal displacements respectively of the 4th (no SPC), 7th and 15th (SPC) cycles.

From a spherical shape (Figure 37, (a)), the cell spread in a cylindrical-like shape (Figure 37, (d)) between the microplates. The cell displacement is composed of repeated cycles. Each

cycle is composed of a linear increase to 5 µm (Figure 36 and Figure 37, (f), (g) and (h)). Then, the cell displacement is immediately decreased to the initial displacement (set as zero displacement in the Figure 36). Finally a resting period of 2.5 min finishes the cycle. The micrograph Figure 37 (e) presents the cell in the initial state (zero-displacement, at t = 0). The initial state of a cell is difficult to define. As explain in the section 2.2.5, at t = 0, the force generated by the cell is unknown, but it is not expected to be far away for the zero force. At the end of the measurement, the zero force value has been determined after cell-adhesion rupture, meaning that the flexible microplate (force sensor) was unloaded. In this situation, the force eventually measured gives the force offset.
Six cycles are imposed on the cell so as to obtain stabilisation of cell deformation and cell adhesion to microplates under periodic displacement. It occurs approximately at the time t = 22 min. The force's decreasing trend reflects the cell adaptation to new constraints. This change of adhesion occurs on a much longer time scale than the time needed for elastic probing of the cell. This is why cell adhesion induced force drift does not contribute substantially to the evaluation of cell's mechanical properties obtained by short time force probing. After the initial period of 35 minutes (which corresponds six cycles), the cell kept in the initial state is treated with 10 µM concentration of SPC. Upon addition of SPC, the cycle duration is extended to approximately 7 min (including 5 min of resting period) in order to reduce perturbations on the cell. Seven of such cycles are applied on the cell before reverting to the original loading conditions at t ~ 80 min. At this time, the SPC has reacted with the cell for 45 minutes which is known to be enough time to obtain a complete effect of SPC.

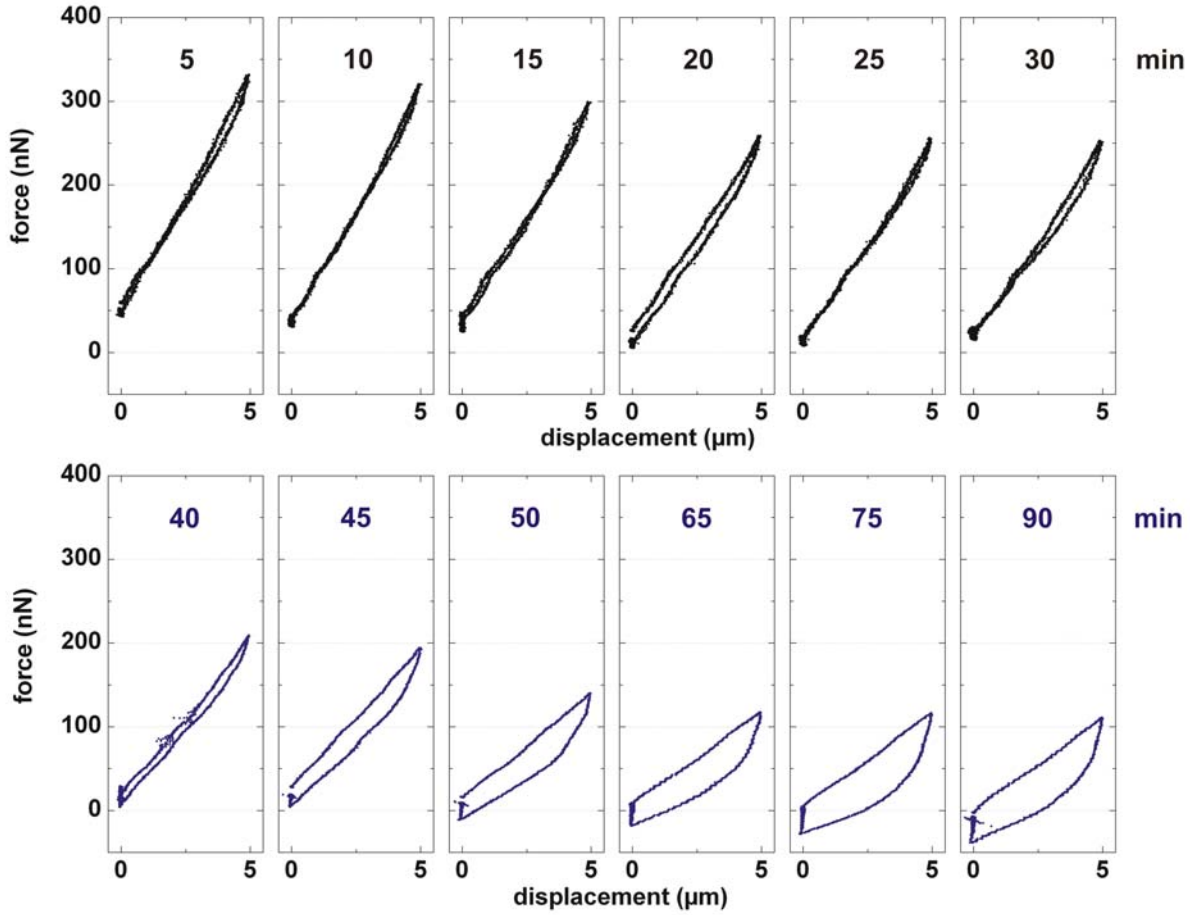

Figure 38: SPC effects on the force-displacement relationship of a Panc-1 cell.
The force has been plotted as a function of displacement for several cell displacement cycles of the Figure 36. Given times (top of each graph) correspond approximately to the beginning of the cycle. The black colour indicates measurement without SPC, whereas the blue colour indicates the presence for 10 µM of SPC.

Two changes occur in presence of SPC: first the amplitude of peaks force decreases and second the displacement rate increases. For a linear displacement of 5 µm, the peak force amplitude drops from ~ 250 nN to ~ 110 nN. For the same control rate (0.05 µm displacement step each 100 ms), the resultant effective displacement rate increases from ~ 0.07 $\mu m.s^{-1}$ to 0.13 $\mu m.s^{-1}$, almost doubled. Force and displacement have been measured simultaneously. Thus, it is possible to plot the force as a function of the displacement for each displacement cycle. Figure 38 present these curves. Before introduction of SPC, force-displacement curves (black colour) show a similar response during the first six cycles, with occasionally a little hysteresis (Figure 28, upper part). In presence of SPC (exactly 15 min after addition of SPC, t = 50 min), the relationship between force and displacement is linear until the set displacement is reached (5 µm), whereas during the unloading to the initial displacement (or zero displacement in the graphs), the force is not a linear function of the displacement (Figure 28, lower part). The jumps in force (*i.e.* force increase at constant displacement) correspond to cell relaxation during the rest periods, which is also clearly remarkable in the Figure 36.
The linear relationship between force and displacement defines the loading/unloading spring constant characteristic of the cell and its biophysical state. This value has been calculated for each displacement cycle. It is the ratio of the loading rate to the displacement rate measured during stretching to 5 µm. In Figure 39, the loading/unloading spring constant has been plotted as a function of the time in units of $\mu N.m^{-1}$ (black curve). The area enclosed in force-displacement graphs, when the cell goes through a displacement cycle, has been also plotted as a function of time in units of energy reported to the cell volume (green curve). It is called hysteretic energy.

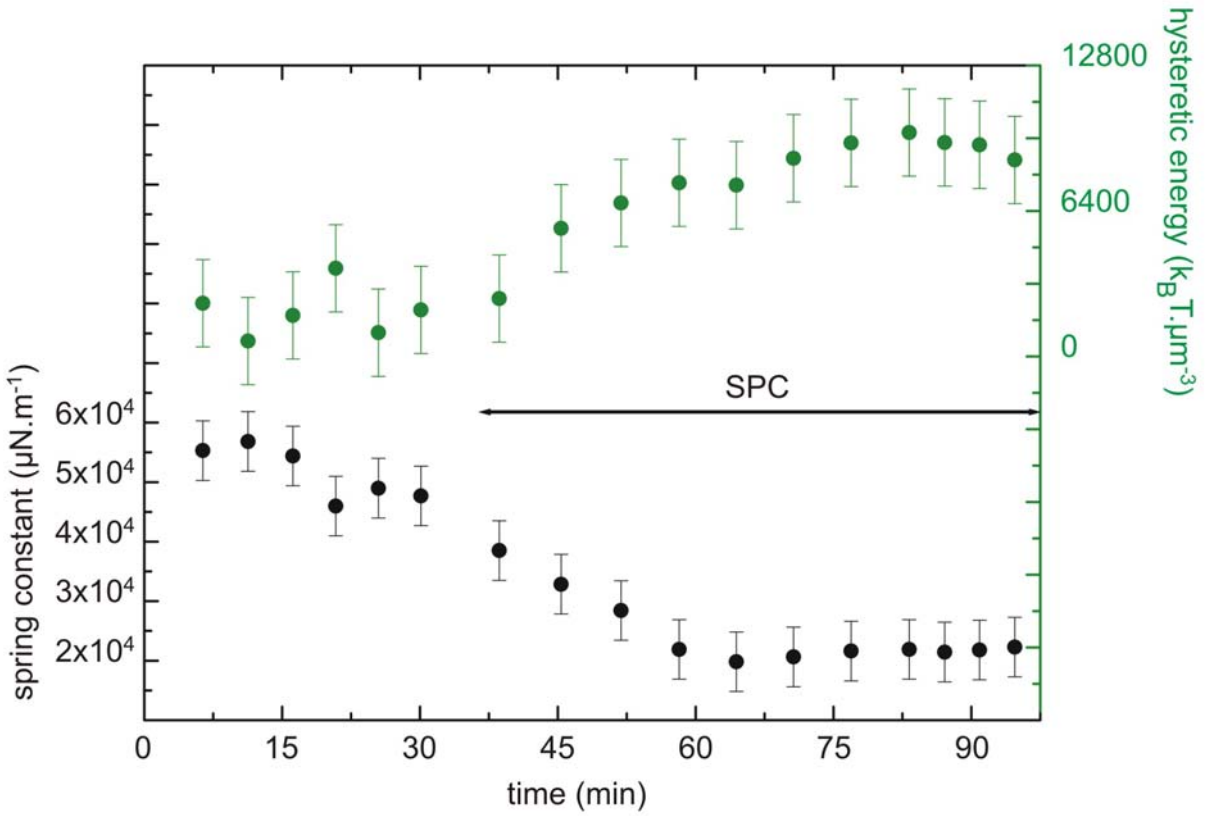

Figure 39: Effective spring constant and hysteretic energy variations under addition of SPC
Loading/unloading effective spring constant (black curve) and hysteretic energy (green curve) are plotted as a function of the time. The energy unit is in $k_B.T$ unit per cell volume in μm^3, where k_B is the Boltzmann constant, T = 310.15 K. The cell diameter equals 22.3 µm.

4.3.2 Discussion

The loading/unloading effective spring-constant decreases gradually after the addition of SPC of a factor ~ 3. It shows a softening of the cell. The system seems to settle in a new biophysical state in presence of SPC. During 35 min, the effective spring-constant and the hysteretic energy do not vary anymore (Figure 39) demonstrating the stability of the system. The cell adhesion does not change until the time t = 100 min, at which it is clearly suddenly depredated. This progressive softening of the cell is attributed to the SPC-mediated reorganisation of the keratin. The perinuclear reorganisation of the cytoskeleton depletes the rest of the cytoplasm of keratin. As a result, a greater volume of cytosol could undergo viscous deformation. It could explain the greater viscous energy dissipation that is manifested as increasing the hysteresis loop area.

4.4 Mechanical Behaviour of Human Pancreas Cancer Cells in Presence of Lysophosphatidic Acid only or with Sphingosylphosphorylcholine

The measurement, which will be presented in this section, is similar to the one showed in the previous section. The mechanical assay is composed of repeated cycles. However, it presents three differences in comparison with the previous measurement. First, the force is controlled and the cell response can be read in the cell displacement. Second, during a cycle, the cell is not only stretched, but also compressed. Third, as the cell adheres between the microplates, it is pre-treated with LPA, before being treated with SPC. The measurement cumulates mechanical assays on the same Panc-1 cell under three different biochemical stimulations: first no stimulation (serum-free medium), second LPA stimulation (at 10 µM) and third LPA and SPC (both at 10 µM) stimulation.

4.4.1 Results

Figure 40 presents a force controlled mechanical assay on a Panc-1 cell. The force (green colour) is plotted as a function of time. Repeated tensile stretching (positive forces values) and compression (negative forces values) are applied on the cell.

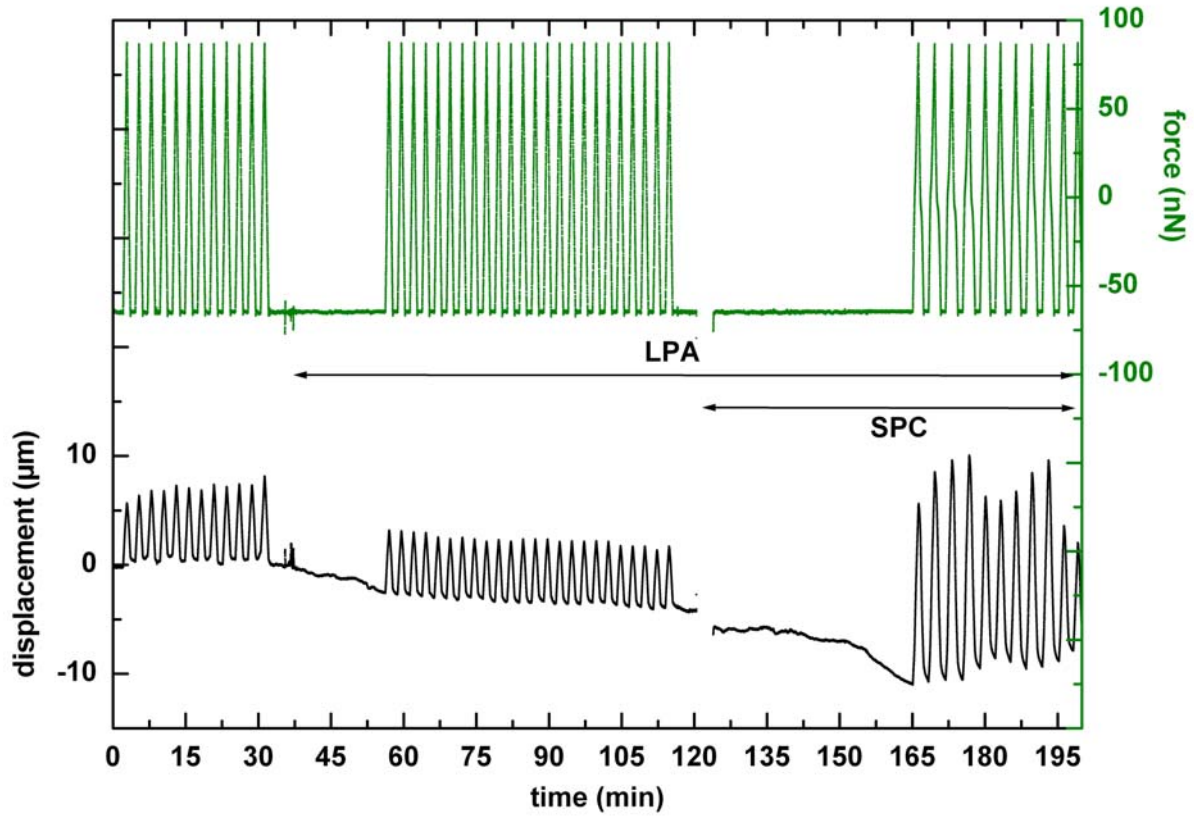

Figure 40: LPA and SPC effects on a Panc-1 cell under controlled periodic force.
A uniaxial 150 nN amplitude and periodic force (green curve) is imposed to a cell. The cell is stretched (positive force values), but also pressed (negative force values). Cell response is recorded as the displacement (black curve) as a function of time. LPA is added in the liquid chamber to reach a concentration of 10 µM at the time t = 35 min. Later, at t = 120 min, SPC is added also at a final concentration of 10 µM.

A force cycle is composed of an increase in the force of 150 nN from the force reference-level. Then, the force is brought back to the force reference-level. The cycle ends with a rest period lasting 1 min. The cell displacement – simultaneously measured – is plotted also as a function of time (Figure 40, black colour). It represents the cell's mechanical response. During 12 successive force cycles over a period of 30 min, the peak displacement increases slightly from 5.6 µm to 8.1 µm. At the time t = 35 min, LPA is added to a final concentration of 10 µM in the liquid-chamber. The force is maintained at the reference level during 20 min in order to allow LPA-induced cytoskeletal reorganisation, without any mechanical perturbations. The cell displacement decreases of ~ 2.5 µm. This is connected with an increase of the cell adhesion area by cell spreading. It can be observed on micrographs (d) and (j) in Figure 41. The increase of the cylinder-like cell diameter can be measure, but the exact adhesion-area increase is not a measurable value due to the set-up configuration. 24 force cycles are applied in presence of LPA. Over all these cycles (60 min), the displacement amplitude is remarkably constant at 5.6 µm. Subsequently, at t = 120 min, SPC is also added in the liquid-chamber to obtain a concentration of 10 µM. As before for the incubation with LPA, the force is maintained at the reference level during 45 min in order to allow complete SPC-induced keratin reorganisation. During this period, the cell displacement decreases, but no cell spreading is seen on pictures (Figure 41, (f) and (l)). At the end of this period, a third series of 10 cycles begins. Now, in presence of LPA and SPC, the displacement amplitude increases of a factor ~ 3-4 in comparison with the amplitude in presence of LPA only. The displacement-amplitude value appears to be unstable in comparison with the measurement in presence of LPA only.
At constant control rate (0.05 µm each 100 ms), the force rate varies between compression and stretching, and depends on the presence of bioactive lipids. For example, during cell stretching, in presence of LPA, the force rate is constant at a value of ~ 3.3 $nN.s^{-1}$ and, in presence of LPA and SPC, it equals ~ 2.2 $nN.s^{-1}$, indicating that the same unit step of 0.05 µm induces less force generation in presence of SPC.

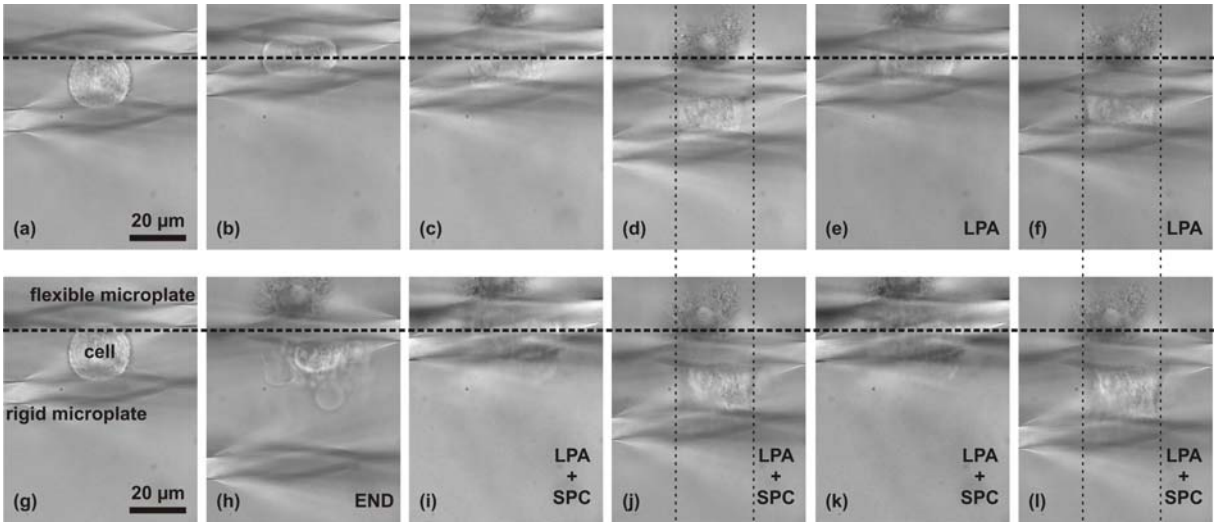

Figure 41: Micrographs of a Panc-1 cell under controlled periodic force.
(a) and (g) are the same micrograph: the panc-1 cell before adhesion. Flexible and stiff microplates are indicated. (b) The cell has been pressed between microplates: cell spreading begins. Reference positions: (c) without any bioactive lipids, (e) with LPA, (i) and (k) with LPA and SPC. Position at maximal force: (d) without any bioactive lipids, (f) with LPA, (j) and (l) with LPA and SPC. Flexible microplate translation in direction of picture bottom leads to an increase of the force. The horizontal dashed line indicates the position of the zero force. Vertical dashed lines allow comparison of cell spreading between the microplates. Addition of LPA coincides with increasing of spreading, whereas addition of SPC does not influence strongly the cell spreading.

Figure 42 presents the force as a function of displacement for several force cycles from the Figure 40. Force cycles before any treatments (black lines), after the introduction of 10 µM

LPA (purple lines) and after subsequent addition of 10 µM of SPC (blue lines) are plotted. In absence of bioactive lipid or in presence of LPA, the force-displacement relationship is almost the same during either increase or decrease of the force. In contrast, in presence of LPA and SPC together, this relationship shows a strong difference between the force increase and the force decrease.

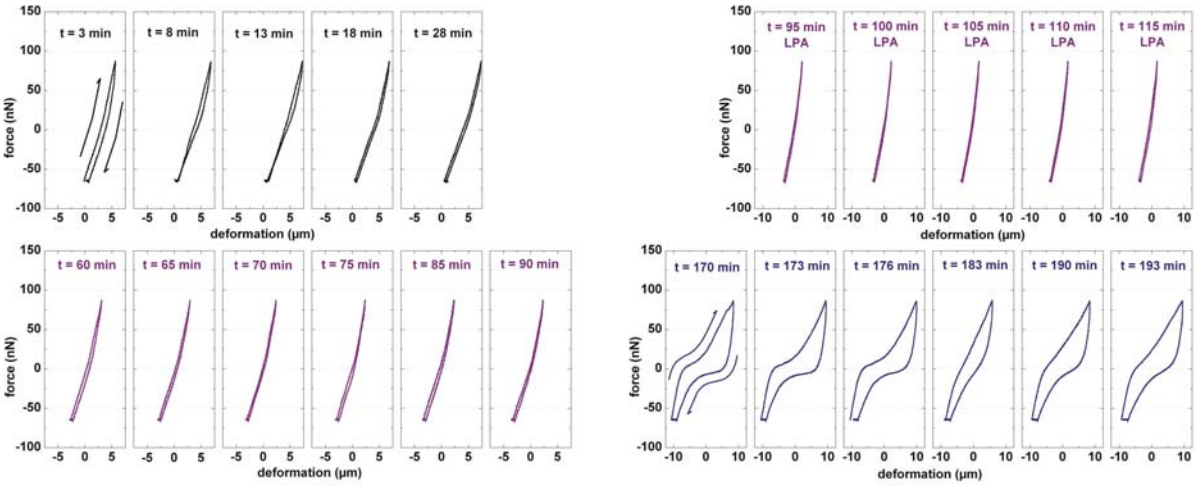

Figure 42: LPA and SPC influence on force-displacement relationship of a Panc-1 cell.
Plots of the force as a function of displacement for several cell force cycles of the Figure 40. The time given at the top of each graph corresponds approximately to the cycle beginning. Black colour indicates measurement without LPA and without SPC, purple colour the presence of 10 µM concentration LPA and blue colour, 10 µM concentration SPC in addition to10 µM concentration LPA .

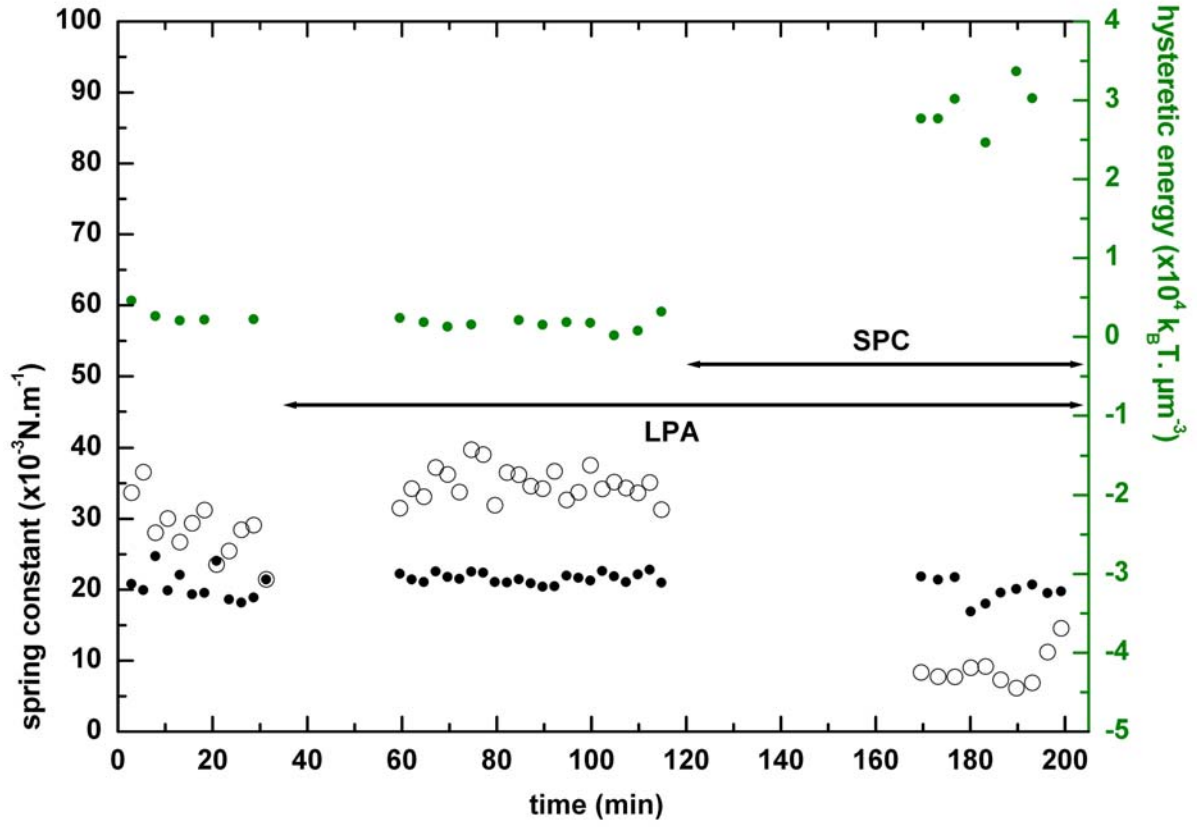

Figure 43: LPA and SPC influence on effective spring constant and hysteretic energy.
Effective spring constant (black curve) and hysteretic energy (green curve) plotted as a function of the time

For each force cycle, the force-displacement relation presents different linear regimes. The loading/unloading spring constant is calculated during stretching in the linear part of the cycle (*i.e*. before the maximal force is reached). This value is plotted in the Figure 43, open circles. In the same way, the linear compression regime can be also characterised by an effective spring constant. The value remains constant at the value ~ 22 10^{-3} $N.m^{-1}$ over the whole measurement (Figure 43, filled circles). The hysteresis loop area of each cycle is also plotted (green curve) as a function of time in Figure 43. As previously, this energy is reported to unit of cell volume. The cell was approximated as a sphere of 22.3 µm in diameter at the beginning of the measurement (Figure 41, (a)).

4.4.2 Discussion

LPA induces the formation of actin stress fibres, as SPC does, but does not affect the keratin cytoskeleton architecture. The choice of LPA-pre-treatment, instead of treating the cell with SPC directly, is motivated by the fact that the SPC-effect should consequently be limited to keratin reorganisation and not simultaneously actin and keratin reorganisation.
LPA and SPC are detectable with the help of the loading/unloading spring-constant value. In DMEM supplemented with L-glutamine (serum free medium), the loading/unloading spring-constant in stretching regime decreases slightly from ~ 35 10^{-3} $N.m^{-1}$ to ~ 25 10^{-3} $N.m^{-1}$ during the 12 cycles. After LPA-treatment, it stabilises at a plateau-value of ~ 35 10^{-3} $N.m^{-1}$. The remarkable stability of the value and its slight increase are interpreted as an activation of the cell contractility mediated by the LPA. It is confirmed by the cell spreading, which is observed. It is also consistent with the LPA-mediated contraction and spreading observed in REF52 cells (section 3.5). Fortunately (because it allows to continue the measurement), the Panc-1 cells do not flatten between the microplates as much as the REF52 cell do, and as observed the cell settles in a stable state regarding adhesion and mechanics. The relationship force-displacement in presence of LPA displays a high reproducibility (Figure 42, purple lines). After 45 min incubation with SPC, the loading/unloading spring constant deceases suddenly of a factor ~ 4.7 indicating softening of the cell. It is attributed to keratin perinuclear reorganisation. The loading/unloading spring-constant in compression regime remains constant demonstrating that the mechanical properties of the nucleus and the perinuclear region do not depend notably on LPA- or SPC-mediated cytoskeletal reorganisation. In compression and in presence of SPC, it could be expected to observe a hardening. It depends on the relative rigidity of the nucleus to the collapsed keratin cytoskeleton on the nucleus. These measurements could indicate that the nucleus gives the main contribution to the mechanical behaviour of the nuclear and perinuclear region of a cell. It is coherent with the measurement of Caille, N. and *al.*, who measured a nuclear elasticity of 5000 Pa to be compare to the cytoplasmic elasticity of 20 Pa (Caille, N. 2002).

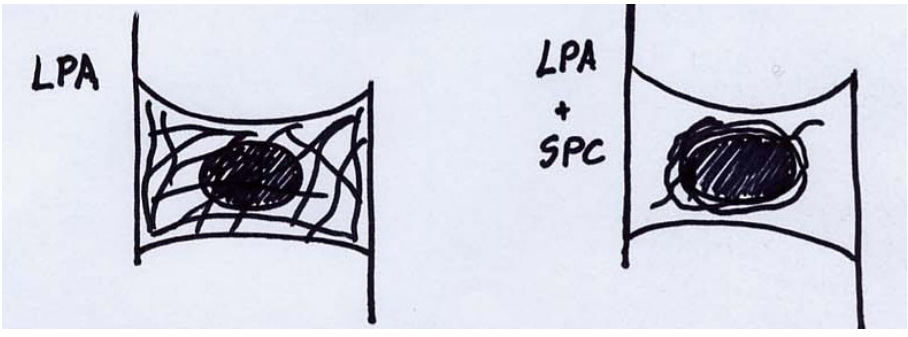

Figure 44: Schematic representation of a Panc-1 cell between the microplates.
(a) with LPA and (b) with LPA and SPC

As before, the sudden increase of the hysteretic energy could be interpreted as an increase of the volume in which viscous dissipations can be produced. This volume is the parts of the cell between nucleus and microplates (Figure 44, (b)).
Furthermore, changes in the actin fibre structure induced by prior treatment with LPA (which does not modify keratin) appear to have no bearing on the effects of SPC in reducing the elastic modulus of cell by reorganising keratin observed in section 4.3.

The migration of Panc-1 cells through size-limited pores in response to SPC has been studied. The migration ability of Panc-1 cells is ~ 2 times higher in presence of SPC in comparison with the control (Micoulet, A. 2003). In this work, it has been proved by a direct measurement that SPC induces cell softening in correlation with specific cellular architecture reorganisation. This softening could explain the increase ability of Panc-1 cells to migrate. As already mentioned, SPC is found in high amounts in malignant ascites. The metastatic process is defined as the invasion of basal membrane and endothelial layer by cancer cells originating in most of the cases from epithelium. Metastases are these epithelial cells, which acquire the ability to migrate through tissues. The SPC-mediated softening of epithelial cancer cells, Panc-1, could facilitate the metastatic process.

5 Conclusions and Outlook

Several insights in cell mechanical behaviour have been presented in this work. It has been shown that the microplate technique could address various questions concerning cell mechnical behaviour. The advantages of this technique are the 'three dimensional-like' situation of the cell between the microplates, the possibility to expose the cell to an adhesion-contrast. The weak point is that one need a statistic on several measurements to reflet the mechanical properties of a cell type.

The coating of the microplates with fibronectin is homogeneous. The entire surface of the microplate is a potential adhesion surface for the cell. Fibroblasts attempt to have a large interaction area with surfaces in culture; typically a surface equivalent to a disk of ~ 50-70 µm in diameter (Figure 45, (b)). The spreading process can be very different between cell lines. REF52 cells spread in ~ 3 hours, whereas Swiss 3T3 cells do need ~ 2-3 times longer. As a consequence, measurements with fibroblasts on FN-coated microplates are possible only if one begins to stretch the cell actively a few minutes after the contact. If not, the cell reduces the distance between microplate to less than 1 µm and not mechanical assay can be conducted.

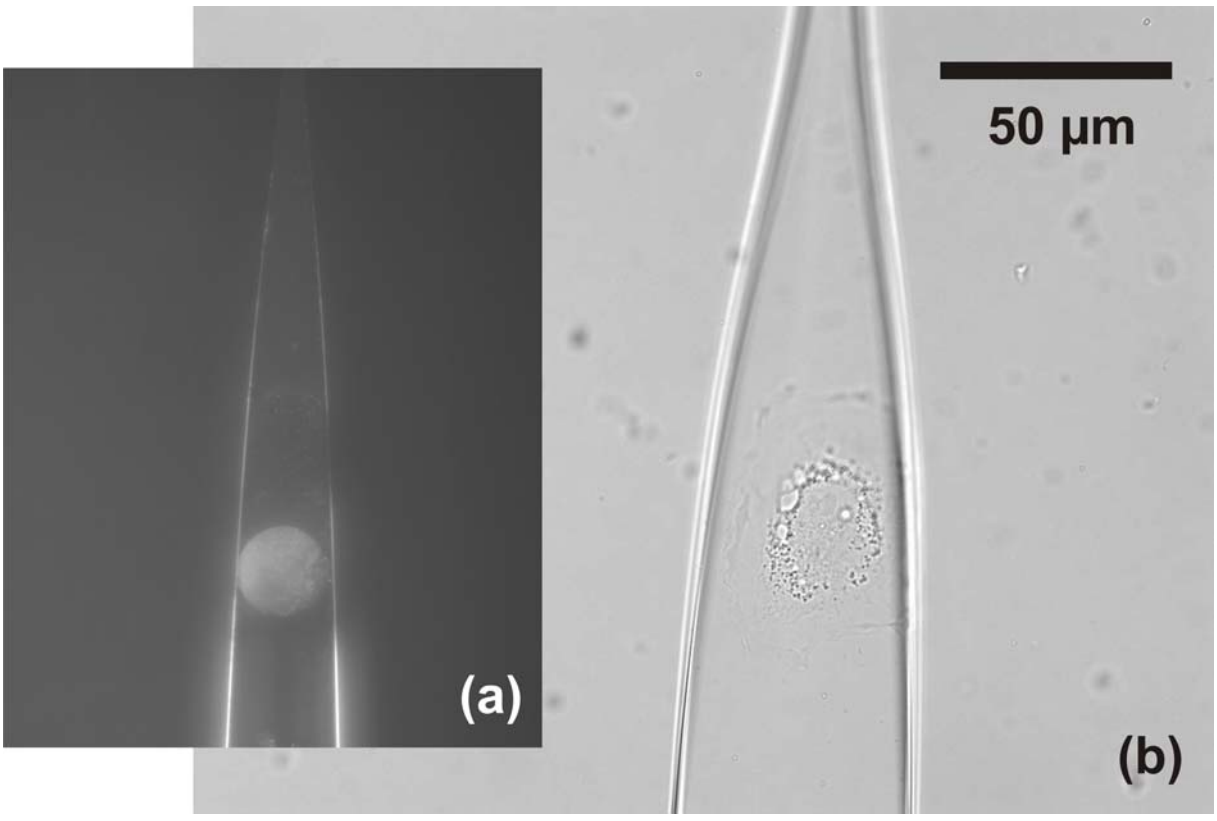

Figure 45: Cell spreading on microplate.
(a) Fluorescence micrograph reveals the presence of FN on a 20 µm disk. The microplate tip has been incubated with a polyclonal anti-body against FN. (b) REF52 cell spread on a microplate. The scale bar is valid for the both micrographs.

Because of this unstable spreading state interpretations of measurements are more difficult and the characterisation of cell's mechanical properties is strongly dependent on it (see section 3.2). The straightforward solution to this difficulty is to stabilise the spread. In order to do so, the 'chemical adhesion' can be used or potential area of adhesion can be reduced. The first solution has been used. It works well for the Swiss 3T3 cells (see section 3.3). In the section 3.2, it has been shown that the adhesion influence the mechanical properties of a cell in the few micrometers close to the surface. The 'chemical adhesion' results in stiffening of the cellular material, which likely disrupts locally instead of adapt to stress because of a lack of organisation. The second method is to provide a 'biological adhesion' to the cell but only on a defined area. The FN is adsorbed or covalently bond to the surface only on a disk of 20 µm in diameter at the tip of the microplate (Figure 45, (a)). This has been achieved by using the micro-channel technique described in the section 2.5. The surface around the disk is coated with BSA which provides an efficient surface passivation regarding cell adhesion. To prove it, FN has been adsorbed on cover-slips using a series of parallel ~ 5 µm wide micro-channels distant of ~ 250 µm. Each 250 µm a channel widens in a circular shape. It results that cells have the possibility to adhere on FN coated patterns: ~ 5 µm wide lines and disks of greater diameter. Two MEF-3T3 cells cannot spread side by side on the 5 µm FN-bands (Figure 46, (a)). 4-5 MEF-3T3 can spread on a disk of ~ 40 µm in diameter (Figure 46, (b)).

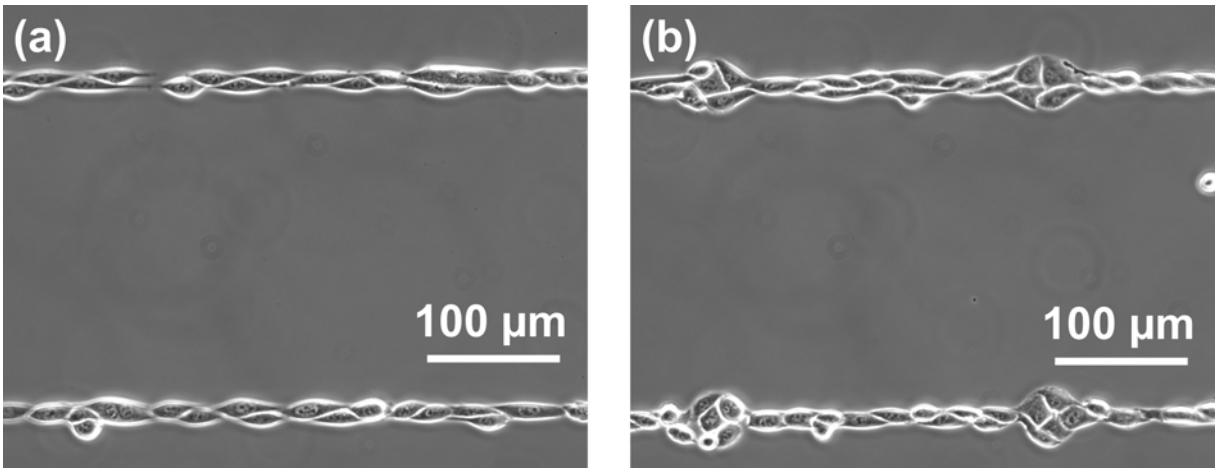

Figure 46: Growth of Swiss-3T3 cells on FN micro-patterned cover-slip.
(a) Phase-contrast micrograph of Swiss-3T3 cells spreading and growing on ~ 5 µm wide FN-coated bands. (b) Phase-contrast micrograph of Swiss-3T3 cells spreading and growing on ~ 5 µm wide FN-coated bands and ~ 40 µm diameter disks.

If all technical problems to achieve the patterning are solved at this date, no experiment has been conducted with such a micro-patterned microplate yet. Measuring the force during the cell spreading between microplates, it is expected to observe a clear limitation of the contraction force observed in the section 3.2, and simultaneously a limitation of the cell displacement. It will be very interesting to measure the mechanical behaviour of the cell in such situation. Does the cell reach a stable state?
Does the cell try periodically to spread further? Stochastic, transient extension periods (STEPs) have been observed in cell spreading (Dubin-Thaler, B.J. 2004). STEPs occur at a rate of ~ 30 events over 10 min. The event consists in an extension followed by a retraction all around the perimeter of the cell. If this extension is associated to a force generation in the range of several nN, it could be measurable with the microplate technique.

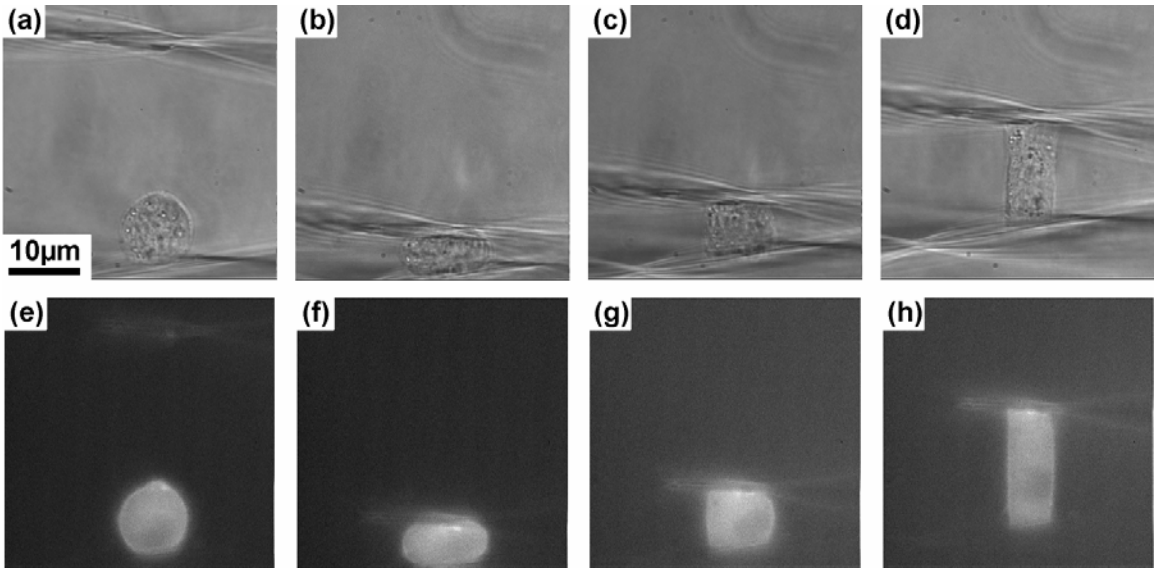

Figure 47: Stretching of a Swiss-3T3 cell
(a) - (d) Micrographs of a Swiss-3T3 cell. In (d) the cell is stretched of 10 µm.
(e) - (h) Fluorescence micrographs of Swiss 3T3 cell

Another interesting measurement stimulated is to observe the live-reorganisation of actin in a fibroblast in response to applied forces. The set-up configuration is ideal for such a measurement. Swiss-3T3 cells transfected with actin-GFP can be placed between the microplates and stretched. Such an experiment has been conducted with 'chemical adhesion' (*Figure 47*Figure 47). The formation of stress-fibres has not been observed. The principal reason for this is the lack of FN or other cell-adhesion protein on the surface. The micro-structured microplates appear as a much better 'tool' to achieved this qualitative measurement because they allow using of FN-coating for experiments with fibroblasts.

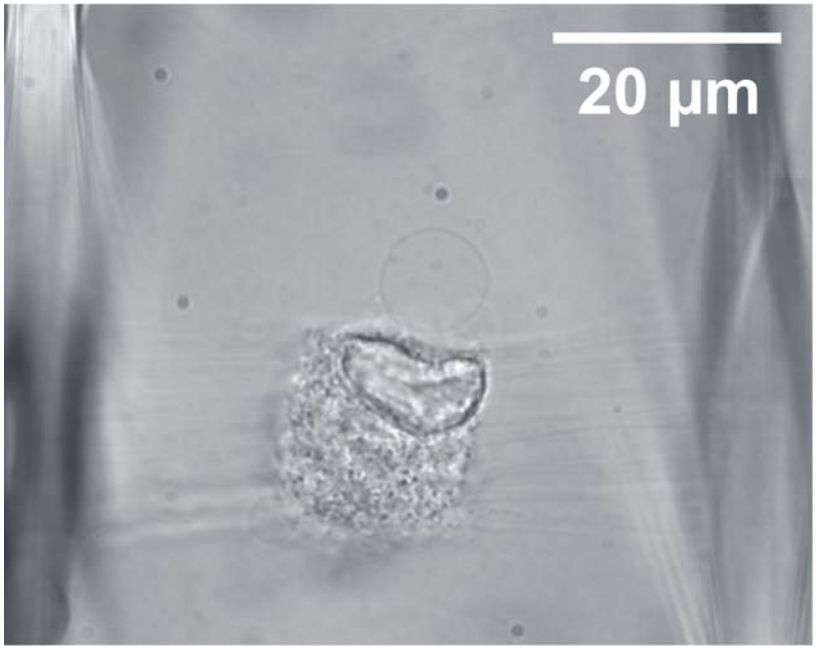

Figure 48: Dead Panc-1 cell.

The Figure 48 is the micrograph of a Panc-1 cell between FN-coated microplates. The cell lost adhesion, probably because it died. The cell did not round as it happens if it dies through apoptosis. The cell is on the middle of the micrograph. It remains a cubic shape. It is hold by many tethers which are pulled out of the plasma membrane. It demonstrates that the strong and local anchorage of the cell to the FN-coated microplates. In contrast to fibroblast spreading, the spreading of Panc-1 cells on FN-coated microplates reaches a stable state faster and thus facilitates measurements and their interpretations (section 4.3 and 4.4). An explanation could be that these cells maintain a certain volume on the surface (obvious in cell culture) or between the microplates because of their epithelial-like morphology, probably connected to the presence of the keratin.

Acknowledgments

I would like to thank Prof. J. Spatz for his constant support and for the possibility, he offered me, to come to Germany to begin my PhD. It was, during one year, in Ulm in the group of Prof. M. Möller.

I thank Prof. B. Fourcade, who supports me from Grenoble in France.

I thank Prof. H. Horner, who accepted to be my supervisor at the faculty of Physics in the University of Heidelberg.

I thank Prof. A. Ott (University of Bayreuth). My interest for biophysics grew in his group, as he was at the Institut Curie, Paris, France.

I thank H. Weiss, the chief of the workshop of the Physical-Chemistry Institut at the University of Heidleberg and his group, and H. Gruchmann, the chief of the workshop of the University of Ulm. My work depended on their work.

I thank our Secretary Frau Boczek, who is always present to solve administrative problems. I thank R. Morlang, who provides materials.

I thank all my colleges here in Heidelberg the Spatz group. Special thanks for Wouter and Wiebke, for Ada, for Jens, for Jacques, for Christian, for Stefan and Frauke, who are in China, and for Moyu, who is in London. All the other for the good atmosphere of work in the lab!

From the time in Ulm, I thank Claudia and Ahmed (Aachen), Vanessa and Mark (Philadelphia), Paul (Toronto), Julien (Ulm) and Olivier for cooking together or for jogging together!

In Heidelberg, I thank Fabiola, Max for playing squash and tennis!

In France, I thank my mother and my family. Bertrand, Jean-Yves and Céline for the vacations in the montains!

6 References

Alberts, B. 2002	Molecular Biology of the Cell, 4th edition, Garland Science, New York, 2002
Arnold, M. 2004	M. Arnold, E.A. Cavalcanti-Adam, R. Glass, J. Bluemmel, W. Eck, M. Kantlehner, H. Kessler, J.P. Spatz, *ChemPhysChem* **2004**, *5*(3), 383-388
Aszodi, A. 2003	A. Aszodi, E.B. Hunziker, C. Brakebusch, R. Fässler, *Genes Dev.* **2003**, *17*, 2465-2479
Ballestrem, C. 1998	C. Ballestrem, B. Wehrle-Haller, B.A. Imhof, *J. Cell Sci.* **1998**, *111*, 1949-1658
Ballestrem C. 2004	Cell Motility, John Wiley & Sons, Chichester, West Sussex, UK, Chapter 5
Balaban, N.Q. 2001	N.Q. Balaban, U.S. Schwarz, D. Riveline, P. Goichberg, G. Tzur, I. Sabanay, D. Mahalu, S. Safran, A. Bershadsky, L. Addadi, B. Geiger, *Nature Cell Biol.* **2001**, *3*, 466-472
Bausch, A.R. 1998	A.R. Bausch, F. Ziemann, A.A.Boulbitch, K. Jacobson, E Sackmann, *Biophys. J.* **1998**, *75*, 2038-2049
Bausch, A.R. 2001	A.R. Bausch, U. Hellerer, M. Essler, M. Aepfelbacher, E. Sackmann, *Biophys. J.* **2001**, *80*, 2649-2657
Bensimon, D. 1996	D. Bensimon, *Structure* **1996**, *4*, 885-889
Block, S.M. 1995	S.M. Block, *Quart. Rev. Biol.* **1995**, *70*, 217-218
Boguslawski G., 2000	G. Boguslawski, D. Lyons, K.A. Harvey, A.T. Kovala, D. English, *Biochem. Biophys. Res. Commun.* **2000**, *272*(2), 603-609.
Boal, D. 2002	Mechanics of the Cell, Cambridge University Press, Cambridge, UK, 2002
Bray, D. 2001	D. Bray, Cell Movements from Molecules to Motility, 2nd ed., Garland Publishing, New York, **2001**
Caille, N. 2002	N. Caille, O. Thoumine, Y. Tardy, J.J. Meister, *J. Biomech.* **2002**, *35*, 177-187
Cavalcanti-Adam, E.A. 2002	E.A. Cavalcanti-Adam, I.M. Shapiro, R.J. Composto, E.J. Macarak, C.S. Adams, *J. Bone Miner. Res.* **2002**, *17*(12), 2130-2140
Cramer, L.P. 1997	L. P. Cramer, M. Siebert, T. J. Mitchison, *J. Cell Biol.* **1997**, *136*(6),1287-1305
Cremers, B. 2003	B. Cremers, M. Flesch, E. Kostenis, C. Maack, A. Niedernberg, A. Stoff, M. Südkamp, O. Wendler, M. Böhm, *J. Mol. Cell. Cardiol.* **2003**, *35*, 71-80
Chang, L. 2004	L. Chang, R.D. Goldmann, *Nature Reviews Mol. Cell Biol.* **2004**, *5*(8), 601-613
Chrétien, D. 1996	D. Chrétien, J. M. Kenney, S. D. Fuller, R. H. Wade, *Structure* **1996**, *4*, 1031-1040
Choquet, D. 1997	D. Choquet, D.P: Felsenfeld, M.P. Sheetz, *Cell* **1997**, *88*, 39-48
Chou C. F. 1993	C. F. Chou, C. L. Riopel, L. S. Rott, M. B. Omary, *J. Cell Sci.* **1993**, *105*, 433-445
Coulombe, P.A. 2002	P. A. Coulombe, M. B. Omary, *Curr. Op. Cell Biol.* **2002**, *14*, 110-122
Cuvelier, D. 2003	D. Cuvelier, O. Rossier, P. Bassereau, P. Nassoy, *Eur. Biophys. J.* **2003**, *32*, 342–354
Döbereiner, H.-G. 2004	H.-G. Döbereiner, B. Dubin-Thaler, G. Giannone, H. S. Xenias, M. P. Sheetz, *Phys. Rev. Let.* **2004**, *93*(10), 108105-1 – 108105-4
Dorow, C. 2003	C. Dorow, N. Krstin, F.-G. Sander, *J. Orofac. Orthop.* **2003**, *2*, 100-107
Dubin-Thaler, B.J. 2004	B. J. Dubin-Thaler, G. Giannone, H.-G. Döbereiner, M. P. Sheetz, *Biophys. J.* **2004**, *86*, 1794–1806

Fang, X. 2000	X. Fang, S. Yu, R. LaPushin, Y. Lu, T. Furui, L.Z. Penn, D. Stokoe, J.R. Erickson, R.C. Bast, Jr., G.B. Mills, *Biochem. J.* **2000**, *352*, 135-143
Finer, J.T. 1994	J.T. Finer, R.M. Simmons, J.A. Spudich, *Nature* **1994**, *368*, 113-119
Freshney, R.I. 2000	Culture of Animal Cells, 4th edition, Wiley-Liss, New York, 2000
Fuchs, E. 1998	E. Fuchs, D.W. Cleveland, *Science* **1998**, *279*, 514-519
Fung, Y.C. 1993	Biomechanics, Mechanical Properties of Living Tissues, 2nd edition, Springer-Verlag, New York, 1993
Fygenson, D.K. 1997	D.K. Fygenson, J.F. Marko, A. Libchaber, *Phys. Rev. Let.* **1997**, *79*(22), 4497-4500
Galbraith, C.G. 2002	C.G. Galbraith, K.M. Yamada, M.P. Sheetz, *J. Cell. Biol.* **2002**, *159*(4), 695-705
Glogauer, M. 1997	M. Glogauer, P. Arora, G. Yao, I. Sokholov, J. Ferrier,C.A.G. McCulloch, *Journal of Cell Science* **1997**, *110*, 11-21
Graber, T.M. 1994	T.M. Graber, R.L.Jr. Vanarsdall, Orthodontics, Current Principles and Techniques, 2nd edition, Mosby, St. Louis, 1994
Gray, H. 1995	Gray's Anatomy, 15th edition, Barnes & Noble, New York, 1995
Guck, J. 2001	J. Guck, R. Ananthakrishnan, H. Mahmood, T.J. Moon, C.C. Cunningham, J. Käs, *Biophys. J.* **2001**, *81*, 767–784
Heidemann, S.R. 2004	S.R. Heidemann, D. Wirtz, *Trends Cell Biol.* **2004**, *14*(4), 160-166
Hermann, H. 1999	H. Hermann, M. Haner, M. Brettel, N.O. Ku, U. Aebi, *J. Mol. Biol.* **1999**, *286*(5), 1403-1420
Hochmuth, R.M. 2002	R.M. Hochmuth, W.D. Marcus, *Biophys. J.* **2002**, *82*, 2964-2969
Hollenbeck, P.J. 1989	P.J. Hollenbeck, A.D. Bershadsky, O.Y. Pletjushkina, I.S. Tint, J.M. Vasiliev, *J. Cell Sci.* **1989**, *92*(4), 621-631
Hood, J.D. 2002	J.D. Hood, D.A. Cheresh, *Nat. Rev. Cancer* **2002**, *2*, 91-100
Hörner, B. 1988	B. Hörner, S. Citi, J. Kendrick-Jones, B.M. Jockusch, *J. Cell. Biol.* **1988**, *107*(6), 2181-2189
Hornberger, T.A. 2004	T.A. Hornberger, D.D. Armstrong, T.J. Koh, T.J. Burkholder, K.A. Esser, *Am. J. Physiol. Cell Physiol.* **2004**, Sep 15, Epub ahead of print
Howard, J. 2001	Mechanics of Motor Proteins and the Cytoskeleton, Sinauer Associates, Inc., Sunderland, Massachussetts, USA, 2001
Janmey, P. 1998	Janmey, P.A., *Physiol. Rev.* **1998**, *78*(3), 763-781
Joanny, J.-F. 2004	J.-F. Joanny, F. Julicher, J. Prost, *Phys. Rev. Lett* **2003**, *90*(16), 168102/1-168102/4
Kainulein, T. 2002	T. Kainulainen, A. Pender, M. D'Addario, Y. Feng, P. Lekic, C.A. McCulloch, *J. Biol. Chem.* **2002**, *277*(24) ,21998–22009
Kemkemer, R. 2002	R. Kemkemer, S. Schrank, W. Vogel, H. Gruler, D. Kaufmann, *Proc. Natl. Acad. Sci. USA* **2002**, *99*(21), 13783-13788
Kovács, M. 2003	M. Kovács, F. Wang, A. Hu, Y. Zhang, J. R. Sellers, *J. Biol. Chem.* **2003**, *278*(40), 38132-38140
Lehnert, D. 2004	D. Lehnert, B. Wehrle-Haller, C. David, U. Weiland, C. Ballestrem, B.A. Imhof, M. Bastmeyer, *J. Cell Sci.* **2004**, *117*, 41-52
Lieber, M. 1975	M. Lieber, J. Mazzetta, W. Nelson-Rees, M. Kaplan, G. Todaro, *Int. J. Cancer* **1975**, *15*, 741-747
Lim, C.T. 2004	C.T. Lim, M. Dao, S. Suresh, C.H. Sow, K.T. Chew, *Acta Materialia* **2004**, *52*(13), 4065-4066
Lo, C.-M. 2000	C.-M. Lo, H.-B. Wang, M. Dembo, Y.-l. Wang, *Biophs. J.* **2000**, *79*, 144-152
Ma, L. 1999	L. Ma, J. Xu, P.A. Coulombe, D. Wirtz, *J. Biol. Chem.* **1999**, *274*(27), 19145-19151
Maniotis A.J. 1997	A.J. Maniotis, C.S. Chen, D.E. Ingber, *Proc. Natl. Acad. Sci. USA* **1997**, *94*, 849–854
Matzke, R. 2001	R. Matzke, K. Jacobson, M. Radmacher, *Nature cell Biol.* **2001**, *3*, 607-610
Merckel, R. 1999	R. Merkel, P. Nassoy, A. Leung, K. Ritchie, E. Evans, *Nature* **1999**, *397*, 50-53

Micoulet, A. 2003	A. Micoulet, M. Beil, G. von Wichert, S. Paschke, P.Walther, M. Bishr Omary, P. P. Van Veldhoven, U. Gern, E. Wolff-Hieber, J. Eggermann, J. Waltenberger, G. Adler, T. Seufferlein, J. Spatz, *Nat. Cell Biol.* **2003**, *5*(9), 803-811
Moore, P.B 1970	P. B. Moore, H. E. Huxley, D. J. DeRosier, *J. Mol. Biol.* **1970**, *50*(2), 279-288
Moyano, J.V. 2003	J.V. Moyano, A. Maqueda, B. Casanova, A. Garcia-Pardo, *Mol. Biol. Cell* **2003***, 14*, 3699–3715
Nobe, H. 2003	H. Nobe, K. Nobe, F. Fazal, P de Lanerolle, R.J. Paul, *Am. J. Physiol. Cell Physiol.* **2003***, 284*, C599-C606
Obara, K. 1995	K. Obara, G. Nikcevic, L. Pestic, G. Nowak, D.D. Lorimer, V. Guerriero, Jr., E.L. Elson, R.J. Paul, P de Lanerolle, *J. Biol. Chem.* **1995***, 270*(32), 18734-18737
Omary, M.B., 1998	M. B. Omary, N.-O. Ku, J. Liao, D. Price, *Sub. Biochem.* **1998**, *31*, 105-140
Peckham, M. 2001	M. Peckham, G. Miller, C. Wells, D. Zicha, G. A. Dunn, *J. Cell Sci.* **2001**, *114*(7), 1367-1377
Pelham, R.J. 1997	R.J. Pelham, JR., Y.-L. Wang, *Proc. Natl. Acad. Sci. USA* **1997**, *94*, 13661–13665
Pender, N. 1991	N. Pender, C.A. McCulloch, *J. Cell Sci.* **1991**, *100*(1), 187-193
Polte, T.R. 2004	T.R. Polte, G.S. Eichler, N. Wang, D.E. Ingber, *Am. J. Physiol. Cell Physiol.* **2004***, 286*, C518-C528
Pollard, T.D. 2001	T.D. Pollard, L. Blanchoin, R.D. Mullins, *J. Cell Sci.* **2001**, *114*, 3
Prost, J. 1994	J. Prost, J.-F. Chauwin, L. Peliti, A. Ajdari, *Phys. Rev. Lett.* **1994**, *72*(16), 2652-2655
Ren, X.-D., 1999	X.-D. Ren, W.B. Kiosses, M.A. Schwartz, *EMBO J.* **1999***, 18*(3), 578-585
Revenu, C. 2004	C. Revenu, R. Athman, S. Robine, D. Louvard, *Nature Reviews, Mol. Cell Biol.* **2004***, 5*(8), 635-646
Riveline, D. 2001	D. Riveline, E. Zamir, N.Q. Balaban, U.S. Schwarz, T. Ishizaki, S. Narumiya, Z. Kam, B. Geiger, A.D. Bershadsky, *J. Cell Biol.* **2001***, 153*(6), 1175–1185
Roberts, W.E. 1981	W.E. Roberts, D.C. Chase, *J. Dent. Res.* **1981**, *60*, 174-181
Russel, D. 2004	D. Russell, P.D. Andrews, J. James, E. B. Lane, *J. Cell Sci.* **2004**, *117*, 5233-5243
Sinard, J.H. 1989	J.H. Sinard, W. S. Stafford, T. D. Pollard, *J. Cell Biol.* **1989**, *109*, 1537-1547
Seufferlein, T. 1994	T. Seufferlein, E. Rozengurt, *J. Biol. Chem.* **1994***, 269*(12), 9345-9351
Shelden, E. 1995	E. Shelden, D.A. Knecht, *J. Cell. Sci.* **1995***, 108*, 1105-1115
Shirinsky, V. 1989	V.P. Shirinsky, A.S. Antonov, K.G. Birukov, A.V. Sobolevsky, Y.A.Romanov, N.V. Kabaeva, G.N. Antonova, V.N. Smirnov, *J. Cell Biol.* **1989***, 109*, 331-339
Stenger, D.A. 1992	D. A. Stenger, J. H. Georger, C. S. Dulcey, J. J. Hickman, A. S. Rudolph, T. B. Nielsen, S. M. McCort, J. M. Calvert, *J. Am. Chem. Soc.* **1992**, *114*, 8435-8442
Strelkov, S.V. 2003	S.V. Strelkov, H. Hermann, U. Aebi, *Bioessays* **2003**, *25*(3), 243-251
Suresh, S. 2005	S. Surech, J. Spatz, J.P. Mills, A. Micoulet, M. Dao, C.T. Lim, M. Beil, T. Seufferlein, *Acta Biomat.* **2005**, *1*(1), 15-30, to be published
Svitkina, T.M. 1996	T.M. Svitkina, A.B. Verkhovsky, G.G. Borisy, *J. Cell Biol.* **1996**, *135*(4), 991-1007
Svitkina, T.M. 1997	T.M. Svitkina, A.B. Verkhovsky, K.M. McQuale, G.G. Borisy, *J. Cell Biol.* **1997**, *139*(2), 397-415
Svitkina, T.M. 1999	T.M. Svitkina, G.G. Borisy, *J. Cell Biol.* **1999**, *145*(5), 1009-1026
Tan J.L , 2003	J.L. Tan, J. Tien, D.M. Pirone, D.S. Gray, K. Bhadriraju, C.S. Chen, *Proc Natl Acad Sci U S A.* **2003***, 100*(4), 1484-1489
Tangkijvanich, P. 2002	P. Tangkijvanich, A.C. Melton, T. Chitapanarux, J. Han, H. F. Yee, Jr., *Exp. Cell Res.* **2002**, *281*, 140-147
Toivola, D.M. 2000	D.M. Toivola, H. Baribault, T. Magin, S.A. Michie, M.B. Omary, *Am. J. Physiol. Gasteointest. Liver Physiol.* **2000***, 279*, G1343-G1354
Theriot J.A. 1991	J. A. Theriot , T. J. Mitchison, *Nature* **1991**, *352*, 107-108
Thoumine, O. 1997	O. Thoumine, A. Ott, *J. Cell Sci.* **1997***, 110*, 2109-2116

Thoumine, O. and Ott, A. 1997	O. Thoumine, A. Ott, *Biorheo.* **1997**, *34*(4/5), 309-326
Verkhovsky, A.B. 1993	A.B. Verkhovsky, G.G. Borisy, *J. Cell Biol.* **1993**, *123*(3), 637-652
Verkhovsky, A.B. 1999	A. B. Verkhovsky, T. M. Svitkina, G. G. Borisy, *Curr. Biol.* **1999**, 9, 9-11
Von den Hoff, J.W. 2003	J.W. Von den Hoff, *J. Periodont. Res.* **2003**, *38*, 449–457
White, J.R. 1983	J. R. White, P. H. Naccache, R. I. Sha'afi, *J. Biol. Chem.* **1983**, *258*(22), 14041-14047
Wang, F. 2003	F. Wang, M. Kovács, A. Hu, J. Limouze, E. V. Harvey, J. R. Sellers, *J. Biol. Chem.* **2003**, *278*(30), 27439-27448
Xu, J. 1998	J. Xu, A. Palmer, D. Wirtz, *Macromol.* **1998**, *31*, 6486-6492
Xu, J. 2000	J. Xu, Y. Tseng, D. Wirtz, *J. Biol. Chem.* **2000**, *275*(46), 35886-35893
Yamada, S. 2000	S. Yamada, D. Wirtz, S.C. Kuo, *Biophys. J.* **2000**, *78*, 1736–1747
Yamada, S. 2002	S. Yamada, D. Wirtz, P.A. Coulombe, *Mol. Biol. Cell,* **2002***, 13*, 382-391
Yoon, K.H. 2001	K.H. Yoon, M. Yoon, R.D. Moir, S. Khuon, F.W. Flitney, R.D. Goldman, *J. Cell Biol.* **2001***, 153*(3), 503-516
Zamir, E. 1999	E. Zamir, B.-Z. Katz, S.-I. Aota, K.M. Yamada, B. Geiger, Z. Kam, *J. Cell Sci.* **1999**, *112*, 1655-1669
Zatloukal, K. 2004	K. Zatloukal, C. Stumptner, A. Fuchsbichler, P. Fickert, C. Lackner, M. Trauner, H. Denk, *J. Pathol.* **2004***, 204*, 367-376
Zhong B., 2004	B. Zhong, Q. Zhou, D.M. Toivola, G.-Z. Tao, E. Z. Resureccion, M. B. Omary, *J. Cell Science* **2004**, *117*, 1709-1718

Abbreviations

actomyosin	protein complex, actin filament and myosin
APT	adenosin triphosphate
ADP	adenosine diphospahte
BSA	bovine serum albumin
CT	connective tissue
DMEM	Dulbecco's modified Eagle medium
EGF	epidermal growth factor
ECM	extra-cellular matrix
FBS	foetal bovine serum
FN	fibronectin
GFP	green fluorescent protein
IF	intermediate filament
LPA	lysophosphatidic acid
MF	microfilament
MT	microtubule
NMM	non-muscle myosin
Panc-1	cancerous cell line from the pancreas
PBS	phosphate buffer saline
PDGF	platelet-derived growth factor
PDL	periodontal ligament
PSD	position sensitive diode
RBC	red blood cell
REF 52	rat embryonic fibroblast 52 cell line
RGD	arginine-glycine-aspartic acid peptide
ROI	region of interest
SFC	scanning force cantilever
SPC	sphingosylphosphorylcholine